SATURATION MAGNETIZATION AND CRYSTAL CHEMISTRY OF FERRIMAGNETIC OXIDES

E. W. GORTER

SATURATION MAGNETIZATION AND CRYSTAL CHEMISTRY OF FERRIMAGNETIC OXIDES

PROEFSCHRIFT

TER VERKRIJGING VAN DE GRAAD VAN DOCTOR IN DE WIS- EN NATUURKUNDE AAN DE RIJKSUNIVERSITEIT TE LEIDEN, OP GEZAG VAN DE RECTOR MAGNIFICUS Mr J. M. VAN BEMMELEN, HOOGLERAAR IN DE FACULTEIT DER RECHTSGELEERDHEID, PUBLIEK TE VERDEDIGEN OP WOENSDAG 9 JUNI 1954 TE 15 UUR

DOOR

EVERT WILLEM GORTER

GEBOREN TE LEIDEN IN 1912

PROMOTOR:
PROF. DR A. E. VAN ARKEL

CONTENTS

	Blz.
INTRODUCTION	2
1. THE SPINEL STRUCTURE	4
1.1 The geometry of the spinel lattice	4
1.2 Crystal chemistry of oxidic spinels	9
1.2.1 Metallic ions occuring in oxidic spinels	9
1.2.2 Cation distribution in binary oxide spinels	10
1.2.3 Long-range order in oxidic spinels	11
1.2.4 The hausmannite structure	13
1.2.5 Factors influencing the cation distribution and the stability of oxidic spinels	13
1.2.5.1 Coulomb energy and repulsive energy	14
1.2.5.2 Short-range order	17
1.2.5.3 Magnetic interaction energy	18
1.2.5.4 Individual preference of cations for 4- or 6-fold coordination	18
1.2.6 Spinels containing three of more different cations	20
References	21
2. THEORY OF FERRIMAGNETISM	22
2.1 Introduction	22
2.2 Outline of the theory of ferrimagnetism	24
2.2.1 Néel's theory	24
2.2.1.1 Paramagnetic behaviour	25
2.2.1.2 Ferromagnetic behaviour	27
2.2.2 Non-parallel ionic moments inside each sublattice	29
2.2.3 Spinels containing two or more magnetic ions	31
2.3 The nature of the exchange interactions	31
2.3.1 Indirect exchange interaction	31
2.3.2 Dependence of superexchange interaction on the angle Me-O-Me	32
2.3.3 Influence of the type of magnetic ion	33
2.3.4 Influence of angles and distances on superexchange interaction in spinels	34
References	35

Blz.

3. EXPERIMENTAL PROCEDURES 36

3.1 Magnetic measuring methods used in sections 4-9 36
3.2 Preparation of the materials 38
3.2.1 The final sintering operation 38
3.2.2 Methods of preparation of the powder to be sintered 40
3.3 X-ray analysis 41
3.4 Chemical analysis 41
References 43

4. EXPERIMENTAL EVIDENCE FOR THE CORRECTNESS OF NEEL'S HYPOTHESIS: THE FERRITES 44

4.1 Introduction 44
4.2 Preparation and analysis of the ferrites 44
4.3 Saturation moments of the single ferrites ($Me^{II}Fe_2^{III}O_4$ and $Li_{0.5}Fe_{2.5}^{III}O_4$) 45
4.3.1 Effective g-factors 49
4.4 Saturation moments of the mixed crystals of the ferromagnetic ferrites with zinc ferrite ($Me_{1-a}^{II}Zn_aFe_2O_4$ and $Li_{0.5-0.5a}Zn_aFe_{2.5-0.5a}O_4$) 50
References 55

5. EXPERIMENTS ON THE ANGLE DEPENDENCE OF THE SUPEREXCHANGE INTERACTION 57

5.1 The angle A-O-B in spinels 57
5.1.1 Introduction 57
5.1.2 CaZn ferrite 57
5.1.2.1 Experimental 57
5.1.2.2 Discussion 59
5.2 Prediction of magnetic behaviour in other crystal structures from Anderson's theory 61
5.2.1 Introduction 61
5.2.2 Application to $BaFe_{12}^{III}O_{19}$ and $KFe_{11}^{III}O_{17}$ 62
5.2.3 Application to $BaFe_2^{II}Fe_{16}^{III}O_{27}$ 66
References 66

6. SATURATION MOMENT AND CRYSTAL CHEMISTRY OF FERRIMAGNETIC SPINELS CONTAINING TITANIUM 67

6.1 Introduction to the sections 6-8 67
6.2 The system $Ni_{1+a}^{II}Fe_{2-2a}^{III}Ti_a^{IV}O_4$ ($NiFe_2O_4$-$Ni_{1.5}FeTi_{0.5}O_4$) 68
6.2.1 Experimental 68

Blz.

6.2.2 Discussion of the results for the annealed samples and neutron diffraction evidence 71
6.2.3 Discussion of the results for the quenched samples 73
6.3 The system $Ni^{II}_{1.5-a}Zn^{II}_{a}Fe^{III}Ti^{IV}_{0.5}O_4$ ($Ni_{1.5}FeTi_{0.5}O_4$-$NiZn_{0.5}FeTi_{0.5}O_4$) 74
6.3.1 Experimental 74
6.3.2 Discussion of the results 76
6.4 The system $Ni^{II}_{1.5-a}Mn^{II}_{a}Fe^{III}Ti^{IV}_{0.5}O_4$ ($Ni_{1.5}FeTi_{0.5}O_4$-$Mn_{1.5}FeTi_{0.5}O_4$) 77
6.4.1 Experimental 77
6.4.2 Discussion of the results 80
References 82

7. FERRIMAGNETIC OXIDES CONTAINING CHROMIUM: THE SYSTEM $Li_{0.5}Fe^{III}_{2.5-a}Cr^{III}_{a}O_4$ ($Li_{0.5}Fe_{2.5}O_4$-$Li_{0.5}Fe_{0.5}Cr_2O_4$) 83

7.1 Experimental 83
7.2 Discussion of the magnetic measurements 86
7.2.1 Saturation moments 86
7.2.2 Curie temperatures 88
7.2.3 Anomalous temperature dependence of saturation magnetization and effective g-factor 89
7.3 Discussion of the cation distribution 91
References 91

8. FERRIMAGNETIC SPINELS CONTAINING ALUMINIUM 92

8.1 Discussion of data published on the systems $Fe^{II}Fe^{III}_{2-a}Al_aO_4$ and $MgFe^{III}_{2-a}Al_aO_4$ 92
8.2 The system $Ni^{II}Fe^{III}_{2-a}Al_aO_4$ ($NiFe_2O_4$-$NiFeAlO_4$) 94
8.2.1 Experimental 94
8.2.2 Discussion of the saturation moments 97
8.2.3 Discussion of the cation distribution 98
8.2.4 Discussion of the shapes of the σ-T curves 99
References 101

9. OTHER FERRIMAGNETIC OXIDES CONTAINING CHROMIUM: THE SYSTEM $Mn^{II}Fe^{III}_{2-a}Cr_aO_4$ ($MnFe_2O_4$-$MnCr_2O_4$) 102

9.1 Introduction 102
9.2 Experimental 102
9.3 Discussion 105
Reference 106

Summary

Measurements of the saturation magnetization (σ) against temperature have been carried out for a number of mixed crystal oxides with spinel structure. The results are in agreement with Néel's theory of ferrimagnetism: the resultant magnetic moment m is the difference of the moments of the tetrahedral (A) and octahedral (B) sublattices, either (a) with complete parallelism of the ionic moments inside each sublattice, or (b) with angles between the ionic moments inside one of the sublattices.

The spinel structure is described in section 1.1, experimental and theoretical data from literature on cation distribution are summarized in section 1.2. Néel's theory is reviewed in section 2.2.1, with Yafet and Kittel's modification (section 2.2.2). When the moments of the two sublattices are approximately equal, Néel predicts a number of anomalous σ-T curves. All of these should occur in a series of mixed crystals of type (a) in which the resultant moment m changes sign.

Our experimental methods are given in section 3.

The measurements on the single ferrites $Me^{II}Fe_2^{III}O_4$, with $Me^{II} = Mn^{2+}$, Fe^{2+}, Co^{2+}, Ni^{2+}, Cu^{2+}, Mg^{2+} or $(0{\cdot}5\ Li^{+} + 0{\cdot}5\ Fe^{3+})$ show that these belong to group (a); the mixed crystals $Me_{1-a}\ Zn_aFe_2O_4$ from $a >$ appr. 0·4 belong to group (b) (section 4).

The moment of $Ca_{0{\cdot}35}Zn_{0{\cdot}65}Fe_2O_4$ is higher than that of any MgZn ferrite, perhaps because the angle A-O-B is increased by the presence of the greater part of the large Ca ions in the B sites, thus increasing the AB interaction; this behaviour would be in agreement with Anderson's theory (section 5.1; Anderson's theory is reviewed in section 2.3.2). The moments of ferrimagnetic oxides with other crystal structures may be predicted from the angles (metal ion)-(O^{2-} ion)-(metal ion); cf. $BaFe^{III}_{12}O_{19}$ and $KFe^{III}_{11}\ O_{17}$ (section 5.2).

In a number of mixed crystal series anomalous σ-T curves have been looked for: these are not found in the systems $Ni_{1+a}Fe^{III}_{2-2a}Ti_aO_4$ and $Ni_{1{\cdot}5-a}Zn_aFe^{III}Ti_{0{\cdot}5}O_4$ because of the unexpected presence of Ti^{4+} ions in tetrahedral sites, proved for $Ni_{1{\cdot}5}Fe^{III}Ti_{0{\cdot}5}O_4$ by measurements of the effective g-factor (section 6.1-2).

In the system $Li_{0{\cdot}5}Fe^{III}_{2{\cdot}5-a}Cr_aO_4$ $(0<a<2{\cdot}0)$ the distribution of the Li^{+} and Fe^{3+} ions is anomalous as a result of short-range order. The resultant moment remains positive, and only one type of anomalous σ-T curve, viz. that for which the spontaneous magnetization changes sign with temperature, occurs in a wide range of compositions. For $a \leqslant 1{\cdot}25$ the materials belong to group (a) (section 7).

A change of sign of the resultant moment does occur in the system $NiFe^{III}_{2-a}Al_aO_4$. Anomalous σ-T curves are here found in a narrow range of compositions, but not all types predicted by Néel: the reasons are discussed (section 8).

The presence of Mn^{2+} ions apparently promotes the formation of angles between the ionic moments in B sites: the complete system $MnFe^{III}_{2-a}Cr_aO_4$ belongs to group (b) (section 9), as well as $MnFe_2O_4$ prepared by other authors (section 4) and part of the system $Ni_{1{\cdot}5-a}Mn_aFe^{III}Ti_{0{\cdot}5}O_4$ (section 6.3). In the first-named system m probably changes sign only as a result of these angles.

Introduction

Largely as a consequence of Snoek's work, the "ferrites", i.e. oxides with a formula $MeO.Fe_2O_3$ or $Me^{II}Fe_2^{III}O_4$, are becoming increasingly important as high-frequency core materials because they combine useful ferromagnetic properties with a high electrical resistivity. In the above formula Me^{II} represents divalent Mn, Fe, Co, Ni, Cu, Zn, Cd, Mg, ($0{\cdot}5Li + 0{\cdot}5\ Fe^{III}$), or two or more of these in mixed crystals. In recent years the fundamental ferromagnetic properties have been investigated extensively. In the following we shall deal with the saturation magnetization of these ferrites and similar materials.

Practically all these materials have the same crystal structure as the mineral spinel, which structure (Bragg, 1915) may be regarded as a cubic, approximately close-packed arrangement of oxygen ions ($r = 1{\cdot}32$ Å), with metal ions having radii of 0·4-1·0 Å distributed amongst two kinds of interstices A and B, surrounded by 4 and 6 oxygen ions respectively. The structure is described in some detail in section 1.1.

X-ray and theoretical investigations, mainly by Verwey et al., have shown that the distribution of the different metallic ions amongst A and B sites is determined mainly by the Coulomb energy, including ordering energy inside each sublattice A or B, and by an individual preference of a number of ions for four- or sixfold coordination. One type of ion often occurs in both lattice sites. These investigations are summarized in section 1.2.

The ferromagnetic moment per formula unit, obtained from saturation magnetization (σ) measurements at low temperatures, is not simply the sum of the moments of the magnetic moments present, but much lower; $ZnFe_2O_4$ and $CdFe_2O_4$ are not even ferromagnetic. Néel in 1948 gave a theory for these materials using the basic assumption that a preponderant negative (AB) interaction between the magnetic moments of the A and B sublattices causes these to have antiparallel orientation, so that the resultant moment m equals the difference between the moments of sublattices A and B. This non-compensated antiferromagnetism Néel calls *ferrimagnetism*. With the aid of this theory he could explain such susceptibility and saturation data as were at the time available, and predicted the occurrence of several types of anomalous magnetization vs temperature curves, which are expected to occur when the moments of the A and B sublattices are not very different. This anomalous behaviour can only occur in ferrimagnetism.

The equally negative AA and BB interactions may be either negligible against the AB interaction, so that the moment of each sublattice is the sum of the ionic moments in that sublattice, or they may be comparable

to the AB interaction, for which case the moment of one of the sublattices is smaller than the sum of the ionic moments it contains. Yafet and Kittel (1952) have shown theoretically that in this case this sublattice splits up in 2 or 4 different parts: in each of these parts the ionic moments are parallel, but the moments of different parts form angles with each other.

The nature of the exchange coupling is an indirect exchange interaction involving the diamagnetic oxygen ions, the theory of which was outlined by Kramers in 1934. A treatment by Anderson (1950) shows that the strength of this superexchange interaction is dependent on the angle (metal ion)-(oxygen ion)-(metal ion). These theories are reviewed in section 2.

The object of the present investigation was primarily to obtain experimental evidence supporting Néel's theory. The results of our measurements of the saturation magnetization of a number of series of mixed crystals with spinel structure can almost all be accounted for by Néel's theory. For a group of materials, which mostly have relatively high Curie temperatures, the resultant moments are in agreement with the theory for the case of a perponderant AB interaction.

In several cases the ionic distribution, as obtained from these measurements, appears to be different from what knowledge on binary spinels would lead one to expect. The cation distribution can in most cases be understood from statistical considerations, assuming a certain order of preference of the cations for the A position inside one series of compositions. In some cases the influence of short-range order is noticeable.

In one series this could be confirmed by X-ray diffraction, in another case the effective g-factor was used in addition to the saturation data to find the ionic distribution. Some of the anomalous σ-T curves predicted by Néel have been found, a.o. in one series in which m changes sign with composition. It is shown that the absence in this series of those σ-T curves for which σ is zero at some temperature between 0 °K and the Curie temperature is due to the inhomogeneity of the cation distribution. In another system we have found materials for which such σ-T curves do occur.

For another group of materials, which have relatively low Curie temperatures, the results are in agreement with the theory for the case of comparable AB and BB interactions. In one system the resultant moment m changes sign, which when assuming parallel ionic moments in each sublattice would not occur for any ionic distribution.

Experimental indications for the dependence of the strength of the interaction on the angle (metal ion)-(oxygen ion)-(metal ion) are discussed and it has been shown that this relationship enables one to account for the resultant moment in other crystal structures.

1. THE SPINEL STRUCTURE

1.1. The Geometry of the Spinel Lattice

As we shall deal extensively with the magnetic properties of oxidic spinels in relation to the crystal structure, we shall give a fuller description of the structure than is found in literature, drawing attention to those features that are of interest in connection with these magnetic properties.

As only oxides will be discussed, the words oxygen ion will be substituted for anion throughout the description.

The crystal structure was determined for the minerals magnetite (Fe_3O_4) and spinel ($MgAl_2O_4$) by W.H. Bragg [1]) in 1915 and at the same time by Nishikawa [2]).

The space group is O_h^7-F3dm [3]) (cubic). The atomic positions in the spinel structure are [4])

8-fold position: 8 metal ions in (a) *) 0 0 0; $\frac{1}{4}\ \frac{1}{4}\ \frac{1}{4}$;

16-fold position: 16 metal ions in (d) *) $\frac{5}{8}\ \frac{5}{8}\ \frac{5}{8}$; $\frac{5}{8}\ \frac{7}{8}\ \frac{7}{8}$; $\frac{7}{8}\ \frac{5}{8}\ \frac{7}{8}$; $\frac{7}{8}\ \frac{7}{8}\ \frac{5}{8}$;

32-fold position: 32 oxygen ions in (e)

$u\ u\ u$; $u\ \bar{u}\ \bar{u}$; $\frac{1}{4}-u,\ \frac{1}{4}-u,\ \frac{1}{4}-u$; $\frac{1}{4}-u,\ \frac{1}{4}+u,\ \frac{1}{4}+u$;

$\bar{u}\ u\ \bar{u}$; $\bar{u}\ \bar{u}\ u$; $\frac{1}{4}+u,\ \frac{1}{4}-u,\ \frac{1}{4}+u$; $\frac{1}{4}+u,\ \frac{1}{4}+u,\ \frac{1}{4}-u$;

with the translations + (0 0 0; 0 $\frac{1}{2}$ $\frac{1}{2}$; $\frac{1}{2}$ 0 $\frac{1}{2}$; $\frac{1}{2}$ $\frac{1}{2}$ 0).

A centre of symmetry exists at each point of the 16-fold position.

The unit cell is seen to contain eight formula units or "molecules" $MgAl_2O_4$, or generally Me_3O_4, if Me represents any number of metal ions in any proportions.

From the translations + (0 0 0; 0 $\frac{1}{2}$ $\frac{1}{2}$; $\frac{1}{2}$ 0 $\frac{1}{2}$; $\frac{1}{2}$ $\frac{1}{2}$ 0) it is seen that the unit cell (cube edge = a) consists of two different groups of four cubes with edges $\frac{1}{2}a$ (octants) with identical ionic positions.

The ionic positions are different in two octants sharing a face and identical in two octants sharing only an edge. Thus a simple picture is obtained if the positions of the ions are drawn in two adjacent octants only (fig. 1).

Fig. 1 is drawn for the "idealized" structure with the oxygen parameter $u = \frac{3}{8}$. In reality u usually is slightly larger: for $u > \frac{3}{8}$ the oxygen ions move from their ideal position in a [111] direction away from the nearest tetrahedral ion. The radii of the ions in the figs 1-5 are completely arbitrary and rather too small.

It is seen from fig. 1 that each octant contains four oxygen ions (large spheres) on the body diagonals of the octants and lying on the corners of a tetrahedron, thus forming a face-centred cubic lattice for $u = \frac{3}{8}$, and four interpenetrating face-centred cubic lattices for $u \neq \frac{3}{8}$. The left-hand

*) In several publications another position of the unit cell has been used for which there are 8 metal ions in ($8f$) and 16 metal ions in ($16c$).

octant contains in the centre a metal ion in the (8*a*) position (small sphere, unhatched), lying in the centre of a tetrahedron of oxygen ions. We shall call this an ion in a tetrahedral site, or tetrahedral ion. The right-hand octant shows four metal ions in the (16*d*) position (small spheres, hatched), each surrounded by an octahedron formed by six oxygen ions. We shall call each of these an ion in an octahedral site, or octahedral ion.

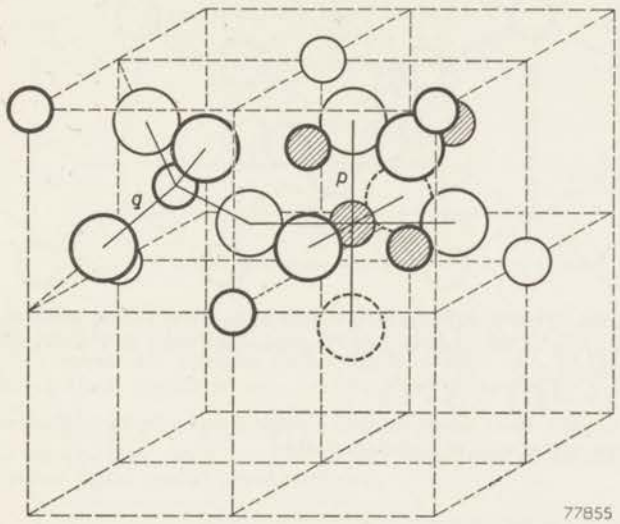

Fig. 1. Unit cell of spinel structure. The position of the ions in only two octants is shown. The dashed circles belong to other octants. The drawn lines indicate the fourfold and sixfold coordination of the respective metal ion positions.
) $x = 0 - \frac{1}{2}$) $x = \frac{3}{8} - \frac{5}{8}$) $x = \frac{3}{4} - 1$
Large circles: oxygen ions; small hatched circles: metal ions at octahedral sites; small unhatched circles: metal ions at tetrahedral sites. The figure is drawn for $u = \frac{3}{8}$.

Each octant moreover contains metal ions in the (8*a*) position (i.e. tetrahedral ions) in every other corner, in such a way that nearest neighbour tetrahedral ions (e.g. those in corners and centre of the left-hand octant) are not separated by an oxygen ion.

Figs 2 and 3 show the positions of the metal ions on tetrahedral sites only, and of the metal ions on octahedral sites only, respectively. Figs 4 and 5 show one octahedral ion surrounded by tetrahedral ions, and one tetrahedral ion surrounded by octahedral ions, respectively; in figure 5 the origin is in $\frac{1}{2}\ \frac{1}{2}\ \frac{1}{2}$.

We shall see that in superexchange interaction, to be discussed in section 2.3.2, the distances Me-Me do not play a rôle. The distances Me-O and the angles Me-O-Me are important here. Therefore a number of triangular configurations Me-O-Me have been drawn in fig. 6 (thick drawn lines),

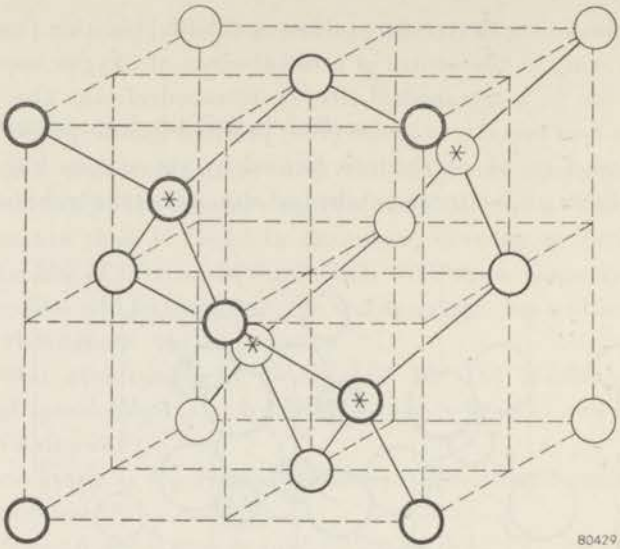

Fig. 2. The position of the metal ions on tetrahedral sites only. Each ion is surrounded by a regular tetrahedron of tetrahedral ions. The asterisks refer to a superstructure to be discussed in section 1.2.3.
) $x = 0 - \frac{1}{2}$) $x = \frac{3}{8} - \frac{5}{8}$) $x = \frac{3}{4} - 1$
Large circles: oxygen ions; small hatched circles: metal ions at octahedral sites; small unhatched circles: metal ions at tetrahedral sites.

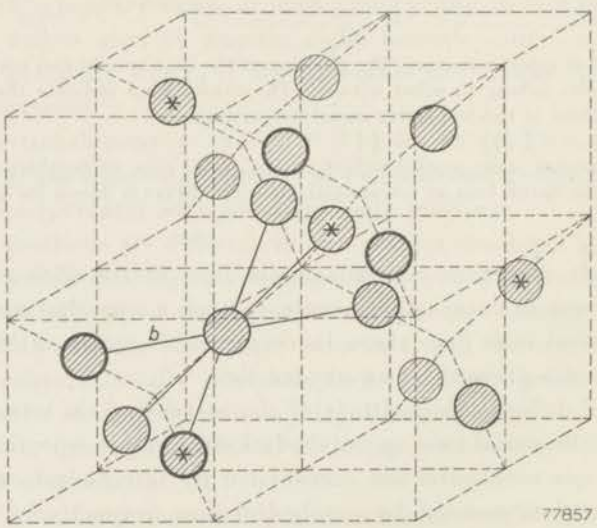

Fig. 3. The position of the metal ions on octahedral sites only. Each ion forms part of two regular tetrahedra of octahedral ions having only this one ion in common. The asterisks refer to another superstructure to be discussed in section 1.2.3.
) $x = 0 - \frac{1}{2}$) $x = \frac{3}{8} - \frac{5}{8}$) $x = \frac{3}{4} - 1$
Large circles: oxygen ions; small hatched circles: metal ions at octahedral sites; small unhatched circles: metal ions at tetrahedral sites.

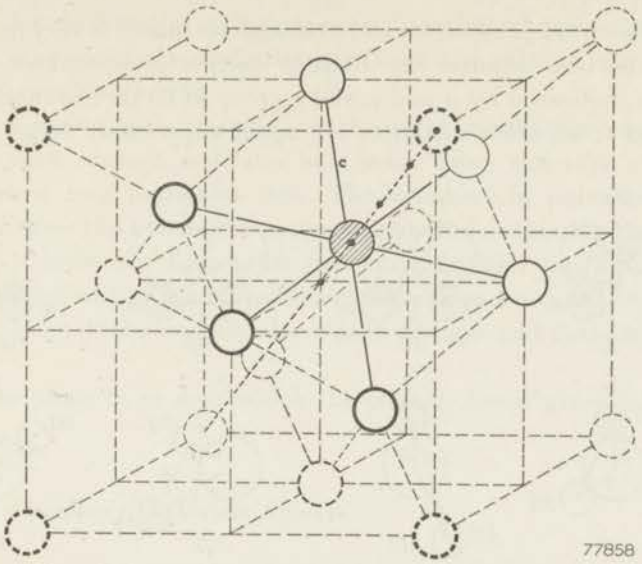

Fig. 4. The position of the metal ions on tetrahedral sites only and one octahedral ion: its six nearest neighbour tetrahedral ions are indicated by drawn circles. The six neighbours form two equilateral triangles each lying in a plane cut by the body diagonal perpendicular to them (indicated by ----) at short distances ($\pm \frac{1}{24} a\sqrt{3}$) from the octahedral ion.

) $x = 0 - \frac{1}{2}$) $x = \frac{3}{8} - \frac{5}{8}$) $x = \frac{3}{4} - 1$

Large circles: oxygen ions; small hatched circles: metal ions at octahedral sites; small unhatched circles: metal ions at tetrahedral sites.

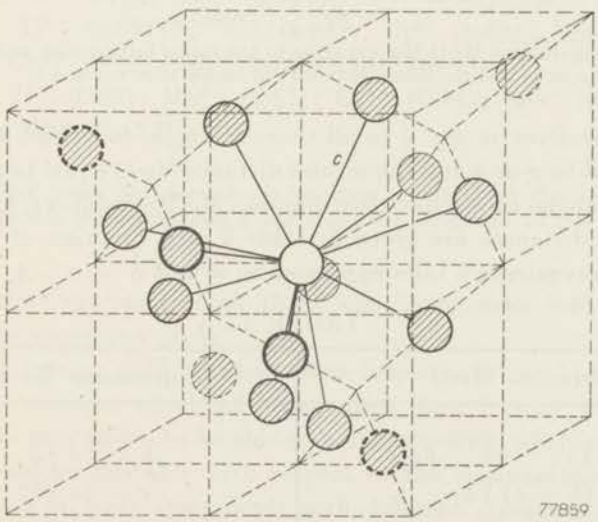

Fig. 5. The octahedral sublattice and one tetrahedral ion; the origin has been moved to $\frac{1}{2}\,\frac{1}{2}\,\frac{1}{2}$ in order to show the tetrahedral ion with its twelve nearest neighbour octahedral ions; these ions are indicated by drawn circles.

) $x = 0 - \frac{1}{2}$) $x = \frac{3}{8} - \frac{5}{8}$) $x = \frac{3}{4} - 1$

Large circles: oxygen ions; small hatched circles: metal ions at octahedral sites; small unhatched circles: metal ions at tetrahedral sites.

for u slightly above $\frac{3}{8}$, which for all ferrimagnetic spinels is very probably the case. The shortest distances Me-O fall in distinct groups: those of nearest neighbours, indicated by p and q, and a group of larger distances indicated by r, s and t; all other distances are again appreciably larger. We have

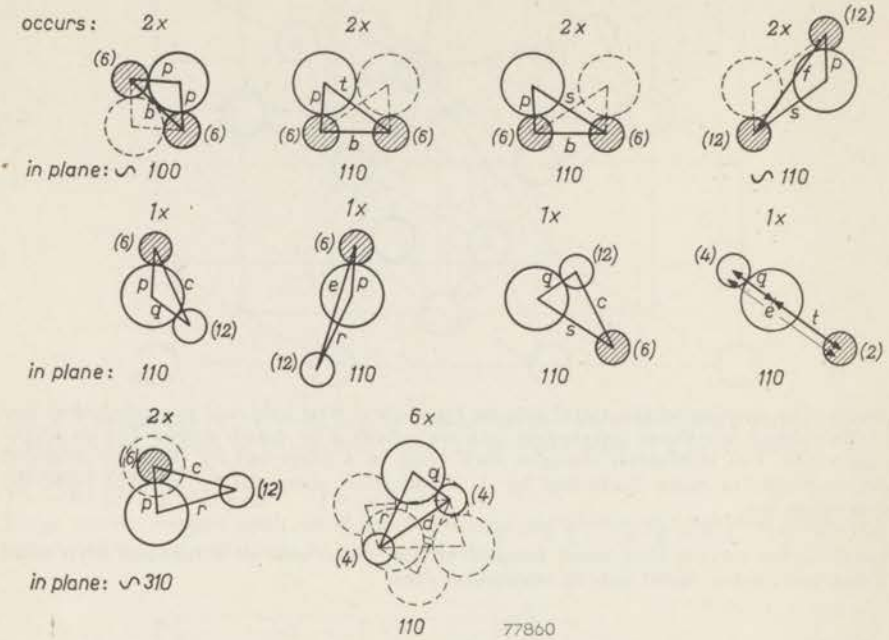

Fig. 6. The configurations Me-O-Me occurring in the spinel lattice with at least one short distance Me-O (p or q) and the other distance not larger than r, s and t.

restricted ourselves in fig. 6 to all those triangles for which one distance Me-O is equal to p or q and the second distance Me-O equal to p, q, r, s or t.

The ten triangles shown have five different Me-Me distances: b, c, d, e and f.

These ten distances are given in table I as a function of a and u, or rather for convenience's sake expressed in a and $\delta = u - \frac{3}{8}$.

TABLE I

distances Me-O	distances Me-Me
$p = a\sqrt{\frac{1}{16} - \frac{1}{2}\delta + 3\delta^2}$	$b = \frac{1}{4}a\sqrt{2}$
$q = a\,(\frac{1}{8} + \delta)\sqrt{3}$	$c = \frac{1}{8}a\sqrt{11}$
$r = a\sqrt{\frac{11}{64} + \frac{1}{4}\delta + 3\delta^2}$	$d = \frac{1}{4}a\sqrt{3}$
$s = a\sqrt{\frac{3}{16} + \frac{1}{2}\delta + 3\delta^2}$	$e = \frac{3}{8}a\sqrt{3}$
$t = a\,(\frac{1}{4} - \delta)\sqrt{3}$	$f = \frac{1}{4}a\sqrt{6}$

In fig. 6 hatched circles again represent octahedral ions, open circles tetrahedral ions and large circles oxygen ions; the ratio of the radii and distances is roughly correct.

The figure above each triangle, or the total number of oxygen ions drawn near each triangle, indicates how many times this type of triangle occurs between two particular ions. The numbers in parentheses near each ion indicates the number of cation neighbours at this Me-Me distance with which it moreover forms this particular triangle (cf. *pre* and *tqe*). Thus the number of times a particular triangle occurs around a particular ion is the product of the number above each triangle and that near the ion concerned.

Finally the plane in or near which the triangle lies is given below each triangle.

1.2. Crystal Chemistry of Oxidic Spinels

1.2.1. Metallic Ions Occurring in Oxidic Spinels

The metallic ions that have been found to occur on oxidic spinels are given below; their Goldschmidt radii are given between parentheses.
H^+(—); Li^+ (0·78); Cu^+ (1·01?)?; Ag^+ (1·13).
Mg^{2+} (0·78); Ca^{2+} (1·06) *); Mn^{2+} (0·91); Fe^{2+} (0·83);
Co^{2+} (0·82); Ni^{2+} (0·78); Cu^{2+} (0·85?); Zn^{2+} (0·82); Cd^{2+} (1·03).
Al^{3+} (0·57); Ti^{3+} (0·69)??; V^{3+} (0·65); Cr^{3+} (0·64); Mn^{3+} (0·70)?;
Fe^{3+} (0·67); Ga^{3+} (0·62); Rh^{3+} (0·68); In^{3+} (0·93).
Ti^{4+} (0·69); V^{4+} (0·65); Mn^{4+} (0·52); Ge^{4+} (0·44); Sn^{4+} (0·74).
Mo^{6+} (0·62?); W^{6+} (0·63?).

A question mark inside the parentheses indicates doubt about the ionic radius; a question mark outside the parentheses doubt about the occurrence of this ion in oxidic spinels.

It is seen that the radii of all these ions lie between 0·44 and appr. 1·0 Å, with the exception of Ag^+.

Several ions having radii between these limits have not been found in oxidic spinels, amongst which all pentavalent ions. It may well be that several of these may prove to be able to occur in spinels, whereas for others the spinel would be unstable with respect to the constituting oxides, or generally to one or more compounds with different structure. Failure to obtain binary spinels has been reported for Zr^{4+}.

Binary spinels are known of the following types

*) Only up to 0·35 per formula unit Me_3O_4.

$Me^{I}_{1/2}\,Me^{III}_{5/2}O_4$, $Me^{I}_{4/3}\,Me^{IV}_{5/3}O_4$ *), $Me^{I}_{2}\,Me^{VI}O_4$;
$Me^{II}\,Me^{III}_{2}O_4$, $Me^{II}_{2}\,Me^{IV}O_4$.

In addition to these types there are known two spinels that are reported to contain trivalent ions only and vacant lattice sites (γ-Fe_2O_3, γ-Al_2O_3), i.e. to have the formula $Me^{III}_{8/3}\,\square_{1/3}O_4$ ($\square$ = vacant lattice site). Mixed-crystal formation between all types containing mono-, di-, tri-, and tetravalent ions has been reported in a great number of cases. A few cases are known of mixed-crystal series with a miscibility gap, e.g. the system $CoFe_2O_4$-Co_3O_4 [5]), various systems reported by Romeijn [6]) and some systems investigated by Jonker [7]), e.g. $MgFe_2O_4$-$MgAl_2O_4$.

When metal ions are present that can occur in different states of valency, it is possible by chemical analysis to determine only the average state of valency. Thus the states of valency of the individual ions in e.g. Fe_3O_4, Co_3O_4, Mn_3O_4, $MnFe_2O_4$. Mn_2TiO_4 and Fe_2TiO_4 cannot be found by analysis.

Here the ionization potentials of the respective ions have to be considered in addition to the other factors determining the lattice energy of the spinels to be discussed in section 1.2.5.

The difference in ionization potentials for the different possibilities is usually not large, and it must be borne in mind that the possible error in the literature values of the 3rd and 4th ionization potentials is very large.

In many spinels, however, little doubt exists about the states of valency of the ions, either because of the known physical properties, or from analogy with similar compounds.

1.2.2. Cation Distribution in Binary Oxide Spinels

The distribution of the metallic ions in binary spinels $MeMe'_2O_4$ may be [9])

(1) "Normal", with 1 Me in the tetrahedral position and 2 Me′ in the octahedral position. Whenever we wish to indicate the ionic distribution in a formula, we shall in the following write the ions in octahedral sites between brackets, and here therefore $Me[Me'_2]O_4$.

(2) "Inverse", with the Me in the octahedral position, and one Me′ in the octahedral position and in the tetrahedral position each. This arrangement will be indicated by $Me'[MeMe']O_4$.

(3) "Intermediate", e.g. $Me'_{1-x}Me_x[Me_{1-x}Me'_{1+x}]O_4$.

In several cases, e.g. in spinels containing several metal ions of the first transition series, the ionic distribution cannot be determined by X-rays to any great accuracy, in view of the small difference in scattering power. This is true even when ions like Mg^{2+}, Al^{3+} etc. are present as well, because the intensities depend on x as well as on the oxygen parameter u.

*) Dr G. H. Jonker has obtained strong indications that a spinel $Li_{4/3}Ti_{5/3}O_4$ does exist, contrary to F. Bertaut and A. Durif (C.R. Acad. Sci., Paris **236**, 212-214, 1953), who report a spinel $LiTi_{7/4}\square_{1/4}O_4$ (private communication Dr Jonker).

The method most often used is that of comparing the intensities of two reflexions with small difference in Σh^2, which vary strongly and in a different sense with x and are least sensitive to differences in u. This method has been used for the determination of the cation distribution of several spinels. The factor limiting the accuracy of this method is the error in the scattering factors used [10]).

For the ferrites an indirect method has also been used. According to X-ray evidence the chromites $MeCr_2O_4$ have a "normal" distribution. The ferrites $ZnFe_2O_4$ and $CdFe_2O_4$ are normal, but $MgFe_2O_4$ and $CuFe_2O_4$ inverse *). The difference in lattice constant between the chromites and the corresponding ferrites is 0·12 Å for Zn^{2+} and Cd^{2+}, but about 0·05 Å for all other ions, amongst which Mg^{2+} and Cu^{2+}. From this data it has been concluded [9]) that the ferrites $MeFe_2O_4$ for which Me = Mn^{2+}, Fe^{2+}, Co^{2+}, Ni^{2+}, Cu^{2+} and Mg^{2+} are inverse.

The aluminates are all normal [8]) [6]), except $NiAl_2O_4$ for which the approximate distribution $Al_{0.75}Ni_{0.25}[Ni_{0.75}Al_{1.25}]O_4$ has recently been found [6]).

MgV_2O_4, ZnV_2O_4, $MgRh_2O_4$ and $ZnRh_2O_4$ are normal [11]), $MgIn_2O_4$ and probably $MgGa_2O_4$ [8]) inverse.

$Li_{0.5}Fe_{2.5}O_4$ is inverse: $Fe[Li_{0.5}Fe_{1.5}]O_4$ [12]).

Several titanates $Me_2^{II}Ti^{IV}O_4$ [9]) as well as $Zn_2Sn^{IV}O_4$ [9]) and $Mg_2V^{IV}O_4$ [11]) have been found to be inverse: it is almost certain that all such titanates and stannates are inverse. Ni_2GeO_4 and Co_2GeO_4 are, however, normal [6]).

1.2.3. Long-range Order in Oxidic Spinels

Originally it had been assumed that the distribution of different cations inside one sublattice is random [8]). In some spinels long-range order has since been found to occur in one of the sublattices. Three types have so far be found:

(1) 1 : 1 order in the octahedral position.

The ionic positions are approximately **) as follows

Me at $\frac{1}{8}\frac{5}{8}\frac{1}{8}$; $\frac{5}{8}\frac{1}{8}\frac{1}{8}$; $\frac{3}{8}\frac{7}{8}\frac{1}{8}$; $\frac{7}{8}\frac{3}{8}\frac{1}{8}$; $\frac{1}{8}\frac{1}{8}\frac{5}{8}$; $\frac{3}{8}\frac{3}{8}\frac{5}{8}$; $\frac{5}{8}\frac{5}{8}\frac{5}{8}$; $\frac{7}{8}\frac{7}{8}\frac{5}{8}$.

Me′ at $\frac{3}{8}\frac{5}{8}\frac{3}{8}$; $\frac{5}{8}\frac{3}{8}\frac{3}{8}$; $\frac{1}{8}\frac{7}{8}\frac{3}{8}$; $\frac{7}{8}\frac{1}{8}\frac{3}{8}$; $\frac{1}{8}\frac{3}{8}\frac{7}{8}$; $\frac{3}{8}\frac{1}{8}\frac{7}{8}$; $\frac{5}{8}\frac{7}{8}\frac{7}{8}$; $\frac{7}{8}\frac{5}{8}\frac{7}{8}$.

Successive (001) layers of octahedral sites are occupied alternatively by Me and Me′.

Every Me ion has 4 Me′ and 2 Me ions as octahedral neighbours and vice versa.

This structure was proposed for $Fe[Fe^{II}Fe]O_4$ below 120 °K by Verwey and Haayman [13]), who deduced it from the resistivity jump at 120 °K.

*) Magnetic investigation has shown that these latter ferrites are only approximately inverse, see section 4.

**) It is clear that the long-range order is accompanied by a change of space group, so that ionic positions slightly different from these "ideal" ones may occur. (see e.g. [12]).

The structure is essentially orthorhombic. It has recently been shown by various methods that Fe_3O_4 below 120 °K has indeed orthorhombic symmetry (see, however, [6]) for literature data).

(2) 1 : 3 order in the octahedral position.

The ionic positions are approximately *) as follows

Me at $\frac{5}{8}\,\frac{5}{8}\,\frac{5}{8}$; $\frac{1}{8}\,\frac{7}{8}\,\frac{3}{8}$; $\frac{7}{8}\,\frac{3}{8}\,\frac{1}{8}$; $\frac{3}{8}\,\frac{1}{8}\,\frac{7}{8}$.

Me′ at $\frac{1}{8}\,\frac{5}{8}\,\frac{1}{8}$; $\frac{5}{8}\,\frac{1}{8}\,\frac{1}{8}$; $\frac{3}{8}\,\frac{7}{8}\,\frac{1}{8}$; $\frac{7}{8}\,\frac{1}{8}\,\frac{3}{8}$; $\frac{3}{8}\,\frac{5}{8}\,\frac{3}{8}$; $\frac{5}{8}\,\frac{3}{8}\,\frac{3}{8}$;
$\frac{1}{8}\,\frac{1}{8}\,\frac{5}{8}$; $\frac{3}{8}\,\frac{3}{8}\,\frac{5}{8}$; $\frac{7}{8}\,\frac{7}{8}\,\frac{5}{8}$; $\frac{1}{8}\,\frac{3}{8}\,\frac{7}{8}$; $\frac{5}{8}\,\frac{7}{8}\,\frac{7}{8}$; $\frac{7}{8}\,\frac{5}{8}\,\frac{7}{8}$.

The distribution of the ions is shown in fig. 3, see asterisks. Every row of octahedral ions in the [110] directions contains an ion Me in every fourth site. Every Me ion is surrounded by six ions Me′, every Me′ ion has 2 Me and 4 Me′ ions as neighbours.

This type of order has been found by Braun [12]) to occur in $Fe[Li_{0.5}Fe_{1.5}]O_4$, of which he determined the structure.

The structure is essentially cubic (space group very probably $P4_33$ (or $P4_13$) [12]). The same superstructure lines are found in $Al[Li_{0.5}Al_{1.5}]O_4$ and in γ-Fe_2O_3 (which probably is a mixed crystal $Fe[H_{1/2}Fe_{3/2}]O_4$-$Fe[\square_{1/3}Fe_{5/3}]O_4$ [12])), and it is probable that these compounds as well as γ-Al_2O_3 have the same superstructure.

For $Fe[Li_{0.5}Fe_{1.5}]O_4$ the transition temperature to the non-ordered spinel structure, which still contains all Li^+ in the octahedral position, is situated between 1008 and 1028 °K.

(3) 1 : 1 order in the tetrahedral position.

The ionic positions are

Me at 0 0 0; 0 $\frac{1}{2}$ $\frac{1}{2}$; $\frac{1}{2}$ 0 $\frac{1}{2}$; $\frac{1}{2}$ $\frac{1}{2}$ 0.

Me′ at $\frac{1}{4}\,\frac{1}{4}\,\frac{1}{4}$; $\frac{1}{4}\,\frac{3}{4}\,\frac{3}{4}$; $\frac{3}{4}\,\frac{1}{4}\,\frac{3}{4}$; $\frac{3}{4}\,\frac{3}{4}\,\frac{1}{4}$.

Every Me ion is surrounded by four Me′ ions and vice versa. This superstructure has recently been found to occur in our preparation $Li_{0.5}Fe^{III}_{0.5}[Cr_2]O_4$ [14]), to be discussed in section 7. The distribution of the ions is shown in fig. 2, see asterisks.

For all of these three superstructures it has been shown that the long-range order gradually disappears on departing from the 1 : 1, 1 : 3, or 1 : 1 ratios respectively.

(1) Verwey and Haayman showed that when the ratio Fe^{3+}/Fe^{2+} in magnetite is increased above 2·0, i.e. the ratio Fe^{3+}/Fe^{2+} in the octahedral position above 1·0 (a few cation vacancies are thereby introduced as well), the jump in the resistivity becomes smaller and moves to lower temperatures. It disappears for a ratio Fe^{3+}/Fe^{2+} in the octahedral position equal to 1·1.

(2) The superstructure lines of $Fe[Li_{0.5}Fe_{1.5}]O_4$ become weaker as the ratio Fe/Li in the octahedral position is increased above 3·0, e.g. by mixed-

*) See second footnote on previous page.

crystal formation with $ZnFe_2O_4$. For $Zn_{0.15}Fe_{0.85}[Li_{0.42_5}Fe_{1.57_5}]O_4$ the superstructure lines have disappeared.
(3) The 1 : 1 order in the tetrahedral position, indicated by the (200) reflexion, is just perceptible in $Fe_{0.64}\,Li_{0.36}\,[Li_{0.14}\,Fe_{0.26}\,Cr_{1.60}]O_4$ [14]).

1.2.4. The Hausmannite Structure

Some compounds of the type Me_3O_4, viz. $CuFe_2O_4$ [16]), $CuCr_2O_4$ [17]), Mn_3O_4 [15]) and $ZnMn_2O_4$ [19]), have a tetragonal crystal structure, the hausmannite structure, after the mineral hausmannite, Mn_3O_4. This structure is most suitably described as a spinel structure elongated in the [001] direction; this description is different from that given in [15]). $CuFe_2O_4$ has an axial ratio = 1·06 when annealed at e.g. 300 °C: at higher temperatures the axial ratio decreases to become unity at 760 °C [16]).
Like Mn_3O_4, $CuFe_2O_4$ forms mixed crystals with cubic spinels: in the systems $Cu_{1-a}Me^{II}_aFe_2O_4$ in which Me^{II} represents Zn, Ni or Co, the axial ratio decreases with the Me^{II} content a [18]).
In the system $\left.\begin{matrix}Mn_3O_4\\ZnMn_2O_4\end{matrix}\right\rangle - \left\langle\begin{matrix}MnFe_2O_4\\ZnFe_2O_4\end{matrix}\right.$ [19]), where the same decrease of axial ratio in the hausmannite phase occurs, a miscibility gap between hausmannite and spinel phases has been found: it is not known if this is a general phenomenon.

The cause of the occurrence of this elongated spinel structure is not known (see also [6]): the X-ray diffraction pattern of $CuFe_2O_4$ does not show any superstructure lines [16]).

1.2.5. Factors Influencing the Cation Distribution and the Stability of Oxidic Spinels

To a first approximation the chemical bond in oxidic spinels may be regarded as purely ionic, so that the main part of the lattice energy is formed by the Coulomb energy and the Born repulsive energy. Other effects that contribute terms to the lattice energy are polarization, an individual preference of certain ions for fourfold or sixfold coordination as a result of their electronic configuration, and other factors, amongst which the magnetic interaction will be considered.

The energy terms are all dependent on a, u and the ionic distribution. The equilibrium cation distribution could in principle be calculated by minimizing the total energy with respect to these variables, but as quantitative relationships between the various energy terms and these three variables are not known, this is at present not possible.

In the following a quantitative discussion of the Coulomb energy is given as a function of the unit-cell edge a, the oxygen parameter u and the charge distribution amongst the lattice sites of the cations. The contri-

bution of some other terms to the lattice energy is probably of a smaller order of magnitude.

1.2.5.1. *Coulomb Energy and Repulsive Energy*

The Coulomb potential energy per "molecule",

$$V_C = -\frac{Me^2}{a},$$

is dependent on the charge distribution, on the oxygen parameter u and, of course, on the unit-cell edge a. Madelung constants (M) have been calculated by Verwey, De Boer and Van Santen [20]) as a function of u for an average ionic charge of 4, 3 or 2 in the tetrahedral position and 2, 2·5 and 3 respectivily in the octahedral position.

As we are interested in mixed crystals, often containing a broken number of charges per formula unit in both positions, the results are given here in a generalized form.

The M values for $u = 0{\cdot}375$ ($\delta = 0$) are given by the formula

$$M = 139{\cdot}8 - 10{\cdot}84\ q_a + 2{\cdot}61\ q_a^2 \quad [21]),$$

in which q_a represents the average ionic charge per formula unit in the tetrahedral position.

The curves giving the dependence of M on u for different values of q_a are very nearly straight lines [20]). We have assumed these to be straight, and further that the slope of these lines ($\Delta M/\Delta u$) varies linearly with q_a, which for $q_a = 4$, 3 and 2 is very nearly true.

The Madelung potentials expressed in units e^2/a as a function of q_a, for different values of u, are given by a set of parabolae represented in fig. 7. From this figure it is clear that a high Madelung potential is obtained:
(1) with low average charge in the tetrahedral position for large values of u;
(2) with high average charge in the tetrahedral position for small values of u.

Thus, as far as the Madelung constant is concerned, an ion that has a low charge and is large with respect to the other cations present will seek the tetrahedral position, if for other cation distributions the Madelung constant derived from fig. 7 is appreciably lower.

Perhaps this effect should account for the fact that in $CdFe_2O_4$ the large Cd^{2+} ions are found in fourfold coordination, whereas in CdO with NaCl structure they have sixfold coordination (see, however, also section 1.2.5.4). From the same point of view an ion with high charge will seek the tetrahedral position only if it is small with respect to the other cations present, and if for other cation distributions the Madelung constant derived

from fig. 7 is appreciably lower. In fact, amongst the Me^{4+} ions only Ge^{4+} is found to occupy solely the tetrahedral position.

It must be kept in mind that the unit-cell edge a is also dependent on the cation distribution, so that a distribution with high M may not give the largest Coulomb energy.

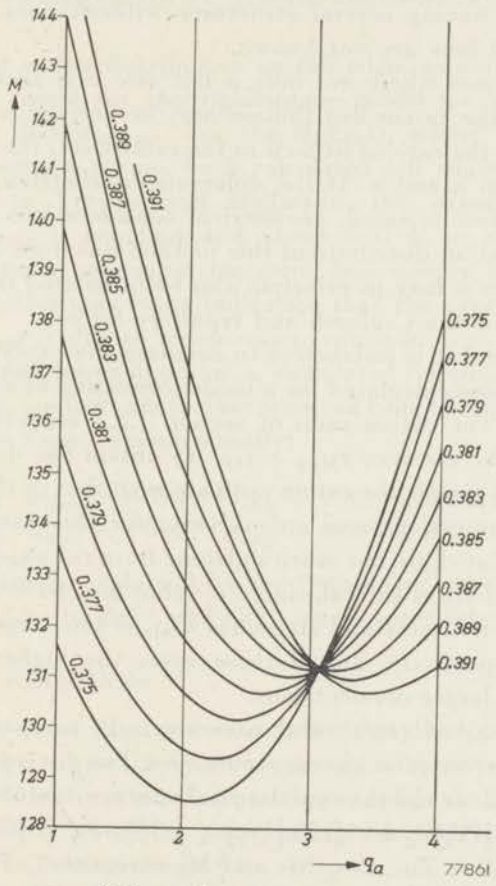

Fig. 7. Madelung constant (M) as a function of the ionic charge in the A position (q_a) for different values of the oxygen parameter (u).

The repulsive potential energy per molecule may be represented by

$$V_R = \frac{B}{a^n}.$$

For equilibrium between Coulomb and repulsive forces this expression gives a repulsive energy that is a constant fraction $1/n$ of the Coulomb energy (n is of the order of 10).

An exponential Born-Mayer expression might give a better approximation, but both expressions contain a constant (n and ϱ respectively) to be derived from compressibility data. For oxides of the transition metals no compressibility measurements are known, and the values of n and ϱ may be appreciably different from those of the alkali halides, which have so far been used [22]). Moreover the compressibilities should be measured for binary oxides having crystal structures without parameters, which for trivalent metal ions are not known.

For those few cases where not only a but also u is accurately known from experiment, the cation distribution may be derived from fig. 7 (e.g. for $GeCo_2O_4$ [6])) if the cations fit well in the interstices, the sizes of which are calculated from a and u. If the difference in Madelung constant for different distributions is small, geometrical considerations alone may be used to find the cation distribution: this method has been used for Fe_3O_4 [22a]). The parameter u may in principle also be calculated from the equilibrium condition for the Coulomb and repulsive forces.

On the other hand it is instructive to compare the experimental values of a and u with those calculated for a model consisting of a dense packing of rigid spheres. The cation radii of section 1.2.1 are used, and 4% is subtracted from the distance $r_{Me_A} + r_{O^{2-}}$ to obtain the distance Me_A-O.

For a number of spinels the cation radii are such that in this model there is contact between cations and anions only; for this case the unit-cell edges a thus calculated are not much different from the experimental ones.

For the inverse ferrites the calculated a value is 0·4-1·0% too large *); for the (inverse) titanates and stannates a_{calc} is too large by 0·9-2·8% and 0·7-1·9% respectively. In all these cases the higher discrepancies are found for the larger divalent ions.

When the cations on tetrahedral sites are large compared with those on octahedral sites, anion-anion contact occurs. The discrepancies between the calculated a values and the experimental ones are now often appreciably larger: i.e. for $Cd[Fe_2]O_4$ 4·5%, $Zn[Fe_2]O_4$ 1·3%; for $Cd[Cr_2]O_4$ 4·5%, for (normal) Mn-*), Fe-, Zn-, Co-, Ni- and Mg-chromite 3, 2·2, 1·5, 1·5, 1·1 and 1·0% respectively; for (normal) Mn-*), Fe-, Zn-, Co- and Mg-aluminate 5·8, 5·0, 5·0, 5·0, and 4·0 % respectively.

From the above figures it appears that the Goldschmidt radii of the oxygen ion (1·32 Å) and of the *larger* divalent ions are too large to account satisfactorily for the unit-cell edges of the oxidic spinels, i.e. these ions may be "squeezed" in this structure with respect to the crystal structures with sixfold coordination, from which their radii were deduced.

---

*) For $MnFe_2O_4$, $MnCr_2O_4$ and $MnAl_2O_4$ the unit-cell edges have been redetermined for preparations made by the author with correct valency states, and were found to be 8·499 Å, 8·425 Å and 8·202 Å respectively.

It is comprehensible that such a squeezing effect, whatever may be its cause, tends to increase with ionic diameter and decrease with ionic charge, and the more so for fourfold coordination. This effect is not sufficiently accounted for by deducing 4% from the radius sums $r_{Me_A} + r_{O^{2-}}$ and nothing from the sums $r_{Me_B} + r_{O^{2-}}$.

From the above it follows that the room required for the smaller ions and those with a high charge (cf. [6])) in the first instance determine the cation distribution.

An effect of cation distribution on cell edge, as noted by Verwey and Heilmann, is found for the rigid-sphere model for $MnFe_2O_4$: a_{normal} is 1·5 % larger than $a_{inverse}$. For the $MgFe_2O_4$ model, however, where no anion-anion contact occurs, both calculated cell edges are equal.

According to Verwey and Heilmann the experimental difference $a_{normal} - a_{inverse}$ is constant and about 0·07 Å, or about 0·8%. As the repulsion potential of course increases less steeply than for the rigid-sphere model, this may be an indication that the experimental difference $a_{normal} - a_{inverse}$ is due to anion-anion repulsion.

The upper and lower limits of u, calculated for the rigid-sphere model for anion-anion contact, are further removed from the ideal value $u = 0{\cdot}375$ than has been found experimentally:

for $Zn[Fe_2]O_4$ $u_{calc} = 0{\cdot}390$, $u_{exp} = 0{\cdot}385 \pm 0{\cdot}002$;
for $Ge[Co_2]O_4$ $u_{calc} = 0{\cdot}369$, $u_{exp} = 0{\cdot}375 \pm 0{\cdot}003$.

This may also be explained by the "squeezing" of the larger ions with lower charge, i.e. the Zn^{2+} and Co^{2+} ions respectively.

1.2.5.2. *Short-Range Order*

The formation of the superstructures described in section 1.2.3. is accompanied by a gain in Coulomb energy with respect to the random distribution inside the octahedral position or inside the tetrahedral position respectively. These "ordering energies" for the first two superstructures mentioned have been given in [23]).

The position of the Me and Me′ ions in the 1 : 1 order in the tetrahedral position is equal to that of Zn and S in the zincblende structure, for which the Madelung potential is known from literature.

These ordering energies, like M expressed in e^2/a (a = cube edge of the unit cell) are given in table II.

A very rough computation indicates that polarization tends to increase these energies by something of the order of one quarter [23]). These ordering energies are large compared with the energy of thermal motion at the transition temperatures, so that one may conclude that above the transition temperatures a very pronounced short-range order must persist [23]).

TABLE II

Ordering energies in units e^2/a

charge difference $(q_{Me'} - q_{Me})$	1 : 1 order in oct. position	1 : 3 order in oct. position	1 : 1 order in tetr. position
1	1·001	0·712	0·946
2	4·004	2·848	3·783

The values given in fig. 7 must therefore be corrected for a strong short-range order, the energy of which is approximately equal to the values for long-range order given above.

1.2.5.3. *Magnetic Interaction Energy*

We shall see that for ferrimagnetic spinels the magnetic (superexchange) interaction energy is strongly dependent on the distribution of the magnetic ions amongst the crystallographic positions. The question might be asked whether this energy will influence the ionic distribution. The Curie temperatures Θ, i.e. the temperatures at which the long-range order of the magnetic moments is destroyed, range up to 950 °K from which we might conclude that this energy is only of the order of $k\Theta \approx 2$ kcal/mole.

It must be borne in mind, however, that a short-range order of the moments may persist above the Curie temperature, i.e. up to temperatures at which ionic diffusion takes place.

An indication to this effect is the fact that very weak reflexions resulting from magnetic spin order in the neutron diffraction pattern of antiferromagnetic MnO [24]) (see section 2) persist up to 3Θ (Θ = Néel temperature, at which the long-range order of the moments is destroyed).

As far as energy is concerned, however, it seems likely that the magnetic interaction energy above the Curie temperature is very small, like for nickel, for which the excess specific heat becomes negligible above the Curie temperature.

1.2.5.4. *Individual Preference of Cations for 4- or 6-fold Coordination*

The influence of diameter and charge of a cation on its preference for the tetrahedral or octahedral sites in an oxidic spinel is not properly called an individual property, as the diameters and charges of the other ions present must be taken into account.

Apart from the influence of diameter and charge on the Coulomb energy and on other energy terms, individual differences between the cations exist as regards their tendency towards four- or sixfold coordination. This is shown by the fact that cations with equal diameter and charge, such as Zn^{2+} and Co^{2+}, or Ni^{2+} and Mg^{2+}, show quite different behaviour as regards ionic distribution in spinels with otherwise equal compositions.

One cause for such individual behaviour is the difference in electronic configuration between different cations: we shall differentiate between five groups with different electron configurations. Of course the resulting ionic distribution cannot be discussed without taking into account diameter and charge of the ions.

(1) The ions Zn^{2+} and Cd^{2+} with a filled 3d shell are known for their tendency to form covalent bonds with sp^3 orbitals. They therefore preferably occupy the tetrahedral sites in spinels. Zn^{2+} in ZnO has fourfold coordination, but Cd^{2+} in CdO, with NaCl structure, sixfold coordination. In the latter case the effect of size, in accordance with Pauling's rule, counteracts the individual preference for fourfold coordination.

The ions with filled d shells:
3d: Cu^{+}, Zn^{2+}, Ga^{3+}, Ge^{4+},
4d: Ag^{+}, Cd^{2+}, In^{3+}, Sn^{4+},
probably all have an individual preference for fourfold coordination in oxides, but this may be counteracted in spinels by the dependence of the lattice energy on q_a, u and a. We have seen that a large tetravalent ion in the tetrahedral position will give a low Madelung constant; as a consequence the stannates $Me_2^{II}SnO_4$ are inverse. Ag_2MoO_4 is probably normal because the inverse arrangement would have very large a.

(2) The ions with noble-gas shells have no individual preference for either coordination. Their distribution will be determined mainly by the dependence of the lattice energy on q_a, a and u. Thus amongst the ions of this kind that occur in spinels:
Li^{+}, Mg^{2+}, Al^{3+}, Ti^{4+}, the tetravalent ion is too large to occupy solely the tetrahedral sites.

(3) The ions with half-filled 3d shell have spherical symmetry. Therefore Mn^{2+}, Fe^{3+} and Co^{4+} will not be expected to have an individual preference for either position (Co^{4+}, if it occurs at all in spinels, which nowadays seems unlikely, might choose the tetrahedral position for electrostatic reasons as discussed above).

The preference of the other transition metal ions is determined by the influence of the crystalline electric field orginating from the neighbouring ions on the average energy level and on the spatial distribution of the 3d electrons, see [6]).

As a result these ions fall into two groups.

(4) Those with $3d^3$ and $3d^8$, which have a strong preference for sixfold coordination: Cr^{3+}, Ni^{2+} and possibly Mn^{4+}.
(5) All other transition metal ions, which have no strong preference for either site.

The above scheme is an extension of the rules on the cation distribution in spinels given by Verwey and Heilmann [9]).

1.2.6. Spinels Containing Three or More Different Cations

Verwey and Heilmann [9]) found by X-ray diffraction that in mixed crystals between normal $Zn[Fe_2]O_4$ and inverse $Fe[CuFe]O_4$ the Zn^{2+} ions still occupied the tetrahedral position and the Cu^{2+} ions the octahedral position, giving a formula e.g. $Zn_{0.5}Fe_{0.5}[Cu_{0.5}\ Fe_{1.5}]O_4$.

As practically no other data were available in 1947 on the ionic distribution in ternary spinels, it was believed that the ions keep their preference for one crystallographic site with respect to other ions in all compounds. This means that a certain order of preference for e.g. the tetrahedral sites can be given, in which the authors placed Fe^{3+} directly after Zn^{2+}, Cd^{2+}, Ga^{3+} and In^{3+} and before the other divalent ions. Recently Romeijn [6]) has shown that in several ternary spinels the behaviour is quite different. Our magnetic measurements to be reported in sections 6-9 will yield further examples of cases where such simple behaviour is not found.

The total energy difference between the normal and inverse arrangements may be found experimentally for those spinels for which the distribution changes measurably with temperature.

For a spinel of the composition e.g. $Me'_{1-x}Me_x[Me_{1-x}Me'_{1+x}]O_4$ the equilibrium distribution is determined by a Boltzmann expression given by Néel [25]):

$$kT \ln \frac{(1-x)^2}{x(x+1)} = E, \qquad (1.1)$$

in which E is the energy involved in the interchange of a Me ion in the octahedral position and a Me′ ion in the tetrahedral position. We have seen that an accurate determination of x from X-ray diffraction data is usually impossible, but Pauthenet and Bochirol [26]) have determined x, and thus E, from magnetic saturation data for $MgFe_2O_4$ and $CuFe_2O_4$ (see section 4): E was found to be fairly constant.

Knowledge of the interchange constants E of two binary spinels containing one cation in common would enable one to calculate the cation distribution in a mixed crystal between them, it if were permissible to use one constant E for a specific pair of cations. This is certainly not the case, as E varies with the charge distribution (q_a), with the cell edge a and with the lattice parameter u: these quantities, as well as the short-range order contribution will be different for different compositions.

REFERENCES

[1]) W. H. Bragg, Nature **95**, 561, 1915; Phil. Mag. **30**, 305-315, 1915.
[2]) S. Nishikawa, Proc. Tokyo math.-phys. Soc. **8**, 199-209, 1915.
[3]) International Tables for X-ray Crystallography, Kynoch Press, Birmingham, 1952, Vol. I, p.340.
[4]) P. P. Ewald and C. Hermann, Strukturberichte, Bd 1913-1926, p. 350 (type *H* 11).
[5]) J. Robin and J. Bénard, C. R. Acad. Sci., Paris **234**, 734-735, 1952.
[6]) F. C. Romeijn, Philips Res. Rep. **8**, 304-342, 1953.
[7]) G. H. Jonker, to be published.
[8]) T. F. W. Barth and E. Posnjak, Z. Kristallogr. **82**, 325-341, 1932.
[9]) E. J. W. Verwey and E. L. Heilmann, J. chem. Phys., **15**, 174-180, 1947.
[10]) F. Bertaut, J. Phys. Radium **12**, 252-255, 1951.
[11]) W. Rüdorff and B. Reuter, Z. anorg. Chem. **253**, 194-208, 1947.
[12]) P. B. Braun, Nature **170**, 1123, 1952.
[13]) E. J. W. Verwey and P. W. Haayman, Physica **8**, 979-987, 1941; E. J. W. Verwey, Nature, **144**, 327, 1939.
[14]) P. B. Braun, Physica, forthcoming.
[15]) G. Aminoff, Z. Kristallogr. **64**, 475-490, 1926.
[16]) L. Weil, F. Bertaut and L. Bochirol. J. Phys. Radium **11**, 208-212, 1950.
[17]) T. R. McGuire, L. N. Howard and J. S. Smart, Ceramic Age **60** (1) 22-24, 1952.
[18]) Results not yet published by the author.
[19]) B. Mason, Amer. Min. **32**, 426-441, 1947.
[20]) E. J. W. Verwey, F. de Boer and J. H. van Santen, J. chem. Phys. **16**, 1091-1092, 1948.
[21]) J. H. van Santen, private communication.
[22]) E. J. W. Verwey, P. W. Haayman and F. C. Romeijn, J. chem. Phys. **15**, 181-187, 1947.
[22a]) E. J. W. Verwey and J. H. de Boer, Rec. Trav. chim. Pays-Bas **55**, 531-540, 1936.
[23]) F. de Boer, J. H. van Santen and E. J. W. Verwey, J. chem. Phys. **18**, 1032-1034, 1950.
[24]) C. G. Shull and J. S. Smart, Phys. Rev. **76**, 1256-1257, 1949.
[25]) L. Néel, C. R. Acad. Sci., Paris **230**, 190-192, 1950.
[26]) R. Pauthenet and L. Bochirol, J. Phys. Radium **12**, 249-251, 1951.

2. THEORY OF FERRIMAGNETISM

2.1. Introduction

In contradistinction to paramagnetics, ferromagnetic substances can be magnetized to saturation by a comparatively small magnetic field (usually 10^2-10^4 oersteds). This is because the magnetic moments of the atoms with partly filled 3d or 4f shells are parallel to their neighbours already in the unmagnetized state, as a result of an electron exchange interaction, which is very much stronger than the interaction forces between magnetic dipoles. The nature of this exchange mechanism does not concern us here. In the unmagnetized (virgin) state the overall magnetization is zero because in each crystal the parallelism of the atomic moments is maintained only within Weiss domains: the direction of magnetization of each Weiss domain is determined by the crystalline, stress and shape anisotropies. The saturating field only has to turn the moments of all Weiss domains against these anisotropies.

Complete parallelism of the atomic moments within the Weiss domains exists only at 0 °K: the saturation magnetization decreases with temperature. At the Curie temperature the long-range order of the atomic moments is destroyed and at higher temperatures only paramagnetism remains. The saturation magnetization at 0 °K per magnetic atom or per "molecule", which we shall call the *saturation moment*, can be expressed in the spin moment of one electron, the so-called Bohr magneton μ_B ($= eh/4\pi mc$, where e, h, m and c have their usual meanings).

In the ferromagnetic metals with partly filled 3d shell the number of unpaired 3d electrons is not simply related to the total number of electrons present, so that the saturation moments cannot be simply predicted.

On the other hand, for compounds that may be considered to be essentially ionic (like the oxides with which we shall concern ourselves) the situation would be expected to be much simpler. Here each magnetic ion contains a known number of unpaired electrons that do not take part in the formation of chemical bonds. For substances containing elements of the first transition series, the ferromagnetic and the paramagnetic behaviours are both almost entirely due to the spins of the unpaired 3d electrons. The ferromagnetic moment of each ion will thus be equal to $2S$ (S = total spin quantum number of the ion), if the orbital contribution is neglected, or gS, if this is taken into account. The g-factor g is $(2mc/e) \times$ (magnetic moment)/(angular momentum).

Table III gives the number of 3d electrons and the number of unpaired 3d electrons ($= 2S$) for these ions. Those ions occurring in the compounds to be discussed have been framed and printed in heavy type.

TABLE III

ions										number of	
										3d electrons	unpaired 3d electrons (2S)
Sc^{3+}	**Ti^{4+}**	V^{5+}	Cr^{6+}	Mn^{7+}						0	0
	Ti^{3+}	V^{4+}	Cr^{5+}	Mn^{6+}						1	1
	Ti^{2+}	V^{3+}	Cr^{4+}	Mn^{5+}	Fe^{6+}					2	2
		V^{2+}	**Cr^{3+}**	Mn^{4+}						3	3
		V^{+}	Cr^{2+}	Mn^{3+}	Fe^{4+}					4	4
				Mn^{2+}	**Fe^{3+}**	Co^{4+}				5	5
					Fe^{2+}	Co^{3+}	Ni^{4+}			6	4
						Co^{2+}	Ni^{3+}			7	3
							Ni^{2+}			8	2
								Cu^{2+}		9	1
								Cu^{+}	**Zn^{2+}**	10	0

In paramagnetic substances containing magnetic ions with partly filled 3d shells, in which the magnetic ions are widely separated from each other, so that no exchange interaction is possible, a magnetic field tends to orient the ionic moments against the thermal motion.

Thus the magnetization per gram ion, I, is

$$I = NgS\mu_B B_S\left(\frac{gS\mu_B H}{kT}\right) \quad \begin{matrix}(N = \text{Avogadro's number},\\ k = \text{Boltzmann's constant}),\end{matrix}$$

in which the Brillouin function B_S is given by

$$B_S\left(\frac{gS\mu_B H}{kT}\right) = \frac{S+\frac{1}{2}}{S}\coth\frac{(S+\frac{1}{2})g\mu_B H}{kT} - \frac{\frac{1}{2}}{S}\coth\frac{\frac{1}{2}g\mu_B H}{kT}.$$

For small values of $gS\mu_B H/kT$ one may write

$$B_S\left(\frac{gS\mu_B H}{kT}\right) = \frac{S+1}{3}\frac{g\mu_B H}{kT},$$

and thus $$I = \frac{Ng^2\mu_B^2 S\,(S+1)H}{3kT} \equiv \frac{CH}{T}.$$

Certain dilute paramagnetic substances e.g. those containing Fe^{3+} ions (e.g. $Fe^{III}NH_4(SO_4)_2 . 12\,H_2O$) indeed follow a Curie law $I/H = \chi = C/T$ (χ and C per gramion) in a wide range of temperatures, and the Curie constant C agrees closely with the theoretical value, thus proving that each magnetic ion contributes with its theoretical moment $gS\,\mu_B$. Other dilute paramagnetic substances in a limited temperature range follow a Curie-Weiss law $\chi = C/(T-\vartheta)$ with small positive or negative values of ϑ, caused by the coupling of the orbital moment with the crystalline electric field.

The exact calculation of the variation of the saturation magnetization with temperature in a crystal is not yet possible, and any such calculation, even with simplifying assumptions, is extremely difficult [27]). Therefore a simple approximation, due to Pierre Weiss [28]), is often used, in which each ion is considered to be situated in a fictitious magnetic field, the so-called molecular field, representing the resultant influence of the exchange forces with all surrounding atoms. The total alignment of the moments that exists at 0 °K, tends to be destroyed at higher temperatures, and the saturation magnetization decreases with temperature according to a Brillouin function in which a field $H + h$ acting on each moment figures: the external field H needed to reach saturation, i.e. to align the Weiss domains, at low temperatures usually can be neglected against the very large molecular field h.

At the Curie temperature the long-range order of the moments is destroyed, but the fact that ferromagnetics above the Curie temperature follow a Curie-Weiss law $\chi = C(T-\vartheta)$, with $\vartheta > 0$ *), shows that here exchange interactions, and thus molecular fields, continue to play a rôle. Here h is not large compared to the external fields generally used, and $H + h$ enters into the Brillouin functions.

The exchange interactions may in other cases result in another state of minimum free energy, i.e. in antiparallel orientation of the spins of neighbouring atoms or ions, found in antiferromagnetics such as MnO, α-Fe_2O_3, CrSb. These may be considered to consist of two equal sublattices with equal, mutually antiparallel, spontaneous magnetizations, each decreasing with temperature according to the same Brillouin function in which only the molecular field h appears. The long-range order of the moments is destroyed at the so-called Néel temperature and above this temperature a Curie-Weiss law $\chi = C/(T-\vartheta)$ is usually obeyed with $\vartheta < 0$ *).

2.2. Outline of the Theory of Ferrimagnetism

2.2.1. Néel's Theory

For a ferromagnetic, essentially ionic compound, the moment per formula unit should be expected to be the sum of the ionic moments; thus

*) We have seen that small values of ϑ may occur even without exchange interaction.

for magnetite $Fe^{II}Fe_2^{III}O_4$ assuming g to be 2 for both ions : $4 + 2 \times 5 = 14\ \mu_B$. Weiss and Forrer [29]) in 1929 had found 4·08 μ_B. From earlier work [30]) it was known that the (normal) ferrites $Zn[Fe_2]O_4$ and $Cd[Fe_2]O_4$ are paramagnetic and the (inverse) ferrites of Mn, Co, Ni, Cu and Mg ferromagnetic like $Fe[Fe^{II}Fe]O_4$.

Also it was known that above the Curie temperature several ferrites showed a curvature of the $1/\chi$ vs T curve concave towards the T axis.

Using these data, Néel, who had already contributed a great deal to the theory of antiferromagnetism, in 1948 made the basic hypothesis [31]) that a strong negative interaction, i.e. a tendency to antiparallel orientation, exists between ionic moments on tetrahedral sites on the one hand and octahedral sites on the other hand. Thus the moment of $Fe^{III}[Fe^{II}Fe^{III}]O_4$ should be $(5+4)-5=4$, in close agreement with experiment. This behaviour may be termed non-compensated antiferromagnetism. We shall use the word *ferrimagnetism*, coined by Néel.

At the same time [31]) Néel extended the Weiss molecular-field theory to a lattice with two different lattice sites on which different amounts of magnetic ions (atoms) are found. The theory was given for one kind of magnetic ion (e.g. Fe^{3+}) only.

We shall give the bare essentials of the theory, applying it to spinels only, and thus introducing from the start the fundamental assumption of negative tetrahedral-octahedral interaction.

Like Néel we shall use an index a for the tetrahedral position and b for the octahedral position. Using a slightly different notation from Néel's, we take a spinel

$$Fe^{III}_{x_a}Me_{1-x_a}[Fe^{III}_{x_b}Me_{2-x_b}]O_4, \tag{2.1}$$

in which Me represents non-magnetic ions and x_a and x_b the number of ferric ions on A and B sites respectively.

2.2.1.1. *Paramagnetic Behaviour*

Taking the *paramagnetic* behaviour above the Curie temperature, the total magnetization per mole $\vec{I}$ equals

$$\vec{I} = x_a\vec{I}_a + x_b\vec{I}_b, \tag{2.2}$$

in which $\vec{I}_a$ is the magnetization per gramion on A, and $\vec{I}_b$ idem on B. The molecular field for an ion on A, h_a, originates from the resultant magnetization of its neighbours on B, and also from those on A, and is assumed to be proportional to $\vec{I}_b$ and $\vec{I}_a$ respectively. Thus

$$\vec{h}_a = n(-x_b\vec{I}_b + ax_a\vec{I}_a), \tag{2.3}$$

in which n is a positive constant related to the sum of the exchange integrals AB, and $-\alpha$ is the ratio of the interactions AA and AB. Likewise

$$\vec{h_b} = n\,(-x_a\vec{I_a} + \beta x_b\vec{I_b}), \tag{2.4}$$

in which $-\beta$ is the ratio of the interactions BB and AB. The coefficients $n\alpha$, $-n$ and $n\beta$ are linearly related to the sums of the possible exchange integrals AA, AB and BB respectively. The partial magnetizations of the sublattices $\vec{I_a}$ and $\vec{I_b}$ can be written:

$$\vec{I_a} = \frac{C}{T}\,(\vec{H} + \vec{h_a}), \tag{2.5}$$

$$\vec{I_b} = \frac{C}{T}\,(\vec{H} + \vec{h_b}). \tag{2.6}$$

Eliminating $\vec{I_a}$, $\vec{I_b}$, $\vec{h_a}$ and $\vec{h_b}$ from (3.3-6) one obtains

$$\frac{H}{I_{\text{mole}}} = \frac{T}{C_{\text{mole}}} + \frac{n(2x_ax_b - \alpha x_a{}^2 - \beta x_b{}^2)}{(x_a + x_b)^2} - \frac{n^2C_{\text{mole}}x_ax_b[x_a(1+\alpha) - x_b(1+\beta)]^2/(x_a+x_b)^4}{T - nC_{\text{mole}}x_ax_b(2+\alpha+\beta)/(x_a+x_b)^2} \tag{2.7}$$

or

$$\frac{1}{\chi_{\text{mole}}} = \frac{T}{C_{\text{mole}}} + \frac{1}{\chi_0} - \frac{s}{T-\vartheta}, \tag{2.8}$$

in which the values of $1/\chi_0$, s and ϑ are read from the formula (2.7). It is seen that this expression represents a hyperbolic relation between $1/\chi_{\text{mole}}$ and T, as is found experimentally.

It has since been found that the slope of the experimental asymptote of the hyperbola is not equal to $1/C_{\text{mole}}$, and Néel has assumed that n (but for simplicity's sake not α and β) is linearly dependent on temperature:

$$n = n_0(1 + \gamma T),$$

giving

$$\frac{1}{C_{\text{mole}}} = \frac{1}{C'_{\text{mole}}} + \frac{\gamma}{\chi_0},$$

in which C'_{mole} is the theoretical Curie constant.

From the shape of the experimental curve χ_0, s and ϑ can be deduced.

$x_a + x_b$ is known (2 for $MgFe_2O_4$, 2·5 for $Li_{0\cdot5}Fe_{2\cdot5}O_4$ etc.) and from χ_0, s, ϑ and from the ferromagnetic behaviour x_a, x_b, α, β and n can be found for those cases where only Fe^{3+} is present, when the molecular-field

theory may be used (i.e. in the absence of a pronounced order of the ions in either position and for not too small x_a or x_b). We wish to stress again [32]) that if x_a/x_b changes with temperature, as has been found to be the case e.g. for $MgFe_2O_4$, the paramagnetic measurements do not correspond to one and the same chemical formula, so that calculations like this have no more than qualitative value.

All the same, Néel has been able to show in this way qualitatively for several ferrites that $|\alpha|$ and $|\beta| \ll 1$, which means that the AA and BB interactions are small with respect to the AB interaction. He also found that α and β and thus the AA and BB interactions, are negative.

2.2.1.2. *Ferromagnetic Behaviour*

We shall in the following concern ourselves only with the *ferromagnetic* behaviour. In the ferromagnetic case the molecular fields are

$$\vec{h_a} = n(-x_b\vec{I_{bs}} + \alpha x_a\vec{I_{as}}) \tag{2.9}$$

and

$$\vec{h_b} = n(-x_a\vec{I_{as}} + \beta x_b\vec{I_{bs}}), \tag{2.10}$$

in which $\vec{I_{as}}$ and $\vec{I_{bs}}$ are the spontaneous magnetizations per gram-ion of the A and B sublattices respectively.

$$I_{as} = NgS\mu_B B_S\left(\frac{gS\mu_B h_a}{kT}\right), \tag{2.11}$$

$$I_{bs} = NgS\mu_B B_S\left(\frac{gS\mu_B h_b}{kT}\right), \tag{2.12}$$

The resultant spontaneous magnetization per mole I_s is given by

$$I_s = x_b I_{bs} - x_a I_{as}. \tag{2.13}$$

We shall now consider the different behaviours of I_s when x_a/x_b is varied.

From equation (2.13) it is seen that the spontaneous magnetization at 0 °K (where $I_{as} = I_{bs}$) changes sign for $x_a/x_b = 1$. It can easily be seen from (2.11-12) that I_{as} and I_{bs} remain equal to each other for all temperatures only if h_a and h_b also remain equal, and this happens only if $\alpha = \beta$. Thus for $\alpha \neq \beta$, $I_{as} \neq I_{bs}$ for all temperatures except $T = 0$ °K, and the I_s vs T curve is as depicted in fig. 8 (*d*) (Néel's type (*L*)).

Near the absolute zero and Curie temperatures simplified expressions may be used for the Brillouin functions. Thus Néel calculates that near the Curie temperature, i.e. for small I_{as} and I_{bs}, the slope of the I_s vs T curve,

dI_s/dT, changes sign for $x_a/x_b = (1+\beta)/(1+\alpha)$. I_s at 0 °K is then not equal to zero, so that I_s near the Curie temperature changes sign with respect to that at 0 °K. The I_s vs T curve is then as depicted in fig. 8 (f).

For x_a/x_b between 1 and $(1+\beta)/(1+\alpha)$ the I_s vs T curve becomes as given in fig. 8 (e).

The condition for which dI_s/dT changes sign near 0 °K was found to be $x_a/x_b = (1-\beta)/(1-\alpha)$. Néel notes that for this condition the shape of the I_s vs T curve is equal to that of a normal ferromagnetic, see fig. 8 (b).

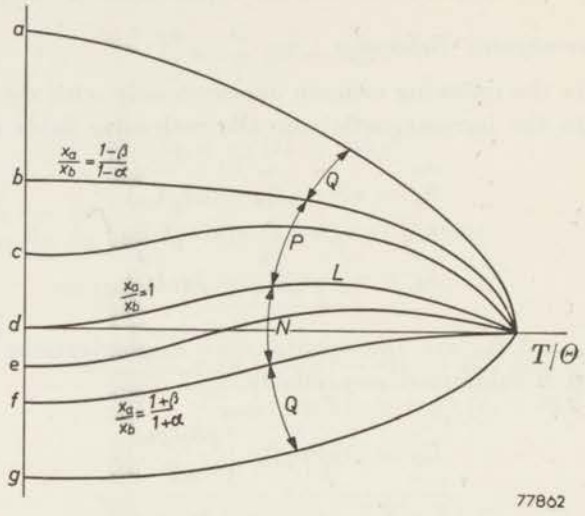

Fig. 8. Spontaneous-magnetization vs temperature curves for different relationships between the number of ferric ions in A and B sites (x_a and x_b respectively) and α and β. The capitals L, N, P and Q refer to Néel's nomenclature for these types of curves.

Thus for x_a/x_b between 1 and $(1-\beta)/(1-\alpha)$ the I_s vs T curve has the shape given in fig. 8 (c).

For x_a/x_b further from 1 than $(1+\beta)/(1+\alpha)$ and $(1-\beta)/(1-\alpha)$ a I_s vs T curve is obtained with a more gradual variation in dI_s/dT with temperature than for a normal ferromagnetic, see fig. 8 (a and g).

Fig. 8 shows that a continuous variation of x_a/x_b will necessarily result in a continuous variation of shape of the spontaneous magnetization vs temperature curve from type a to type g as shown, except for the unlikely case that $\alpha = \beta$.

When x_a/x_b increases, thereby passing unity, the curves will change in the order g-a for negative α and β and for $|\beta| > |\alpha|$, whereas for $|\alpha| > |\beta|$ they would then change in the order a-g.

2.2.2. Non-parallel Ionic Moments Inside Each Sublattice

Néel [31]) showed that the state of minimum energy due to the molecular field at 0 °K is not necessarily that in which all ionic moments inside each sublattice are parallel. Two more possibilities exist, in which on either sublattice A or B the ionic moments are not parallel, as a result of the negative interaction between the ionic moments inside the sublattice. Néel supposed the distribution of the non-aligned magnetic moments to be random. Yafet and Kittel [33]) showed that a lower energy is obtained if the ionic moments with non-parallel orientation form an ordered arrangement inside the A or B sublattices either in the two face-centred sublattices A' and A'' or in the four face-centred sublattices in the B position. In the latter case a simple, although formal, description is obtained when only two sublattices B' and B'' are considered. The ionic moments inside each of the sublattices A', A'', B' and B'' are mutually parallel but the ionic moments in the A' and A'', or in the B' and B'' sublattices form angles with each other as a result of the negative AA or BB interactions competing with the AB interactions.

In Yafet and Kittel's modification of Néel's theory Néel's σ-T curves of the types (V), (R), and (M) ([31]) p. 154), which have non-zero slope at 0 °K, cannot occur since the sublattices A', A'', $B'$and B'' are saturated at 0 °K *).

Whenever curves are found that down to low temperatures resemble curves (V), (R) and (M) they should be regarded as types (N), (Q) and (P) respectively. Thus e.g. even a $\sigma-T$ curve that is convex towards the T-axis is considered as a curve of type (Q).

The possible arrangements of the sublattice magnetizations are shown in figs 9*a* and 9*c* respectively. The resultant magnetizations are

for 9*a* $$I_s = x_b I_{bs} - x_a I_{as} \sin\varphi \quad , \qquad (2.14)$$

for 9*c* $$I_s = x_b I_{bs} \sin\psi - x_a I_{as} \quad , \qquad (2.15)$$

in which $180° - 2\varphi$ and $180° - 2\psi$ are the angles between the directions of the magnetic moments in the A' and A'' sublattices and in the B' and B'' sublattices respectively.

For the case of fig. 9*a* the molecular fields in the A' sublattice due to the B sublattice and to the A'' sublattice have a resultant equal in magnitude to the latter:

$$n(x_b \overrightarrow{I_{bs}} + \alpha_2 x_a \overrightarrow{I_{a''s}}) = n\,\alpha_2 x_a \overrightarrow{I_{a's}} \quad ,$$

in which $-\alpha_2$ is the ratio of the interactions $A'A''/AB$. Since the angle between $\overrightarrow{h_{a'}}$ and $\overrightarrow{h_{a''}}$ is $180° - 2\varphi$, this gives $\sin\varphi = -x_b I_{bs}/\alpha_2 x_a I_{as}$,

*) There is no conflict here with the third law of thermodynamics.

and substitution in (2.14) gives

$$\text{for } 9a \qquad I_s = x_b I_{bs}\left(1 + \frac{1}{a_2}\right) \quad . \qquad (2.16)$$

Similarly one finds

$$\text{for } 9c \qquad I_s = -x_a I_{as}\left(1 + \frac{1}{\gamma_2}\right) \quad , \qquad (2.17)$$

in which $-\gamma_2$ is the ratio of the interactions $B'B''/AB$.

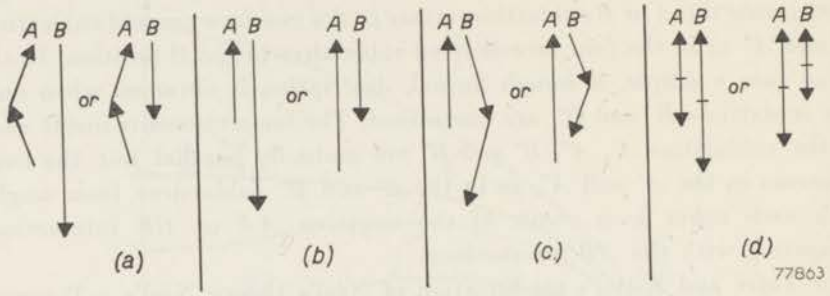

Fig. 9. Four different theoretically possible orientations of the ionic moments in A and B sublattices for different ratios between AA, AB and BB interactions. For each case a-c the figures are drawn for positive and negative I_s, and for d for $I_{a's} <$ or $> I_{b's}$.
(a) Interaction AA comparable to AB, and BB small with respect to AB.
(b) Interactions AA and BB both small with respect to AB.
(c) Interaction AA small with respect to AB, and BB comparable to AB.
(d) Interactions AA and BB large with respect to AB.

A fourth theoretically possible arrangement, viz. for predominant $A'A''$ and $B'B''$ interactions, is shown in fig. 9d. This case will not occur in practice when only one type of magnetic ion is present, because the geometry of the spinel lattice favours the AB interaction.

A series of mixed crystals between two materials that *at all temperatures* have the arrangements shown in figs 9a and 9c respectively, will not give a series of magnetization vs temperature curves as depicted in fig. 8 a-g, Such anomalous curves occur only because they are the difference of two sublattice-magnetization vs temperature curves, each of which, however. is a Brillouin curve. In the present case, where I_s is determined by I_{as} *or* I_{bs} only, the theory predicts normal Brillouin curves for all materials, also for $a_2 \neq \gamma_2$.

Yafet and Kittel have shown, however, that transitions between the arrangements 9a-d may occur for one and the same material, when the temperature is varied. The occurrence of angles between the ionic moments inside one sublattice at 0 °K does not mean, therefore, that the σ-T curves cannot become anomalous at higher temperatures.

It follows from equations (2.16) and 2.17) that for small negative values of α_2 and γ_2 ($|\alpha_2|$ or $|\gamma_2|<1$) the direction of the resultant magnetization is opposite to that of the sublattice magnetization determining its magnitude, i.e. as shown in fig. 9*a* (right) and in fig. 9*c* (left). Only for large negative values of α_2 or γ_2 ($|\alpha_2|$ or $\gamma_2|>1$) are these directions the same, i.e. as shown in fig. 9*a* (left) and in fig. 9*c* (right).

Large negative values of α_2 or γ_2 will not occur in a spinel containing only one type of magnetic ion, in view of the geometry of the spinel lattice, so that in this case the last-named two arrangements will not occur. The spinels containing two types of magnetic ions, Me_1 and Me_2, the interactions Me_1-Me_1, Me_1-Me_2 and Me_2-Me_2 may be widely different, and this may greatly increase α_2 or γ_2 when the simple theory is applied for this case (see however section 2.2.3.). It is quite possible that in this case, especially for γ_2, values $|\gamma_2|>1$ will occur.

We shall in the following sections use the symbols m_a and m_b for the sums of the ionic moments in the A or in the B position respectively, at 0 °K, irrespective of their orientation, expressed in Bohr magnetons per formula unit. We take both quantities positive.

The saturation moment $n_B = |m|$, where generally $m = m_b \sin \psi - m_a \sin \varphi$. Either $\sin \psi$ or $\sin \varphi$, or both, are equal to unity; m may be either positive or negative. The expressions (2.14) - (2.17) then become

$$m = m_b - m_a \sin \varphi = + m_b (1 + 1/\alpha_2) \quad , \qquad (2.18)$$

$$m = m_b \sin \psi - m_a = - m_a (1 + 1/\gamma_2) \quad . \qquad (2.19)$$

2.2.3. Spinels Containing Two or More Magnetic Ions

Many of the materials we have investigated (amongst which several ferrites that have industrial importance) contain in addition to Fe^{3+} ions one or more other magnetic ions. For this reason one should like to extend Néel's theory for this case. For the case of two magnetic ions Me_1 and Me_2 being located on both lattice sites there are 10 different interactions since the AA, AB and BB interactions depend on the type of interacting ions. It is clearly impossible to get any results with this large number of parameters, so that simplifying assumptions have to be made. Néels' assumption that the Me_1-$Me_1(n)$, Me_1-$Me_2(n')$ and Me_2-$Me_2(n'')$ interaction constants are equal is certainly very crude. Niessen [34a-e]) has attempted a refinement of Néel's treatment by introducing three different interaction constants n, n' and n'', but still had to make a number of simplifying assumptions, such as: α and β are constant for these three interactions, $nn'' = n'^2$, $g_1 = g_2$ etc. Assumptions as regards ionic distribution may also be used, but only with care. Expressions may be derived for which the saturation magnetization vs temperature curves shown in fig. 8*a-g* occur.

2.3. The Nature of the Exchange Interactions

2.3.1. Indirect Exchange Interaction

The Heisenberg exchange integral depends on the extent to which the 3d-electron wave functions of adjacent metal atoms overlap. Slater and

Néel have given curves showing the dependence of the magnitude of the exchange integral on D/d and $D-d$ respectively, in which D = the atomic separation and d = the diameter of the 3d orbit. For small values of D/d ($<$appr. 1·5) the exchange interaction is negative, above 1·5 it becomes positive, passes through a maximum at D/d = appr. 1·8 to become small but still positive at values of D/d = appr. 3. In ferromagnetic spinels for which $a \geqslant 8{\cdot}30$ Å the distances of adjacent ferric ions are $A\text{-}A \geqslant 3{\cdot}61$ Å, $A\text{-}B \geqslant 3{\cdot}44$ Å, $B\text{-}B \geqslant 2{\cdot}94$ Å whereas d is of the order of the ionic diameter, i.e. 1·34 Å, giving D/d = appr. 2·7, 2·6 and 2·2 respectively, i.e. values in the region of weak to strong *positive* interaction.

It is to be noted that in spinels the strongest, negative interaction is the AB interaction for which (considering only those configurations with the shortest Me-O distances) fig. 6, triangle *pqc*, shows that the oxygen ion obstructs the direct view between the metallic ions more than is the case for the AA and BB interactions (fig. 6, triangles *qrd* and *ppb* respectively). Néel has suggested that here an indirect exchange mechanism occurs, in which the anions play the rôle of an intermediary, as was first outlined by Kramers. This mechanism is usually called *superexchange*.

It has been proved by neutron diffraction [35]) that in antiferromagnetic MnO with NaCl structure the strongest negative interaction is between Mn^{2+} ions at a distance a, for which the angle Mn^{2+} - O^{2-} - Mn^{2+} is 180°, though there is a shorter distance Mn^{2+}-Mn^{2+} of $\frac{1}{2}a\sqrt{2}$, for which the angle Mn^{2+}-O^{2-}-Mn^{2+} is, however, 90° *).

Here a direct overlap of the 3d wave functions is clearly impossible, showing that the intervening oxygen ion must play a rôle in the exchange mechanism.

2.3.2. Dependence of Superexchange on the Angle Me-O-Me

The collinearity of the Mn^{2+} - O^{2-} - Mn^{2+} configuration must be favourable to superexchange, as it must make up for the increased Mn^{2+}-Mn^{2+} distance with respect to the right-angle configuration

$$\begin{array}{c} Mn^{2+} \\ | \\ Mn^{2+}— O^{2-} \end{array}$$

Anderson [36]) has shown theoretically that this is indeed the case, i.e.

*) Neutrons are scattered by the magnetic moments of the unpaired electrons as well as by the atomic nuclei, and the former magnetic contribution to the scattering power has opposite phase for ions with magnetic moments pointing in opposite directions. Thus the total scattering power has a different value for e.g. $Mn^{2+}\uparrow$ and $Mn^{2+}\downarrow$. The neutron diffraction pattern of MnO below the Néel temperature showed superstructure lines yielding a cell edge twice as large as that found by X-ray diffraction.

that the exchange interaction has a maximum value for an angle Me-O-Me of 180° and a minimum for an angle of 90°.

Qualitatively this may be understood as follows [37]). The ground state of a pair of ions Mn^{2+}-O^{2-} is

$$\begin{array}{lll} & Mn^{2+}(3d^5) & O^{2-}(2p^6) \\ & \downarrow & \uparrow\downarrow \quad 2p^2 \\ 3d^5 & \downarrow & (\uparrow\downarrow) \quad (2p^2) \\ & \downarrow & (\uparrow\downarrow) \quad (2p^2) \\ & \downarrow & \\ & \downarrow & \end{array} .$$

The six 2p electrons of the O^{2-} ions form three pairs, located in three different p orbits with dumb-bell shape: ∞

An excited state exists, in which one of a pair of 2p electrons having the axis of the dumb-bell in the direction of a Mn^{2+} ion goes over to this Mn^{2+} ion and, as the 3d orbit is half-filled, with presumably antiparallel spin to that of the electrons present, giving a configuration

$$\begin{array}{lll} & Mn^{+} & O^{-} \\ & \downarrow\uparrow & \\ & \downarrow & \downarrow \quad 2p \\ 3d^6 & \downarrow & (\uparrow\downarrow) \; (2p^2) \\ & \downarrow & (\uparrow\downarrow) \; (2p^2) \\ & \downarrow & \end{array} .$$

The remaining p electron, having the same dumb-bell axis as that of the electron that has gone to the Mn^{2+} ion, will now presumably be able to interact with the Mn^{2+} ion directly opposite to the one depicted. Provided the two assumptions are correct, Anderson's calculation shows that the disturbing influence of excited states yields a negative exchange coupling between the opposite Mn^{2+} ions of the right order of magnitude.

Because of the dumb-bell shape of the 2p orbits the superexchange interaction for the right-angle configuration must be very weak. A small interaction may in this case also result from hybridization of 2p and 2s wave functions, or from the presence of excited states in which an electron is raised from the 2p to a $3l$ orbit, which, however, takes a considerable energy.

2.3.3. Influence of the Type of Magnetic Ion

If both ions have less than five 3d electrons, the p electron will be accommodated in the 3d orbit with parallel spin, and Anderson therefore expects positive interaction to result in all such cases, citing examples like CrTe (ferromagnetic) vs MnTe (antiferromagnetic). There are, however,

many oxides of metal ions with less than five 3d electrons which are antiferromagnetic, e.g. Cr_2O_3, whereas only a few really ferromagnetic oxides, i.e. with positive interactions, are known. Thus e.g. $CaMn^{IV}O_3$ with perovskite structure is antiferromagnetic, while mixed crystals $La_{1-x}Me_xMn^{III}_{1-x}Mn^{IV}_xO_4$, in which Me = Ca, Sr or Ba, are real ferromagnetics, i.e. with positive interactions [38]).

The interaction between ions with less than five 3d electrons and those with five 3d electrons according to this theory may be either positive or negative.

It may be noted that Zener [39]) proposes another exchange mechanism to account for the ferromagnetism of $La_{1-x}Sr_xMn^{III}_{1-x}Mn^{IV}_xO_4$. This involves the simultaneous transfer of an electron from one metal ion to an adjacent oxygen ion and of another electron from there to another metal ion ("double exchange"). This mechanism would thus occur in semiconductors for which De Boer and Verwey [40]) postulate the presence of two ions of one metal with different valencies in one crystallographic position.

It has been suggested [41]) that Zener's double exchange mechanism plays a rôle in the *BB* interaction in magnetite. It will be seen in the sections 4-9 that all saturation moments can be accounted for on the basis of negative exchange interaction.

The only ion having less than five 3d electrons used in the preparations described in the present paper is the Cr^{3+} ion. It will appear that in the materials described in section 7 the Fe^{3+}_A-Cr^{3+}_B interaction is undoubtedly negative.

2.3.4. Influence of Angles and Distances on Superexchange Interaction in Spinels

Though no theory is known regarding the influence of the distances Me-O on the strength of the superexchange interaction, it is assumed that generally exchange interactions fall off rapidly with increasing distance. We have seen in section 1.1 that the shortest distances Me-O in the spinel structure fall in two groups, that of nearest neighbours, formerly indicated by *p* and *q*, and a group of larger distances, indicated by *r*, *s* and *t* (see section 1.1). Configurations Me-O-Me with larger Me-O distances, as well as those with both distances of the group *r*, *s* and *t* will be assumed to give interactions that are negligible against those with one distance *p* or *q* and the other equal to *p*, *q*, *r*, *s* or *t*. From fig. 6 we see that only for triangle *pqc* both distances Me-O and the angle Me-O-Me are favourable. The arrangements *pre* and *tqe* have very favourable angles but one large distance. The *AB* interaction will therefore be strong. For *qrd* the angle is very unfavourable and one distance large: consequently the *AA* interaction will be very weak.

For *ppb* the angle is very unfavourable, but both distances Me-O are small; for *ptb*, *psb* and *psf* the angles are more favourable, but one of the distances is large. The *BB* interaction therefore will be expected to be intermediate between the *AB* and *AA* interactions.

In literature only those interactions have so far been taken into account for which the distances *AA*, *AB*, and *BB* are shortests (i.e. *d*, *c* and *b* respectively). As long as the relative influence of angles and distances are unknown, there is no reason why the other configurations should be neglected.

It is the merit of the molecular-field approximation that it does not concern itself with the number of configurations that are taken into account, as the molecular-field constants n, α, β etc. comprise all interactions that play a rôle.

When it is attempted, however, to link the molecular-field constants to the exchange integrals, it seems appropriate to take into account all the configurations that contribute to the interactions.

R.S. Weisz [42]) has attempted to draw up an empirical quantitative relationship giving the dependence of the exchange interaction energy, $k\Theta$, as a function of the distance Me-O + O-Me′ (l), and the angle Me-O-Me′ (φ):

$$k\Theta = C\ S_1 S_2\ e^{-10l} \cos^6 \varphi\,,$$

in which C is a constant and S_1 and S_2 the spin quantum numbers of the ions Me and Me′ respectively.

From the Néel temperatures of the antiferromagnetics MnO, FeO and CoO, for which $\cos \varphi = 1$, a constant value of C is found, but not for NiO.

For spinels the formula was applied to obtain the ratio of the exchange energies for the *AA*, *AB* and *BB* interactions: values for α and β were found of the order of 10^{-9} and 10^{-7} respectively. Weisz therefore assumed $E_{\text{exch}(AB)} = k\Theta$; the Curie temperatures thus calculated from the *AB* interaction agree with the experimental values to within 20 %; in a previous communication Weisz uses a factor e^{-7l}, giving agreement to within 15 %. It seems that many experiments described in the following sections cannot be understood with the small values of α and β Weisz derived. Theoretical background for his formula is so far lacking.

REFERENCES

[27]) For a general synopsis of the theoretical work in this field see
J. H. Van Vleck, Rev. mod. Phys. **17**, 27-47, 1945; Physica, **15**, 197-206, 1949.
[28]) P. Weiss, J. Phys. (4) **6**, 661-690, 1907.
[29]) P. Weiss and R. Forrer, Ann. Phys., Paris (10) **12**, 279-374, 1929.
[30]) G. Hilpert, Ber. dtsch. chem. Ges. **42**, 2248, 1909;
H. Forestier, Thèse, Paris, 1925, or Ann. Chim. **10**, 9, 57, 1925;
J. L. Snoek, Philips tech. Rev. **8**, 353-360, 1946.
[31]) L. Néel, Ann. Phys., Paris **3**, 137-198, 1948.
[32]) J. Phys. Radium, **12**, 160, 1951.
[33]) Y. Yafet and C. Kittel, Phys. Rev. **87**, 290-294, 1952.
[34a]) K. F. Niessen, Physica **17**, 1033-1047, 1951.
[34b]) K. F. Niessen, Physica **18**, 449-468, 1952.
[34c]) K. F. Niessen, Physica **19**, 445-450, 1953.
[34d]) K. F. Niessen, Physica **19**, 1127-1132, 1953.
[34e]) K. F. Niessen, Physica **19**, 1035-1045, 1953.
[35]) C. G. Shull and J. S. Smart, Phys. Rev. **76**, 1256-1257, 1949.
[36]) P. W. Anderson, Phys. Rev. **79**, 350-356, 705-710, 1950.
[37]) J. H. Van Vleck, J. Phys. Radium, **12**, 262-274, 1951.
[38]) G. H. Jonker and J. H. van Santen, Physica, **16**, 337-349, 1950.
[39]) C. Zener, Phys. Rev. **82**, 403-405, 1951.
[40]) J. H. de Boer and E. J. W. Verwey, Proc. phys. Soc. **49A**, 59-71, 1937.
[41]) A. Fairweather, F. F. Roberts and A. J. E. Welch, Ferrites, Rep. Progr. Phys. **15**, 142-172, 1952;
C. Zener and R. R. Heikes, Rev. mod. Phys. **25**, 191-198, 1953.
[42]) R. S. Weisz, Ceramic Age, **59**, 35-38, 1952.

3. EXPERIMENTAL PROCEDURES

3.1. Magnetic Measuring Methods used in Sections 4-9

In the following sections we shall report and discuss measurements of the saturation magnetizations of various ferrimagnetic oxides.

The measurements were carried out by the ponderomotor method described by Rathenau and Snoek [43]) (see fig. 10), in which the material (p) is fixed to a horizontal pendulum (P) suspended from four wires (W), moving perpendicularly to an inhomogeneous field. The field varies very nearly as $H = H_0 - \frac{1}{2}\, ax^2$ in the direction x of the oscillations, which is brought about by the shape of the pole-pieces which end in equal spherical segments (N and S). The constant of the restoring force on the magnetic material in this inhomogeneous field is $a\sigma m_p$, in which σ is the saturation magnetization in $\mathrm{cgs_{magn}.cm^3/gram}$, m_p the weight of the sample. The saturation magnetization σ is found from the formula

$$\sigma = \frac{4\pi^2 m_P}{a m_p}\left(\frac{1}{\tau^2} - \frac{1}{\tau_0^2}\right),$$

in which m_P is the weight of the pendulum, τ_0 the period of the oscillations

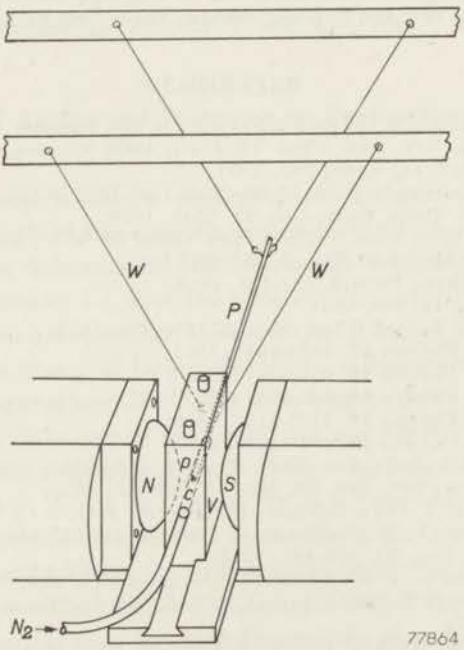

Fig. 10. Apparatus for measuring saturation magnetizations (for symbols see text).

in a magnetic field without the magnetic material fixed to the pendulum, and τ that with the magnetic material present. The constant $4\pi^2/a$ is determined by calibration with very pure iron and nickel.

The measurements reported in sections 4, 7 and 9 were carried out in fields up to 5900 oersteds, those in sections 5, 6 and 8 in fields up to 8000 or 9000 oersteds. For measurements at higher temperatures the end of the pendulum carrying the magnetic material moves in a small tubular furnace; for those at the lowest temperatures it moves in a channel (C) through a vessel (V) containing liquid nitrogen. For temperatures between about 80 °K and room temperature a stream of nitrogen is sucked from a Dewar flask through the vessel (V). By varying the suction rate any constant temperature can be obtained. At liquid-nitrogen temperatures a slow stream of dry nitrogen is passed through the channel in order to prevent condensation of oxygen on the pendulum. Temperatures were measured by means of a thermocouple fixed to the mV meter by very thin leads, so that the movement of the pendulum is not impeded.

Measurements of the saturation magnetization at liquid-hydrogen temperature were carried out by Dr J. Volger or by Mr P. Jongenburger *) by a ballistic method, using a watercooled solenoid for generating the field. These measurements were performed on rods of about $3 \times 3 \times 50$ mm^3 at field strengths up to 7000 oersteds.

Here the flux Φ through the rod is measured. The magnetization in $\mathrm{cgs}_{\mathrm{magn}}$ $I = \Phi/4\pi A$ (A = the area of the cross-section of the rod in cm^2), and σ is obtained from

$$\sigma = \frac{I}{d} = \frac{IAl}{m_{\mathrm{prep}}} = \frac{\Phi l}{4\pi m_{\mathrm{prep}}}.$$

(d = apparent density = (weight)/(external volume), l = length in cm).

The hydrogen liquefactor was not yet available when the measurements reported in section 4 were carried out. Therefore the values given in that section have not been extrapolated to 0 °K and are given in one decimal place less than the values reported in the later sections. The latter values were extrapolated with a T^2 law. Extrapolation with $T^{3/2}$, as postulated by the Bloch spin-wave theory, does not give appreciably different results.

The moment per formula unit Me_3O_4 (n_B) in Bohr magnetons is obtained from $\sigma_{\substack{T=0 \\ H\to\infty}}$ (σ_0) from the formula

$$n_B = \frac{\sigma_0 \times \text{molec. wt } (M)}{(\text{Avogadro's number}) \times (\text{Bohr magneton in ergs/gauss})} = \frac{\sigma_0 M}{5585}.$$

*) The author wishes to express his thanks to Dr J. Volger and Mr P. Jongenburger for performing these measurements.

3.2. Preparation of the Materials

3.2.1. The Final Sintering Operation

The final operation in the preparation of all materials investigated was a sintering process carried out on pressed bars, pellets, etc. placed in an alumina boat inside the gas-tight tube of a molybdenum-wire electric furnace. This operation is carried out at a temperature (900-1350 °C) and in an atmosphere that to a large extent determine the composition. For reducing atmospheres and high temperatures two concentric gas-tight tubes were used and the intervening space was rinsed with the same atmosphere as the preparation.

Practically all materials investigated are spinels, and contain ferric ions, and many also other ions of the transition metals, which can give ions of different states of valency, either higher or lower than that desired. All materials have an equilibrium oxygen pressure that increases with temperature, and which for every different composition will be different.

Because of the special feature of the oxidic spinels to form mixed crystals, containing ions varying from tetravalent to monovalent as well as vacant lattice positions, sintering in an atmosphere with an oxygen content appreciably different from the equilibrium pressure tends to give a spinel with different composition, either alone, like e.g. in the case

$$MnFe_2O_4 + \tfrac{1}{2}x\ O_2 \rightarrow (1-3x)\ MnFe_2O_4 \,.\, x\ Mn_3O_4 \,.\, 3x\ Fe_2O_3,$$

which for $x \ll 1$ may form one phase, or with a second phase, like e.g. in the case

$$MnFe_2O_4 - \tfrac{1}{2}x\ O_2 \rightarrow (1-x)\ (Mn,Fe^{II})Fe_2O_4 + 3x\ (Mn,Fe^{II})O\,.$$

Divalent oxides are usually practically insoluble in the spinel phase.

For practically all materials, except e.g. Fe_3O_4, the equilibrium oxygen pressure exceeds one atmosphere below the melting point; the materials cannot, therefore, be melted in a stream of oxygen at 1 atm without serious decomposition.

The upper temperature limit for the sintering operation is thus primarily determined by the temperature at which the equilibrium oxygen pressure reaches 1 atm.

The possibility of a chemical reaction taking place with the receptacle affords another limiting factor. We have always used recrystallized alumina boats (fired above 1800 °C) or fused-alumina powder underneath the material to be sintered. This material proved to be very unreactive. Even so sintering temperatures have been kept below 1350 °C in order to avoid any reaction with the alumina: where this appeared advisable the surface that had been in contact with the alumina was ground away.

For a number of spinels, containing, apart from noble-gas-shell ions Li^+, Mg^{2+}, Al^{3+}, only Fe^{3+}, Ni^{2+}, Cr^{3+}, Cu^{2+}, the ions with valencies higher than those desired are very unstable, which appears from the fact that even in an oxygen atmosphere, at the minimum temperature required to obtain complete reaction, no ions with higher valencies are formed. These materials were fired in oxygen at a temperature low enough to give no perceptible reduction of Fe^{3+} to Fe^{2+}. The spinels containing Cu^{2+} were markedly reduced in oxygen above 900-1000 °C. Such materials may be kept porous so that any loss of oxygen occurring during firing may be corrected by oxygen take-up during cooling.

The preparation of spinels containing ions for which the valency states lower than those desired are difficult to obtain, e.g. $MnCr_2O_4$, is also fairly easy. Thus $MnCr_2O_4$ may be fired in a wide range of reducing atmospheres, without formation of metallic Mn (or Cr), and with imperceptible amounts of excess oxygen.

The problem of obtaining the correct composition is more difficult for spinels containing ions like Fe^{2+}, Mn^{2+}, and to a lesser extent Co^{2+}, for which higher valency states are stable up to high temperatures, as well as ions like Fe^{3+} for which lower valency states are formed at high temperatures.

In order to obtain the desired composition (i.e. oxygen content) one may choose from two methods:

(1) Using a constant atmosphere, the temperature is adjusted until chemical analysis of the material shows that the correct oxygen content is obtained.

(2) Using a constant temperature, the oxygen content of the atmosphere is adjusted until the material has the correct oxygen content.

It must be kept in mind, however, that an atmosphere in equilibrium with the material at the sintering temperature will reoxidize it at lower temperatures and mostly so at the outside surface, so that the composition becomes inhomogeneous during cooling down.

This might be largely avoided by quenching the material from the sintering temperature, but we shall see that the cation distribution amongst tetrahedral and octahedral sites is often strongly dependent on temperature, so that in this way a different material is obtained, quite apart from the effect of possible reoxidation.

We shall be interested in the properties of the material having the most stable ionic distribution, and therefore have to cool slowly.

The ideal method of obtaining a homogeneous material with the correct oxygen content and the most stable ionic distribution is that of cooling slowly in a continuously changing atmosphere at all temperatures in equilibrium with the oxygen pressure of the material. Smiltens has used

a stepwise changing atmosphere in the preparation of Fe_3O_4 single crystals, using his own equilibrium pressure data [44]).

The determination of the equilibrium oxygen pressure as a function of temperature is difficult and laborious, and has been carried out only for Fe_3O_4.

A method of diminishing reoxidation during cooling down, i.e. sintering to a high apparent density, so that the atmosphere cannot penetrate into the inside of the material through the pores, can sometimes be used with success [45]).

Another method is that of firing in a gas mixture the oxygen content of which changes with temperature (e.g. CO_2, $CO_2 + CO$, H_2O, $H_2O + H_2$). From Smiltens's work it is known that the decrease of oxygen content with decreasing temperature of a CO_2-CO mixture is not sufficient to keep it in equilibrium with Fe_3O_4, and this appears to be very general for the known gas mixtures.

As the firing temperature is decreased, the difference in oxygen pressure between the firing temperature and room temperature is decreased. The minimum sintering temperature is determined by the condition that complete reaction takes place. This temperature may be lowered by a suitable preparation of the powder to be sintered.

In practice we have in most cases left the preparations to cool in the same atmosphere after switching off the furnace. The cooling time was then 7-9 hours. In many cases we have annealed the sample at low temperatures, high enough for ionic diffusion to take place within convenient time intervals. Whenever this has been done, specific reference to this effect will be made.

For a fair comparison of the ionic distribution in a mixed-crystal series we have always fired the whole series at one temperature and therefore often had to use different atmospheres for different members of the series (e.g. the series $MnFe_2O_4$-$MnCr_2O_4$). One sintering temperature cannot be used if certain members of a series do not react completely at a temperature where for other members melting occurs (cf. the series $CaFe_2O_4$-$ZnFe_2O_4$).

In view of the volatility of ZnO and Li_2O care was taken that no free ZnO or Li_2O was present when the final sintering operation was started. As these oxides volatilize even from their compounds under the conditions used, these were sintered at temperatures not above 1300 °C for Zn compounds and not above 1150 °C for Li compounds.

3.2.2. Methods of Preparation of the Powder to be Sintered

Several methods have been used:

(A) Pure oxides, or in certain cases carbonates, are ground together in a chromium-plated steel ball mill or in an agate Bloch-Rossetti mill under

ethanol. The mixture is dried under an electric (infrared) lamp, prefired, usually in air, at a temperature below the final sintering temperature and ballmilled again.

Zinc oxide was heated to 500 °C before being used in order to decompose any $ZnCO_3$ present. The other oxides were heated at 200 °C before chemical analysis and before being used.

(B) The pure metals (or, in some cases, oxides or carbonates) were dissolved in nitric acid, the solution evaporated to dryness under an infrared lamp, often on a sand bath, and the nitrates decomposed to oxides. When the powder was completely dry it was transferred from the porcelain dish to an alumina beaker and heated to about 800 °C. The powder was then ballmilled in an agate Bloch-Rossetti mill. The compounds containing titanium were prepared by adding TiO_2 (anatase, synthetic) to the nitrates solution before evaporation and heating to dryness.

(B′): like (B), but using sulphuric acid instead of nitric acid. The prefiring was interrupted at 600 °C for a milling operation, then continued up to 900 °C, after which the powder was milled again.

(B″): like (B), but ammonia is added to the nitrates solution. The hydroxides are filtered, washed, dried and decomposed at about 800 °C.

(C) To the nitrates or sulfates solution prepared like under (B) (B′) a sodium carbonate solution is added at 100 °C, the precipitate boiled, filtered, washed well, dried and decomposed by prefiring at about 800 °C.

We shall describe in the following sections the preparation of the various materials by giving:

the raw materials with the main impurities if present in amounts above 0·01 %;

the method used;

the temperature and duration of prefiring, and the atmosphere, if different from air (e.g. pref. 2 h 800 °C in O_2);

the temperature and duration of the final sintering and the atmosphere (e.g. sint. 2 h 1200 °C in O_2).

3.3. X-ray Analysis

X-ray diagrams for all materials mentioned have been obtained on a Norelco X-ray Diffractometer. All materials reported show a spinel diagram without additional lines, except for the cases where superstructure lines occur, or in a few other cases which will be mentioned. The lattice constants were determined wit Co $K\alpha_1$, Fe $K\alpha_1$ or Mo $K\alpha_1$ radiation, using the wavelengths Co $K\alpha_1$: 1·78890 Å, Fe $K\alpha_1$: 1·93597 Å and Mo $K\alpha_1$: 0·70926 Å.

3.4. Chemical Analysis

Analysis of the oxygen content of many of the materials has been carried

out. The method used has been worked out by Messrs G. W. van Oosterhout and A. Bol.

The weighed sample is brought in glass tube with 7 mm inner diameter with a constriction. The tube is rinsed with carbon dioxide or with very pure nitrogen; a calibrated solution of Mohr's salt in 6 N hydrochloric acid is then introduced. After a rinse with the same gas the tube is sealed. The tube is heated to 120-200 °C till the material has dissolved, which usually takes 8-24 hours.

The tube is then opened, and the contents are transferred to a titration vessel that is rinsed continuously with carbon dioxide.

The ferrous iron is titrated potentiometrically, using a vacuum tube voltmeter as described by Claassen [46]), against 0·01 or 0·1 N ceric sulphate solution. In this way both an excess and a shortage of oxygen with respect to Fe^{3+}, Mn^{2+}, Co^{2+}, Ni^{2+} or Cu^{2+} can be determined. For the titration of an excess oxygen the amount of Mohr's salt in the hydrochloric acid solution is adjusted so that there is a small excess in every case.

For the determination of a shortage of oxygen a small amount of Mohr's salt is added to the hydrochloric acid in order to reduce dissolved oxygen. The solution is calibrated at least a day after preparation.

It is convenient to store the solutions in flasks; an accurately measured quantity of the solution is passed from these flasks through a silver reductor [47]) to the reaction tube. Calibration of the solution is carried out exactly as described above, leaving out the material.

For the determination of the total iron content the solution of the sample is passed through a silver reductor before the titration.

The titrations were carried out by Mr T. Geraerts for the materials of section 4, for the materials of sections 5-9 at the Analytical Chemistry Department of our laboratories under the supervision of Dr A. Claassen and Mr J. Visser *). A determination of the proportion of the metal ions present was carried out in a few cases. This was found not to deviate from the proportion in the raw materials within the analytical error. Several of the spinels containing volatile oxides were weighed before and after the final sintering.

Provided the material had practically completely reacted at a temperature well below the firing temperature of 1150 °C, the loss in weight of the spinels containing lithium was small, in fact less than 1 % of the Li_2O present. For the spinels containing zinc but no manganous or ferrous ions no loss of zinc was observed; for those containing Zn^{2+} and Mn^{2+} ions no loss of zinc occurred when the presence of free ZnO was avoided at the final

*) The author is indebted to Dr Claassen and to Mr Visser for their help in these investigations.

sintering. For those containing Zn^{2+} and Fe^{2+} ions special measures were taken, to be described in section 4.

The order of magnitude of the amount of impurities present in the raw materials was determined by a semi-quantitative spectrochemical method by Dr N. W. H. Addink *).

*) The author is indebted to Dr Addink for carrying out these analyses.

REFERENCES

43) G. W. Rathenau and J. L. Snoek, Philips Res. Rep. **1**, 239, 1946.
44) J. Smiltens. J. chem. Phys. **20**, 990-994, 1952.
45) J. L. Snoek, New Developments in Ferromagnetic Materials, Elsevier Publ. Comp., New York-Amsterdam, 1947.
46) A. Claassen, Analyt. chim. acta **2**, 602-605, 1948.
47) G. H. Walden, L. P. Hamett and S. M. Edmunds, J. Amer. chem. Soc. **56**, 350-353, 1934.

4. EXPERIMENTAL EVIDENCE FOR THE CORRECTNESS OF NEEL'S HYPOTHESIS: THE FERRITES

4.1. Introduction

In order to obtain experimental evidence supporting Néel's theory, we have prepared the single ferrites $MnFe_2^{III}O_4$, $Fe^{II}Fe_2^{III}O_4$, $CoFe_2^{III}O_4$, $NiFe_2^{III}O_4$, $Cu^{II}Fe_2^{III}O_4$, $MgFe_2^{III}O_4$, $Li_{0.5}Fe_{2.5}^{III}O_4$, $ZnFe_2^{III}O_4$ and $CdFe_2^{III}O_4$ and mixed crystals of the first seven ferrites (reported to have the inverse cation distribution) with zinc ferrite.

The saturation moments expressed in Bohr magnetons have been reported previously [48) 49) 50)]. More complete data on many of these materials have since been reported by other authors, giving the saturation-magnetization vs temperature curves and susceptibility vs temperature measurements above the Curie temperature.

In the present section we shall give no new magnetic data, and discuss the experimental data at present available.

As we shall see that the magnetic properties depend on the ionic distribution, and as this in turn depends on the method of preparation, we shall in section 4.2 give our methods of preparation of the ferrites investigated.

4.2. Preparation and Analysis of the Ferrites

(a) The manganese-zinc ferrites $Mn_{1-a}Zn_a\ Fe_2O_4$ were prepared from
$MnCO_3$ (Ca 0·1%, Mg 0·12%, Zn 0·05 %, Na $<$ 0·04%),
ZnO (Mg $<$ 0·01 %),
Fe_2O_3 (Si 0·04 %, Pb 0·03 %, Mn 0·1 %),
by method (A), pref. 2 h at 1000 °C in air, sint: heating up in O_2 up to 1100 °C, further up to 1250 °C and 2 h at 1250 °C in N_2, containing traces of O_2.
$MnFe_2O_4$ contained 0·05 % Fe^{2+}; those MnZn ferrites for which data have been given $\leqslant$ 0·1 % Fe^{2+}.
(b) The ferrous-zinc ferrites were prepared from
ZnO
Fe_2O_3 } as under (a),
by method (A), pref. 2 h at 900 °C in N_2, sint. 2 h at 1250 °C in N_2 atmospheres containing varying amounts of oxygen.

The material was placed in an envelope of ZnO. For two of the materials analysis showed that the Fe^{2+} and Zn contents were correct to within 0·1 %.
The ferrous ferrite was fired for 2 h at 1350 °C in a CO_2-H_2 mixture and cooled down very slowly in a CO_2-H_2 mixture the composition of which was changed stepwise as Smiltens has indicated. The CO_2-H_2 ratios were the same as the CO_2-CO ratios given by Smiltens. Our Fe_3O_4, however, contained 1·04 Fe^{2+} on 2·00 Fe^{3+}.
(c) The cobalt-zinc ferrites $Co_{1-a}\ Zn_aFe_2O_4$ was prepared from
$CoCO_3$ ($<$ 0·1 % impurities),
ZnO (as under (a)),
Fe_2O_3 (Ni 0·03%, Mn 0·02 %, Si 0·02 %),
by method (A), pref. 2 h at 800 °C in air, sint. 2 h in oxygen or air at 1250 °C.
The $CoFe_2O_4$ contained no Fe^{2+} or excess oxygen, the CoZn ferrites $\leqslant$ 0·1 % excess oxygen.

(d) The nickel-zinc ferrites $Ni_{1-a}\ Zn_a\ Fe_2O_4$ were prepared from
$NiSO_4$ solution (Na < 0·07 %, Ca 0·03 %, Co 0·02 %, Si 0·02 %),
ZnO (as under (a)),
Fe (< 0·01 % impurities),
by method (B′), sint. in oxygen for 2 h at 1200 °C or 4 h at 1250 °C.
The Fe^{2+} contents were negligible, the SO_3 contents small, i.e. < 0·1 %.
(e) The copper-zinc ferrites proved difficult to prepare, as they easily lost oxygen at temperatures where complete reaction took place.
Raw materials were
CuO (Pb 0·03 %, Si 0·02 %),
ZnO (as under (a)),
Fe_2O_3 (as under (c)).
$CuFe_2O_4$: pref. 2 h at 700 °C, sint. 2 h at 900 °C in O_2, annealed 168 h at 360 °C in O_2. The sample showed the tetragonal hausmannite structure with $c = 8{\cdot}68$ Å, $a = 8{\cdot}24$ Å. It contained 0·1 % Fe^{2+} (or Cu^+).
$Cu_{0\cdot5}Zn_{0\cdot5}\ Fe_2O_4$: pref. 2 h at 800 °C, sint. 3½ h at 1050 °C. It contained 0·1 % Fe^{2+} (or Cu^+).
(f) The magnesium-zinc ferrites were prepared from
MgO (Ca 0·2 %, Fe 0·01 %),
ZnO (as under (a)),
Fe_2O_3 (as under (c)),
by method (A), pref. 2 h at 900 °C, sint. 4 h at 1200 °C in O_2. $MgFe_2O_4$ was annealed for 24 h at 700 °C in O_2 and cooled slowly. The materials contained < 0·1 % Fe^{2+}.
(g) The "lithium-zinc ferrites" $Li_{0\cdot5-0\cdot5a}\ Zn_a\ Fe_{2\cdot5-0\cdot5a}O_4$ were prepared from
Li_2CO_3 (Mg 0·02 %, Na 0·1 %, Ca 0·02 %),
ZnO (as under (a)),
Fe_2O_3 (as under (a)).
1 Li_2CO_3 + 1 Fe_2O_3 were milled in an agate ball mill under absolute ethanol, and after drying heated to 700 °C in oxygen for 5 hours. The $LiFeO_2$ thus obtained was used in method (A), pref. 2 h at 750 °C, sint. 4 h at 1150 °C in O_2. Fe^{2+} content ⩽ 0·1 %.
The following materials were quenched by dropping in saturated NaCl solution, which was subsequently rinsed out with boiling water, or in oil, which was rinsed out with benzene.
$NiFe_2O_4$ from 1250 °C;
$CuFe_2O_4$ from 900 °C;
$MgFe_2O_4$ from 1250 °C;
$Li_{0\cdot5}Fe_{2\cdot5}O_4$ from 1150 °C.
These samples all contained < 0·1 % Fe^{2+}.

4.3 Saturation Moments of the Single Ferrites ($Me^{II}Fe_2^{III}O_4$ and $Li_{0\cdot5}Fe_{2\cdot5}^{III}O_4$)

Our results given previously [59) 49)] will be given in table IV together with those since obtained by Pauthenet [51) 52) 53)] and Guillaud et al. [54a-d) or 55)].

Guillaud states that his preparations apart from being stoichiometric to within 0·2 %, contain < 0·05 wt % of metal in lower or higher valency states. Pauthenet gives no data on preparation or purity, except that they were found to be pure spinels.

Contrary to our own results of the present section, which are calculated from the magnetization at 77 °K and 5900 Oe, these authors have measured also at 20 °K, and in fields up to 20 000 Oe, and have extrapolated towards $H = \infty$ and $T = 0$ °K.

We have seen (section 1.2) that according to Verwey and Heilmann the six first-named ferrites are inverse: $Fe[Me^{II}Fe]O_4$.

Thus for these six ferrites antiparallelism of the ionic moments in the *A* and *B* positions respectively as a result of a preponderant *AB*

TABLE IV

Saturation moments of single ferrites

	(1)	(2)	(3)	(4)	(5)
	Gorter [50]) [49])	Guillaud [54]) [55])	Pauthenet [51]) [52]) [53])	other authors	$2S_{Me^{2+}}$
$MnFe_2O_4$	5·0	4·60	4·40±0·04	—	5
$FeFe_2O_4$	4·2	4·03	4·08 (±0·01)*)	4·08 [29])*)	4
$CoFe_2O_4$	3·3	3·67; 3·70	3·94±0·002	—	3
$NiFe_2O_4$	2·3	2·40	2·224	—	2
$CuFe_2O_4$	1·3	—	1·37	⩾1·70 [56])	1
$MgFe_2O_4$	1·1	⩾1·0	0·86	1·1 [57])	0
$Li_{0·5}Fe_{2·5}O_4$	2·6	—	—	—	(2·5)
$ZnFe_2O_4$	0·0	0	—	—	0
$CdFe_2O_4$	0·0	—	—	—	0

*) Natural magnetite

interaction, leads to a saturation moment $(5 + m_{Me^{2+}}) - 5 = m_{Me^{2+}}$. Taking $g_{Me^{2+}} = 2$, $m_{Me^{2+}} = 2S_{Me^{2+}}$. Comparison of columns (1) and (5) shows that our measurements to a first approximation confirmed Néel's hypothesis.

Braun [12]) has found that $Li_{0·5}Fe_{2·5}O_4$ is completely inverse. Thus for $Fe[Li_{0·5}Fe_{1·5}]O_4$ a saturation moment $7·5 - 5 = 2·5$ is calculated. The agreement with the experimental moment shows that $m_{Fe^{3+}} = 5$ as expected.

There are two different causes for the discrepancies between our values and the values of $2S$:

(1) the ferrites under discussion are not completely inverse;

(2) the g-factor of Me^{2+} is not equal to 2.

The first of these hypotheses was originally proposed by Néel [31]) in order to explain the increase of the saturation moments of $CuFe_2O_4$ on quenching [56]).

If a slowly cooled ferrite is not completely inverse or normal, it has not reached a state of lowest free energy. Thus the ionic distribution will be expected to vary with temperature. The highest entropy would be gained for a completely random arrangement i.e. $Fe_{2/3}Me^{II}_{1/3}[Me^{II}_{2/3}Fe_{4/3}]O_4$.

Thus the general formula of a ferrite $Me^{II}Fe_2O_4$ is

$$Fe_{1-x}Me^{II}_x[Me^{II}_{1-x}Fe_{1+x}]O_4. \qquad (4.1)$$

The theoretical limiting value of x, i.e. $x = \frac{1}{3}$, is in practice not reached at the highest temperature to which the ferrite may be raised without decomposition through reduction

of Fe^{3+} to Fe^{2+}. The value of x will further be determined by the cooling rate. When a ferrite is quenched from a high temperature the equilibrium distribution at the quenching temperature may be frozen in to a large extent.

When the ferrite is cooled slowly, the ionic distribution will adjust itself to maintain equilibrium till the temperature is reached where the ionic diffusion will be too slow to maintain equilibrium during cooling, Thus the distributions actually found are also frozen in, and x depends on the cooling rate.

The moment calculated for formula (4.1) is

$$n_B = 10x + m_{Me^{2+}}(1-2x). \qquad (4.2)$$

We had assumed that if $x \neq 0$ it must change with temperature. We therefore subjected several ferrites to a quenching treatment and found [50]) [49]) that for $MgFe_2O_4$ and $CuFe_2O_4$ the saturation moment is increased by quenching, but that for $NiFe_2O_4$ and $Li_{0.5}Fe_{2.5}O_4$ it remains the same. The results are given in table V.

TABLE V

	treatment	n_B	treatment	n_B
$MgFe_2O_4$	24 h 700 °C	1·1	quenched from 1250 °C	1·4
$CuFe_2O_4$	168 h 360 °C	1·3	quenched from 900 °C	2·3
$NiFe_2O_4$	cooled slowly	2·3	quenched from 1250 °C	2·3
$Li_{0.5}Fe_{2.5}O_4$	,, ,,	2·47 *)	quenched from 1150 °C	2·50 *)

*) material of section 7 (new data).

For $MgFe_2O_4$ we deduce from (4.2) $x = 0{\cdot}11$ and $x = 0{\cdot}14$ for annealed and quenched samples respectively.

Pauthenet and Bochirol [52]) have since reported measurements of the saturation moments of $MgFe_2O_4$ and $CuFe_2O_4$ quenched from various temperatures. The values of x calculated from (4.2) lie close to a curve representing a Boltzmann distribution formula

$$\frac{x(1+x)}{(1-x)^2} = e^{-E/kT},$$

in which E is the energy needed to bring an ion Me from the B to the A position and a ferric ion back from A to B. Bertaut [10]) had qualitatively confirmed the x values found by Pauthenet and Bochirol by X-ray intensity measurements but the accuracy of the X-ray method (appr. $\pm 0{\cdot}03$ in x according to Bertaut) is very much lower.

Also neutron diffraction intensities for a sample of $MgFe_2O_4$ with $n_B = 1{\cdot}1$ [57]) show better agreement for $x = 0{\cdot}1_0$ than for $x = 0$ [58]).

For $NiFe_2O_4$ the equality of n_B for quenched and slowly cooled samples lead to the assumption $x = 0$; thus $m_{Ni^{2+}} = 2{\cdot}3$.

Thus we have been led to assume that for $NiFe_2O_4$ the discrepancy between columns (1) and (5) of table IV is due to $g_{Me^{2+}}$ being larger than 2. For $Fe^{II}Fe_2O_4$, $CoFe_2O_4$ and $CuFe_2O_4$ we have also assumed $g_{Me^{2+}} > 2$ in view of the known paramagnetic behaviour of salts containing Fe^{2+}, Co^{2+}, Ni^{2+} and Cu^{2+} ions. The n_B values of $CuFeO_4$ must be accounted for by $g_{Cu^{2+}}$ being larger than 2 as well as by the presence of some Cu^{2+} ions on A sites.

It may be noted that for $Mn^{II}Fe_2O_4$ and $Li_{0{\cdot}5}Fe_{2{\cdot}5}O_4$ the agreement between columns (1) and (5) is very good, in accordance with the fact that $g_{Mn^{2+}} = g_{Fe^{3+}} = 2$, since there is no contribution of the orbital moment.

The g-factors of the magnetic divalent ions may be obtained from measurements of the effective g-factors of the ferrites, when the cation distribution is known. These g-factors will be discussed in section 4.3.1 and such measurements as have been reported in literature will be given.

We shall first discuss the discrepancies between the n_B values found by different authors.

Our own values being obtained for 77 °K and 5900 Oe will generally be expected to be too low. This is especially so for $CoFe_2O_4$, which because of the large crystalline and stress anisotropies is far from saturated under these conditions. Our value for Fe_3O_4 is, however, higher than that of other authors. Our preparation contained an excess of Fe^{2+} [50]) [49]). The FeO, originally present next to the spinel, presumably decomposes on cooling through 570 °C and gives Fe + Fe_3O_4. This may just account for the deviation of our value from that given by Pauthenet [51–53]) and Weiss and Forrer [29]). Our value of 2·3 for $NiFe_2O_4$ has been confirmed by measurements extended to liquid-hydrogen temperature and 9000 Oe (see section 8).

Pauthenet reports like ourselves that the saturation moment of $NiFe_2O_4$ does not change measurably on quenching, and finds the same behaviour for $CoFe_2O_4$. The discrepancies between the values for $NiFe_2O_4$ and $CoFe_2O_4$ in columns (2) and (3) might nevertheless be due to very slight differences in ionic distribution, as a very small amount of divalent metal may freeze in on tetrahedral sites during the formation of the spinel.

The only serious discrepancy in table IV is that between the values for $MnFe_2O_4$. Guillaud has prepared three mixed crystals $MnFe_2O_4$-$NiFe_2O_4$ and one MnNiCo ferrite, in all of which the saturation moments agree with that calculated with $m_{Mn^{2+}} = 4{\cdot}60$, $m_{Ni^{2+}} = 2{\cdot}40$ etc. to within 0·05. This according to Guillaud, adds weight to his assumed value $m_{Mn^{2+}} = 4{\cdot}60$.

Another value for $MnFe_2O_4$ since obtained by us is $n_B = 4{\cdot}85$ (section 9). We believe that the discrepancies in the n_B values are real, and that they are related to different cation distributions in the different preparations. The fact that Guillaud's sample was sintered at 1380 °C [54b]) and ours at 1250 °C lends some support to the latter assumption, which should, however, be checked by further experiments.

We cannot, however, account for the fact that for $MnFe_2O_4$ n_B is sometimes below 5. It might be suggested that $(m_{Mn^{2+}})_A > 5$, i.e. that $(g_{Mn^{2+}})_A > 2$ (see section 4.3.1), but a value $n_B = 4{\cdot}6$ would lead to impossibly high values of $(g_{Mn^{2+}})_A$, so that we assume that $(m_{Mn^{2+}})_A = (m_{Mn^{2+}})_B = m_{Fe^{3+}} = 5$.

Another possibility is that part of the Mn^{2+} and Fe^{2+} ions in the B sites change into Mn^{3+} and Fe^{2+} ions ($m_{Mn^{3+}} \approx m_{Fe^{2+}} \approx 4$), which state might be stabilized by the establishment of a higher degree of short-range order between the di- and trivalent ions, but this seems rather unlikely to us.

Finally it may be that the ionic moments in the B position are not completely parallel. We shall discuss this possibility in section 4.4.

A direct confirmation of Néels's hypothesis of antiparallel moments in A and B positions has been provided by neutron diffraction experiments on Fe_3O_4 [68]), $NiFe_2O_4$ [69]) and $MgFe_2O_4$ [58]) [70]). Moreover, Fe_3O_4 and $NiFe_2O_4$ were found to be qualitatively inverse, for $MgFe_2O_4$ the ionic distribution was even determined quantitatively [70]) ($x = 0{\cdot}12$).

A discussion of $Zn[Fe_2]O_4$ will be given in section 4.4.

4.3.1. Effective g-factors

Effective g-factors of the ferrites may be determined by microwave absorption measurements [60]). The method used in our laboratory will be described elsewhere [59]).

The specimen (here a sphere of 0·8-0·1 mm diameter) is placed in a cavity in a large external field H_z and a microwave field with angular frequency ω perpendicular to it.

The spins perform a precessional movement around H_z, whereby the magnetization M_z is decreased by ΔM and the angular momentum J_z by ΔJ. A resonance peak is observed for a fixed angular frequency ω when the field H_z is varied. The resonance condition for a sphere is $\omega = g(e/2mc)H_z$ For polycrystalline materials with random crystallite orientation the influence of crystalline anisotropy on the resonance condition may be neglected, when H_z is large and the crystalline anisotropy is fairly low. Be M the magnetization and J the angular momentum per unit volume, then Kittel [61]) has shown that

$$g\frac{e}{2mc} = \frac{\Delta M}{\Delta J} = \frac{\Delta(M_{spin} + M_{orb})}{\Delta J_{spin}}. \qquad (4.3)$$

As $M_{spin}/J_{spin} = e/mc$, and the changes (Δ) in M and J are proportional to their absolute values, one obtains

$$g = \frac{2(M_{spin} + M_{orb})}{M_{spin}} = \frac{2(\text{total magnetic moment})}{\text{spin moment}}. \qquad (4.4)$$

For the special case of a ferrimagnetic spinel with antiparallel ionic moments in A and B positions

$$g_{eff} = 2 \cdot \frac{(M_{total})_A - (M_{total})_B}{(M_{spin})_A - (M_{spin})_B}. \qquad (4.5)$$

Such a spinel containing different magnetic ions i (x ions per formula unit in either position) has at 0 °K

$$g_{eff} = \frac{\sum_i (x_i g_i S_i)_A - \sum_i (x_i g_i S_i)_B}{\sum_i (x_i S_i)_A - \sum_i (x_i S_i)_B} = \frac{\overrightarrow{\sum_i} x_i g_i S_i}{\overrightarrow{\sum_i} x_i S_i}. \qquad (4.6)$$

In his first measurement [62]) Beljers found for $NiFe_2O_4$ $g = 2{\cdot}36$, but it has since been shown the spheres he used were not small enough. In his later measurements spheres of 0·8 - 0·1 mm diameter, prepared by a method described by Bond [63]), have been used.

g-factor values, reported in literature for several ferrites are given in table VI.

It is clear from this table that g_{eff}, which for a completely inverse ferrite is equal to $g_{Me^{2+}}$, as is seen from formula (4.5), can qualitatively account for the discrepancies between the experimental saturation moments of columns (1)-(4) and the figures of column (5) in table IV.

4.4. Saturation Moments of the Mixed Crystals of the Ferromagnetic Ferrites with Zinc Ferrite ($Me^{II}_{1-a}\ Zn_a\ Fe_2O_4$ and $Li_{0{\cdot}5-0{\cdot}5a}\ Zn_a\ Fe_{2{\cdot}5-0{\cdot}5a}O_4$)

Verwey and Heilmann have shown that in mixed crystals of $ZnFe_2O_4$ and $CuFe_2O_4$ the divalent ions occupy the same crystallographic positions as in the constituent single ferrites. Assuming the Zn^{2+} ions to occupy the tetrahedral sites only, the mixed crystals of $Zn[Fe_2]O_4$ with a completely inverse ferrite $Fe[Me^{II}Fe]O_4$ have the formula

$$Zn_a\ Fe^{III}_{1-a}[Me^{II}_{1-a}\ Fe^{III}_{1+a}]O_4,$$

which for complete antiparallelism of the ionic moments in the A and B positions respectively gives a saturation moment

$$n_B = m_b - m_a = 10a + (1-a)\, m_{Me^{2+}}, \qquad (4.7)$$

TABLE VI

Experimental values of effective g-factors of various single ferrites *)

ferrite	g_{eff}	temperature (°C)	wavelength (cm)	author(s)	sample
$MnFe_2O_4$	2·05	room temp.	1·24	a)	polycryst.
$MnFe_2O_4$	2·16 ↓ 2·02	room temp.	3·14 ↓ 0·64	b)	polycryst.
$FeFe_2O_4$	2·06	—153	3·35	c)	synth.
	2·08; 2·09	—143	3·35; 1·25		single crystals
	2·17; 2·13	20	3·35; 1.25		
$CoFe_2O_4$	broad peak	room temp.	1·24	a)	polycryst.
$CoFe_2O_4$	2·22 ↓ 2·91 ↓ 2·08	100 ↓ 300 ↓ 480	3·2 3·2 3·2	d)	polycryst.
$NiFe_2O_4$	2·21	room temp.	1·24	a)	polycryst.
	2·19	room temp.	1·25	e)	single crystal
	$2{\cdot}25_5$(av.)	—195-588	3·33	f)	polycryst.
	2·43 ↓ 2·12	room temp. room temp.	3·14 ↓ 0·64	b)	polycryst.
$CuFe_2O_4$	2·20; 2·17 ↓ ↓ 2·05; 2·06	—195 ↓ 450	1·25 1·25	g)	single cryst.; polycryst.
$MgFe_2O_4$	2·03-2·06	room temp.	1·24	a)	
$Li_{0·5}Fe_{2·5}O_4$	2·08	room temp.	3·18	h)	

a) W. A. Yager, F. R. Merritt and C. Guillaud, Phys. Rev. **81,** 477-478, 1951.
b) T. Okamura, Y. Torizuka and Y. Kojima, Phys. Rev. **88,** 1425-1426, 1952.
c) L. R. Bickford, Phys. Rev. **76,** 137-138, 1949.
d) T. Okamura, Y. Torizuka and Y. Kojima, Phys. Rev. **84,** 372, 1951.
e) W. A. Yager, J. K. Galt, F. R. Merritt and E. A. Wood, Phys. Rev. **80,** 744-748, 1950.
f) D. W. Healy, Phys. Rev. **86,** 1009-1013, 1952.
g) T. Okamura and Y. Kojima, Phys. Rev. **86,** 1040-1041, 1951.
h) Unpublished value of Mr H. G. Beljers.

*) Results obtained on too large specimens have been disregarded.

in which m_a and m_b represent the resultant moments per formula unit in the A and B positions respectively. When the possibility of the presence of Zn ions in B sites and of Me^{II} ions in A sites is taken into account, the general formula is

$$Zn_{a-y}Fe_{1-a+y-x}Me^{II}_x[Me^{II}_{1-a-x}Zn_yFe_{1+a-y+x}]O_4,$$

with

$$n_B = m_b - m_a = 10a + (1-a)\, m_{Me^{2+}} + (10-2m_{Me^{2+}})x - 10y. \qquad (4.8)$$

Fig. 11 shows the results of our measurements of the saturation moments of the mixed-crystal series

$Mn_{1-a}Zn_a\ Fe_2O_4$,
$Fe_{1-a}\ Zn_a\ Fe_2O_4$,
$Co_{1-a}\ Zn_a\ Fe_2O_4$,
$Ni_{1-a}\ Zn_a\ Fe_2O_4$,
$Cu_{1-a}\ Zn_a\ Fe_2O_4$ (only for $a = 0$ and $a = 0{\cdot}5$),
$Mg_{1-a}\ Zn_a\ Fe_2O_4$,
$Li_{0{\cdot}5-0{\cdot}5a}\ Zn_a\ Fe_{2{\cdot}5-0{\cdot}5a}\ O_4$.

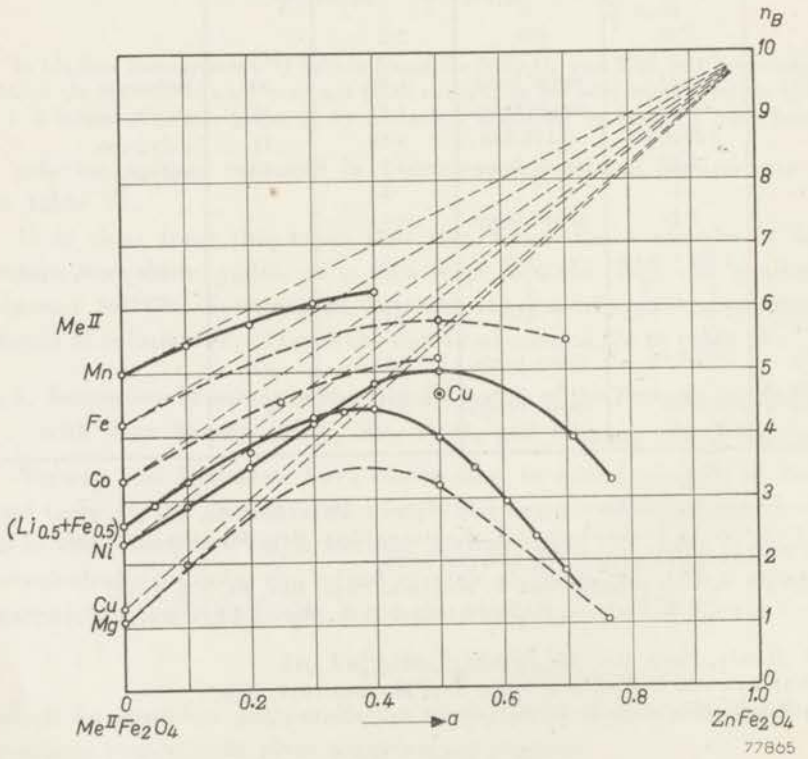

Fig. 11. Saturation moment in Bohr magnetons of various mixed-crystal series $Me^{II}Fe_2O_4$-$ZnFe_2O_4$ (measurements by the author).

The dashed lines represent the n_B values calculated from formula (4.7), or from formula (4.8) assuming x to be a constant fraction of $1-a$ and $y = 0$, i.e. assuming the relative distribution of Me^{2+} amongst the tetrahedral and octahedral sites to be unaffected by mixed-crystal formation with $Zn[Fe_2]O_4$.

It is seen that the saturation moments found for small values of the Zn content a indeed increase with a: the initial slopes of the curves in several cases are practically equal to those of the corresponding dashed lines.

The agreement of these slopes is considerably better for the curves obtained by Guillaud for several of these systems (fig. 12), which, as we have seen, were measured using higher fields and lower temperatures, and extrapolated towards $H = \infty$ and $T = 0$ °K.

The latter results prove (at least up to $a = 0{\cdot}4$) that the Zn^{2+} occupies practically exclusively the tetrahedral position and, incidentally, confirms that $m_{Fe^{3+}} = 5$. The distribution of the Zn ions is, however, dependent on temperature: Pauthenet [53]) has measured the saturation moments also of quenched samples of nickel-zinc ferrites up to $a = 0{\cdot}6$, and found that the

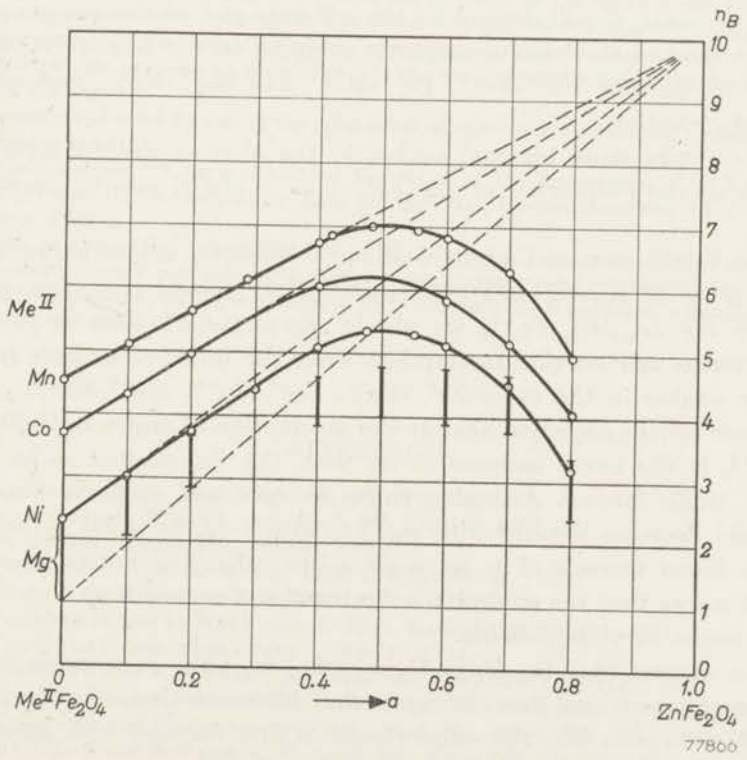

Fig. 12. Saturation moment in Bohr magnetons of various mixed-crystal series $Me^{II}Fe_2O_4$-$ZnFe_2O_4$ (measurements by Guillaud et al.).

slope of the curve then deviates more from the dashed line than for annealed samples. This proves that some Zn^{2+} now occupies the octahedral sites: the difference between the n_B values for annealed and quenched samples is equal to $10y$ (formula 4.8).

The decrease of n_B for higher zinc contents as shown in figs 11 and 12 must be explained as follows:

The number of ferric ions in the A position, and thus m_a, decreases with increasing a. Where the straight line $m = m_b - m_a$ intersects the straight line $m = -m_a\ (1 + 1/\gamma_2)$, angles between the ionic moments in the B position start to occur, according to the theory.

The curvature of the n_B vs a curve has been accounted for by Néel [64]) for NiZn ferrites by fluctuations in the ratio of the numbers of Zn^{2+} and Fe^{3+} ions in A sites surrounding different B sites, i.e. by local fluctuations in the AB interaction. In this calculation he used interaction constants derived from his own susceptibility data [65]). Considering the facts that these materials contain two different magnetic ions, and that this theory should be modified along the lines of Yafet and Kittel's theory, the agreement is satisfactory. The interaction constant β, or γ_2, needs not remain constant: it will depend on the cell edge and on the oxygen parameter, and when Me^{2+} has a magnetic moment, on the relative strengths of the interactions Fe^{3+}-Fe^{3+}, Fe^{3+}-Me^{2+} and Me^{2+}-Me^{2+}, and on the cation distribution.

If the interactions become weaker in the above order, $|\beta|$ or $|\gamma_2|$ will increase as the proportion of the Fe^{3+} ions in the B position increases.

If we would assume that in Guillaud's $MnFe_2O_4$ angles between the moments in the B position occur, formula (2.19) would give $\gamma_2 = -0{\cdot}52$, whereas for $Zn_{0{\cdot}8}Mn_{0{\cdot}2}Fe_2O_4$ we obtain $\gamma_2 = -0{\cdot}17$. This is in itself an argument against this assumption, since the interactions here indeed become weaker in the order Fe^{3+}-Fe^{3+}, Fe^{3+}-Mn^{2+}, Mn^{2+}-Mn^{2+}.

A more serious objection against the assumption of angles in Guillaud's $MnFe_2O_4$ is the linear increase of n_B with the Zn content a he finds for the MnZn ferrites. Assuming angles to exist and γ_2 to be constant, m should decrease linearly with m_a, i.e. with $1-a$. In order to account for the linear *increase* of m we must assume that $|\gamma_2|$ decreases with a in such a way that the angle $180° - 2\psi$ remains very small up to $a = 0.5$, which seems very improbable.

If we assume that for $MnFe_2O_4$ $n_B < m_b - m_a$ only as a result of the above-mentioned local fluctuations in the AB interaction, it still remains difficult to explain why this effect should at first decrease with increasing Zn content a.

The decrease of the Curie temperature with $ZnFe_2O_4$ content [54a, c, d])

can also be accounted for by qualitative considerations. The Curie temperature is primarily determined by the strongest interaction(s), i.e. by the AB interaction as long as this is predominant. The Curie temperature will, therefore, decrease with the number of AB interactions, i.e. with increasing a.

It is clear that angles between the ionic moments in the B position will not occur for materials with very high Curie temperatures.

For normal $ZnFe_2O_4$, prepared by annealing, $n_B = 0{\cdot}0$. Here only BB interactions can occur, and an "antiferromagnetic" arrangement will result, probably with different spin directions in each of the four face-centred sublattices in the B position. A Néel temperature has not so far been found.

When $ZnFe_2O_4$ is quenched, it becomes ferromagnetic [67])[55]) with a high Curie temperature (60 °C). This is clearly caused by AB interaction, which occurs as a result of the presence of some Fe^{3+} in the A position, as has been suggested in both papers cited.

Guillaud has suggested that the presence of a certain amount of Zn^{2+} in the B sites as indicated by the intensities of the X-ray diagrams of his NiZn ferrites [55])[66]) may, apart from all other hypotheses, account for the decrease of the n_B vs a curve for large a values. It seems safe to assume that this effect only plays a secondary rôle. In fact, we shall give examples of materials for which the saturation moment cannot be accounted for at all without the presence of angles between the ionic moments inside the B sublattice (sections 6.4 and 7).

The presence of some Zn ions in the octahedral position must be assumed to account for the following results.

Néel and Brochet [65]) have calculated the ratios of the interactions AA/BB (α) and BB/AB (β) from their susceptibility data for the NiZn ferrites, assuming all Zn^{2+} ions to occupy A sites.

For this case they find extremely high α values for large Zn contents, which according to Anderson's theory are extremely unlikely from geometrical considerations. If it is assumed that a certain small percentage of Zn^{2+} occupies the B positions, α remains small throughout the series of mixed crystals.

REFERENCES

[48]) D. Polder, J. Instn. elect. Engrs **97**, (II), 246-256, 1950.
[49]) E. W. Gorter, C. R. Acad. Sci., Paris **230**, 192-194, 1950.
[50]) E. W. Gorter, Nature **165**, 798-800, 1950.
[51]) R. Pauthenet, C. R. Acad. Sci., Paris **230**, 1842-1843, 1950;
L. Néel, C. R. Acad. Sci., Paris **230**, 190-192, 1950.
[52]) R. Pauthenet and L. Bochirol, J. Phys. Radium **12**, 249-251, 1951.
[53]) R. Pauthenet, Ann. Phys., Paris **7**, 710-747, 1952.
[54a]) C. Guillaud and M. Roux, C.R. Acad. Sci., Paris **229**, 1133-1135, 1949.
[54b]) C. Guillaud and H. Creveaux, C. R. Acad. Sci., Paris **230**, 1256-1258, 1950.
[54c]) C. Guillaud and H. Creveaux, C. R. Acad. Sci., Paris **230**, 1458-1460, 1950.
[54d]) C. Guillaud and M. Sage, C. R. Acad. Sci., Paris **232**, 944-946, 1951.
[55]) C. Guillaud, J. Phys. Radium **12**, 239-248, 1951 (or J. Rech. C.N.R.S. nr 12, 1950).
[56]) M. Fallot, unpublished, 1935, cited from L. Néel, [31]).

[57]) G. O. Jones and F. F. Roberts, Proc. phys. Soc. Lond. **B 65,** 390, 1952.
[58]) G. E. Bacon and F. F. Roberts, Acta cryst. **6,** 57-62, 1953.
[59]) H. G. Beljers and J. S. van Wieringen. Physica, forthcoming.
[60]) See e.g. H. G. Beljers and J. L. Snoek, Philips tech. Rev. **11**, 313-322, 1950.
[61]) C. Kittel, Phys. Rev. **76,** 743-748, 1949.
[62]) H. G. Beljers and D. Polder, Nature, **165,** 800, 1950.
[63]) W. L. Bond, Rev. sci. Instrum. **22,** 344-345. 1951.
[64]) L. Néel, C. R. Acad. Sci., Paris **230,** 375-377, 1950.
[65]) L. Néel and P. Brochet, C.R. Acad. Sci., Paris **230,** 280-282, 1950.
[66]) M. Sage and C. Guillaud, C. R. Acad. Sci., Paris **230,** 1751-1753, 1950.
[67]) F. G. Brockman, Phys. Rev. **77,** 841-842, 1950.
[68]) C. G. Shull, E. O. Wollan and W. C. Koehler, Phys. Rev. **84,** 912-921, 1951.
[69]) J. M. Hastings and L. M. Corliss, Rev. mod. Phys. **25,** 114-121, 1953.
[70]) L. M. Corliss, J. M. Hastings and F. G. Brockmann, Phys. Rev. **90,** 1013-1018, 1953.

5. EXPERIMENTS ON THE ANGLE DEPENDENCE OF THE SUPER-EXCHANGE INTERACTION

5.1. The angle *A*-O-*B* in Spinels

5.1.1. Introduction

The results obtained in many mixed-crystal series, discussed in the previous section, showed that the *BB* interaction was much weaker than the *AB* interaction. Theoretical background for this behaviour was at the time not available *).

Kramers's theory of the superexchange interaction [71]) gave no explicit indications about the order of magnitude of the superexchange interaction, nor about its dependence on the geometrical configuration. Néel, therefore, originally made a crude assumption, called by himself "*certainement inexacte*", that all superexchange interactions Me-O-Me are of equal strength for nearest neighbours Me-Me, and that the *BB* interaction is weak because a direct *positive* interaction Me-Me is active simultaneously with the negative superexchange interaction Me-O-Me.

We supposed that the angle *A*-O-*B* being larger than the angle *B*-O-*B* might play an important rôle.

The angle *A*-O-*B* varies with the parameter *u*, and *u* might be influenced by the size of the ions. Thus the angle *A*-O-*B* might be increased by incorporating a large ion in the *B* position.

We have therefore tried to incorporate Ca^{2+} ions in the spinel structure. $CaFe_2O_4$ is a well-defined compound, but has no spinel structure: the crystal structure is up to now unknown [72]). We found, however, that at high temperatures over a third of the Zn^{2+} ions in $ZnFe_2O_4$ may be replaced by Ca^{2+} ions; these mixed crystals do not decompose when quenched.

It was believed that the Ca^{2+} ions would have a much greater preference for sixfold coordination than Mg^{2+} ions, as in many oxides Ca^{2+} occurs in sixfold or higher coordination.

We supposed that in these CaZn ferrites the large Ca^{2+} ions in the *B* position would cause the *BB* interaction to be less able to compete with the *AB* interaction than in other corresponding ferrites i.e. that the CaZn ferrites would have higher saturation moments.

5.1.2. CaZn ferrite

5.1.2.1 *Experimental*

Materials with the composition $a\,CaO.(1-a)ZnO.1Fe_2O_3$ were prepared, with $a = 0{\cdot}20$, $0{\cdot}30$, $0{\cdot}35$, $0{\cdot}40$, $0{\cdot}50$, $0{\cdot}90$ and $1{\cdot}00$.

*) The magnetic measurements to be given in section 5.1.2.1. were performed after publication of the results described in section 4.4, but before Anderson's theory was known to the author.

The materials were prepared from
$CaCO_3$ (p.a. Merck),
ZnO (Pb 0·01 %, Mg < 0·01 %),
Fe (C 0·03 %),
by method (C), pref. 2 h 1000 °C, milling 4 h. The preparations were sintered at various temperatures and either slowly cooled or quenched.

The X-ray diagrams showed the following results (table VII).

TABLE VII

Phases found for preparations $a\,CaO.(1-a)ZnO.1Fe_2O_3$

a =	1·00	0·90	0·50	0·40	0·35	0·30	0·20
heat treatment	phase(s)						
1200 °C cooled slowly	$CaFe_2O_4$*)		spinel + $CaFe_2O_4$ and/or a-Fe_2O_3				
1250 °C cooled slowly	*melts* ($CaFe_2O_4$)		,,				
1300 °C cooled slowly	—	—	—	—	*melts* spinel + a-Fe_2O_3	spinel + a-Fe_2O_3	spinel
1250 °C quenched	—	—	$CaFe_2O_4$ + spinel		spinel	spinel + a-Fe_2O_3	
1280 °C quenched	—	—	*melts*	spinel + tr. $CaFe_2O_4$	spinel	spinel	
1300 °C quenched	—	—	—	—	*melts*	spinel	

*) An identical pattern is obtained after quenching from 1200 °C.

These results show:

(1) At 1280 °C and 1300 °C equilibrium is obtained for all compositions, but up to 1250 °C no complete reaction is obtained at least for $a = 0{\cdot}20$.

(2) The preparations with $a = 0{\cdot}30$ and $a = 0{\cdot}35$ are pure spinels at $\geqslant$ 1280 °C, but separate into two phases at lower temperatures: only the preparation with $a = 0{\cdot}20$ does not separate into two phases during cooling at the rate used by us.

(3) The temperature for which melting of at least part of the material occurs decreases with increasing a. Only the preparations quenched from 1280 °C are sintered pure spinels for $a = 0{\cdot}20$ - $0{\cdot}35$.

The preparations for which partial melting occurs were not all investigated because the alumina support was slightly porous, so that the correct total composition was not maintained.

Amongst the pure spinels obtained by sintering, those with $a = 0{\cdot}35$, i.e. with the formula $Ca_{0{\cdot}35}Zn_{0{\cdot}65}Fe_2O_4$, obtained by quenching from 1250 °C and 1280 °C gave by far the highest saturation moment (5.30) [74])

and Curie temperature (appr. 300 °C). After heating to the Curie temperature the saturation moment had decreased by 3%, which is an indication of the instability of this composition at low temperatures.

The results for the other spinels are not given here; the saturation moments are below 1·0.

Recently Mr P. B. Braun has made an attempt to determine the cation distribution of $Ca_{0.35}Zn_{0.65}Fe_2O_4$. The intensities observed with a Norelco High-angle X-ray Diffractometer, using Mo $K\alpha$ radiation are given in table VIII.

TABLE VIII

Σh^2	3	8	11	12	16	19	24	27	32
observed	28	102	383	25	62	$\leqslant 1$	41	116	147
calculated	28	112	372	23	71	0	38	114	150

The amount of Ca^{2+} ions in the tetrahedral position per formula unit (t) could not be determined from the present data, because for Mo radiation the scattering power of Fe^{3+} is just intermediate between those of Zn^{2+} and Ca^{2+}.

We therefore write the general formula as follows:

$$Ca_t Zn_{s+t} Fe_{1-s-2t} [Ca_{0.35-t} Zn_{0.65-s-t} Fe_{1+s+2t}] O_4 \quad , \qquad (5.1)$$

in which s could be determined. The best agreement with the observed intensities was found for $s = 0{\cdot}30 \pm 0{\cdot}05$; the intensities calculated for $s = 0{\cdot}30$ are given in table VIII.

The oxygen parameter $u = 0{\cdot}382 \pm 0{\cdot}005$, and slightly decreases with increasing t. The cell edge $a = 8{\cdot}49_5$ Å.

5.1.2.2. *Discussion*

The saturation moment of quenched $Ca_{0.35}Zn_{0.65}Fe_2O_4$ has been given previously. Originally we compared its value ($n_B = 5{\cdot}30$) with that of $Ni_{0.35}Zn_{0.65}Fe_2O_4$ ($n_B = 4{\cdot}8$) [73] [74]) and assumed that all Ca^{2+} ions occupy B sites. The latter assumption has now been proved to be wrong, but also the comparison with the Ni compound is not appropriate, because the replacement of non-magnetic Ca^{2+} by magnetic Ni^{2+} ions will increase the BB interaction more than the AB interaction, i.e. increase $|\beta|$ or $|\gamma_2|$ in the theory for one type of magnetic ion, quite apart from any effect of ionic size.

In the discussion which follows we shall show that the X-ray results since obtained neither prove nor disprove the picture previously proposed.

The general formula for the CaZn and MgZn ferrites is

$$Me^{II}_x Fe_{1-x} [Me^{II}_{1-x} Fe_{1+x}] O_4 , \qquad (5.2)$$

in which Me^{II} represents any mixture of two of the diamagnetic ions Mg^{2+}, Ca^{2+} or Zn^{2+}; x is not known.

The saturation moment is $n_B = 10x$ for antiparallel moments in A and B sites, or below $10x$ when the moments in the B sites are no longer mutually parallel.

It follows that for the CaZn ferrite with $n_B = 5{\cdot}3$, $x \geqslant 0{\cdot}53$ and for the MgZn ferrite with $n_B = 4{\cdot}7$, $x \geqslant 0{\cdot}47$.

For the MgZn ferrites it seems reasonable to assume that γ_2 is independent of an interchange of Mg^{2+} and Zn^{2+} ions between A and B sites, in view of the almost equal ionic radii, so that γ_2, and therefore n_B, will be practically only dependent on x.

A curve n_B vs x for MgZn ferrites has been schematically represented in fig. 13 (I), using a value of γ_2 deduced from $n_B = 3$ for $Zn_{0{\cdot}8}Mg_{0{\cdot}2}Fe_2O_4$, using formula (2.19) and assuming arbitrarily that in the latter material $x = 0{\cdot}82$, i.e. that e.g. all Zn^{2+} ions and 10 % of the Mg^{2+} ions occur in A sites.

The radius of curvature of this curve is determined by the local fluctuations in the AB interactions, and since these radii are similar for different

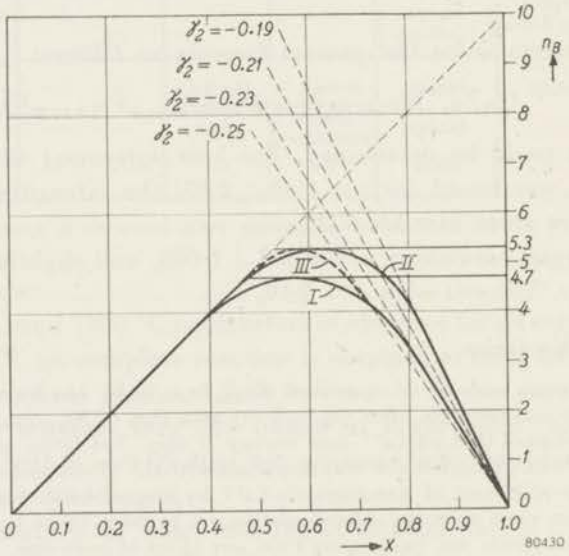

Fig. 13. Schematic representation of saturation moments for materials $Fe_{1-x}\ Me_x[Me_{1-x}\ Fe_{1+x}]O_4$, with Me = non-magnetic ion.
Curve I: Guillaud's experimental saturation moments for MgZn ferrites, schematically redrawn not against the Zn content, but against x.
Curve II: schematic curve drawn through a maximum $n_B = 5{\cdot}3$ with similar radius of curvature as curve I, in order to evaluate γ_2 for $Ca_{0{\cdot}35}Zn_{0{\cdot}65}Fe_2O_4$: γ_2 is then larger than for the MgZn ferrites.
Dashed curve III: schematic curve for $Ca_{0{\cdot}35}Zn_{0{\cdot}65}Fe_2O_4$ with smaller γ_2 than for the MgZn ferrites: the radius of curvature is then very small and therefore unlikely.

MeZn ferrite series (fig. 12), we have drawn a schematic curve II through a maximum $n_B = 5{\cdot}3$ with a similar radius of curvature for our CaZn ferrite, in order to evaluate γ_2.

It is seen that a lower value of $|\gamma_2|$ is thus obtained than for the MgZn ferrites. Only if the radius of curvature is very much smaller (dashed curve III), would $|\gamma_2|$ be larger than for the MgZn ferrites.

We are tempted to conclude that for the CaZn ferrite $|\gamma_2|$ is indeed smaller than for the MgZn ferrites.

This is what we expected for the presence of the greater part of the large Ca^{2+} ions in the B position, i.e. for $t \leqslant 0{\cdot}17_5$. For $t \geqslant 0{\cdot}17_5$ we expected $|\gamma_2|$ to be larger than for the MgZn ferrites.

The minimum value of t is obtained from the X-ray and magnetic measurements: $x = s + 2t \geqslant 0{\cdot}53$, in which $s = 0{\cdot}30 \pm 0{\cdot}05$, gives $t \geqslant 0{\cdot}11_5 \pm 0{\cdot}02_5$.

The values of x for which t is $<$ or $>$ $0{\cdot}17_5$ are deduced from $x = s + 2t$:
$t < 0{\cdot}17_5$ for $x < 0{\cdot}60$;
t either $<$ or $> 0{\cdot}17_5$ for $0{\cdot}60 < x < 0{\cdot}70$;
$t > 0{\cdot}17_5$ for $x > 0{\cdot}70$.

For $x < 0{\cdot}60$ the radius of curvature of the n_B vs x curve would be very small: this is very unlikely, so that we cannot prove that $t < 0{\cdot}17_5$. For $x > 0{\cdot}70$ the radius of curvature would probably be too large, so that a value $0{\cdot}60 < x < 0{\cdot}70$ is most likely. This means that we can only say that the possibility $t < 0{\cdot}17_5$ is not excluded.

The error in the oxygen parameter $u = 0{\cdot}382 \pm 0{\cdot}005$ does not exclude this possibility either.

The fact that the saturation moments of the CaZn ferrites with higher Zn contents are below 1 is no proof either against the picture of large ions influencing the angle A-O-B an thereby the ratio of the interaction BB/AB, because in these materials the values of x may be much larger.

5.2. Prediction of Magnetic Behaviour in other Crystal Structures from Anderson's Theory

5.2.1. Introduction

Anderson's theory provides a useful rule of thumb for predicting the saturation moments of ferrimagnetics when the crystal structure is known: when one kind of magnetic ions is present, the strength of the interactions increases with the angle Me-O-Me from a minimum for 90° to a maximum for 180°; the strength of the interactions, moreover, decreases rapidly with the distances Me-O.

In crystal structures such as the spinel structure and the structures to be discussed in the present section the oxygen ions form an approximately close-packed arrangement with the cations fitting in the interstices. All shortest distances Me-O, therefore, will be of the same order of magnitude (like p and q in the spinel structure, see table I).

The relative directions of the ionic moments in ferrimagnetics, i.e. for the case that only negative interactions occur, may be found by allocating an arbitrary direction to an arbitrary ionic moment, and by

placing antiparallel to it the moments of those surrounding ions for which the angle Me-O-Me is largest and for which the distances Me-O are those of nearest neighbours, say 2·5 Å.

We have applied this rule to some compounds with hexagonal crystal structures, viz. $BaFe^{III}_{12}O_{19}$, $KFe^{III}_{11}O_{17}$ and $BaFe^{II}_{2}Fe^{III}_{16}O_{27}$ [78]).

5.2.2. Application to $BaFe^{III}_{12}O_{19}$ and $KFe^{III}_{11}O_{17}$

The hexagonal unit cells of $BaFe^{III}_{12}O_{19}$ (or $BaO.6Fe_2O_3$) and of $KFe^{III}_{11}O_{17}$ (or $K_2O.11Fe_2O_3$) are shown schematically in fig. 14. The "spinel blocks" consist of 4 horizontal planes containing 4 oxygen ions each, with the cations between these planes. The ionic positions in these "blocks" are not shown: apart from slight differences in parameters they

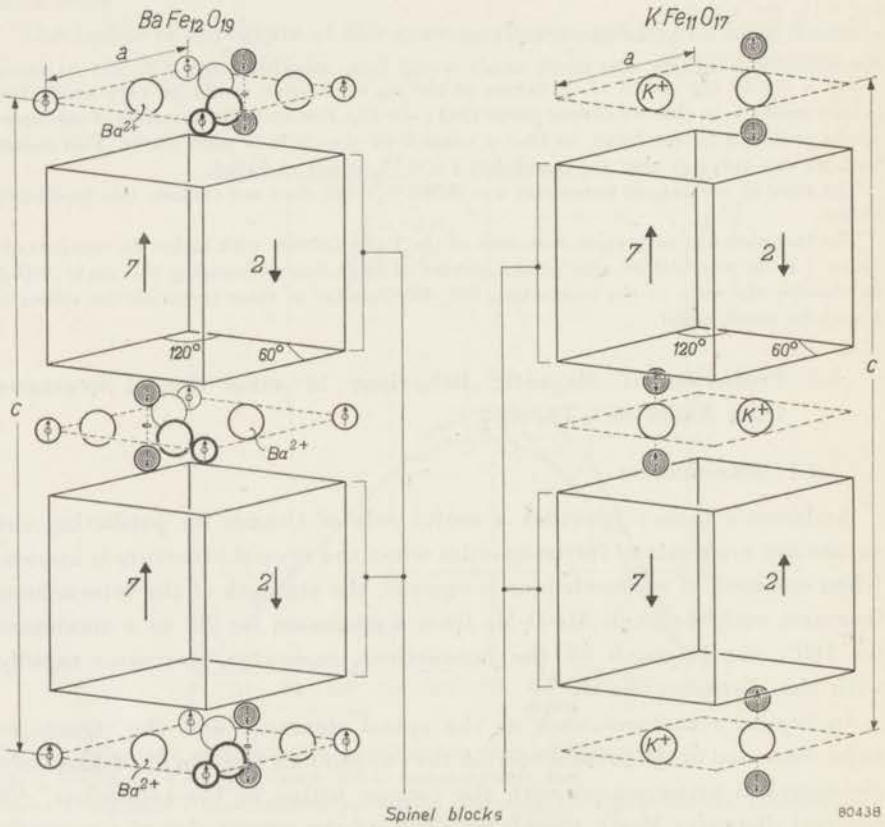

Fig. 14 Unit cells of $BaFe_{12}O_{19}$ and $KFe_{11}O_{17}$ (schematically). Large circles denote oxygen ions, or K^+ or Ba^{2+} ions where indicated; small circles represent ferric ions. The ionic positions inside the "spinel blocks" are not shown: each block contains 4 horizontal planes containing 4 oxygen ions each; between these planes 9 Fe^{3+} are situated, of which 7 have ionic moments pointing in one direction and 2 ionic moments in the opposite direction.

are identical to those in the spinel lattice, with vertical orientation of the [111] axis *).

$BaFe_{12}O_{19}$ *) is isomorphous [75]) with the mineral magnetoplumbite, which has the approximate composition $Pb(Fe_{7\cdot5}Mn_{3\cdot5}Al_{0\cdot5}Ti_{0\cdot5})O_{19}$ [76]). The crystal structure of this mineral was determined by Adelsköld [75]). $KFe_{11}O_{17}$ *) is isomorphous [75]) with "β-alumina", $NaAl_{11}O_{17}$, the structure of which was determined by Beevers and Ross [77]).

The average distances between the horizontal oxygen planes *), and the oxygen-oxygen distances inside the oxygen planes *) are compared with those for a spinel with $a = 8{\cdot}35$ Å (an average cell edge for a ferrite) in table IX.

TABLE IX

Comparison of dimensions in the structures of $BaFe_{12}O_{19}$ and $KFe_{11}O_{17}$ with those of a spinel with $a = 8{\cdot}35$ Å.

structure	c (Å)	a (Å)	average distance between O planes (Å)	distances O-O in O planes (Å)
$BaFe_{12}O_{19}$	$23{\cdot}21_5$**)	5.891**)	$\frac{1}{10}c = 2{\cdot}321_5$	$\frac{1}{2}a = 2{\cdot}945_5$
$KFe_{11}O_{17}$	$23{\cdot}73_9$**)	5·932**)	$\frac{1}{10}c = 2{\cdot}374$	$\frac{1}{2}a = 2{\cdot}966$
spinel	—	(8·35)	$\frac{1}{6}a\sqrt{3} = 2{\cdot}41_0$	$\frac{1}{4}a\sqrt{2} = 2{\cdot}95_2$

**) Values determined by Mr P. B. Braun. These values closely agree with those found by Adelsköld after conversion of the latter from kX into Ångström units.

The slight differences in dimensions shown, and the slight differences in parameter values, which undoubtedly occur but have not been accurately determined, are too small to have any influence on the application of the rule of thumb.

The difference between the two structures is apparent from fig. 14. In the unit cell of the Ba compound the planes containing the Ba^{2+} ion contain in addition three O^{2-} ions, thus giving a twelvefold coordination of the Ba^{2+} ion by oxygen ions, and one Fe^{3+} ion. In the unit cell of the K compound the corresponding planes contain in addition to the K^+ ion only one O^{2-} ion, thus giving a ninefold coordination for the K^+ ion, as has been found in other compounds.

*) For comparison of the complete unit cells see ref. [78]), part III, fig. 2.

Saturation magnetization measurements have been made on oriented single crystals of $BaFe_{12}O_{19}$ [78]) *) and susceptibility measurements on these [78]) and on a polycrystalline specimen of $KFe_{11}O_{17}$. The results may be compared in fig. 15.

$KFe_{11}O_{17}$ was originally prepared by decomposing a solution of K and Fe^{III} nitrates in the stoichiometric proportion, obtained by dissolving in nitric acid
K_2CO_3 (p.a. Merck),
Fe (C 0·03 %).

After prefiring at 800 °C in O_2, milling and sintering for 2 h at 1200 °C in O_2, X-ray diagrams of the resulting preparations, obtained on a Norelco High-angle X-ray Diffractometer, showed strong α-Fe_2O_3 reflexions in addition to those of $KFe_{11}O_{17}$. The preparation became ferromagnetic in humid air, presumably through the presence of $KFeO_2$, which is known to react with water to give γ-Fe_2O_3.

The material was then treated with excess KNO_3 solution, dried, milled and sintered 2h at 1200 °C in O_2: the resulting material shows only $KFe_{11}O_{17}$ reflexions and is stable in humid air.

There is a striking difference in magnetic properties between the two materials: $BaFe_{12}O_{19}$ shows ferromagnetic behaviour with an extrapolated saturation moment of 40 *) (Bohr magnetons) per unit cell. $KFe_{11}O_{17}$ shows antiferromagnetic behaviour (fig. 15). This can be explained by the small difference between the two structures described above and shown in fig. 14. In the Ba compound the pairs of adjacent ferric ions on both sides of the Ba plane (indicated by ◉) have parallel ionic moments, because the (negative) interactions ◉-oxygen-◎ outweigh the ◉-oxygen-◉ interaction, as the angle is nearer to 180° in the former case. In the K compound there is only a large negative interaction ◉-oxygen-◉ between these pairs, so that the ionic moments are antiparallel.

The resultant moments of the spinel blocks are antiparallel to the moments of the adjacent ions, so that in the Ba compound these resultant moments are parallel to those of adjacent blocks, but in the K compound antiparallel.

For the complete unit cells this gives an arrangement $\xrightarrow{16\ Fe^{3+}}\ \xleftarrow{8\ Fe^{3+}}$ with a saturation moment $n_B = 40$ for $BaFe_{12}O_{19}$, and an arrangement $\xrightarrow{11\ Fe^{3+}}\ \xleftarrow{11\ Fe^{3+}}$ with a saturation moment $n_B = 0$ for $KFe_{11}O_{17}$. The agreement between experimental and theoretical values shows that the saturation moment of $BaFe_{12}O_{19}$ may be accounted for without assuming angles to occur between the ionic moments inside one of the sublattices. The $1/\chi$ vs T curve (fig. 15, curve II) shows the hyperbolic shape characteristic for ferrimagnetics.

---

*) Recent measurements on polycrystalline $BaFe_{12}O_{19}$ at liquid-hydrogen temperature and in fields up to 26000 oersteds show that σ_0 is very near to 100 $cgs_{magn}\cdot cm^3/g$, i.e. that $n_B = 40$ (A. L. Stuyts and P. Jongenburger, to be published).

The $1/\chi$ curve of $KFe_{11}O_{17}$ (fig. 15, curve III) shows a break at about 530 °C: this is almost certainly the antiferromagnetic Néel temperature. In view of the above discussion it is not surprising that this is situated near, i.e. slightly above, the Curie temperature of $BaFe_{12}O_{19}$.

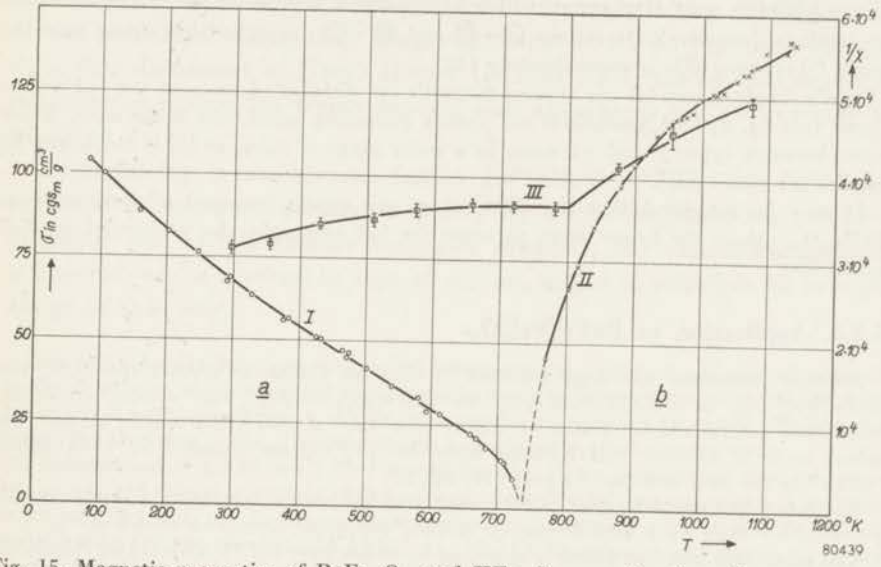

Fig. 15. Magnetic properties of $BaFe_{12}O_{19}$ and $KFe_{11}O_{17}$ as a function of temperature.
Curve I: saturation magnetization (σ) of $BaFe_{12}O_{19}$ (left-hand scale).
Curve II: the inverse of the susceptibility per gram ($1/\chi$) for $BaFe_{12}O_{19}$ above the Curie temperature (right-hand scale).
Curve III: the inverse of the susceptibility per gram ($1/\chi$) for $KFe_{11}O_{17}$ (right-hand scale).

The anomalous slope of the $1/\chi$ vs T curve of $KFe_{11}O_{17}$ below the Néel temperature cannot at present be accounted for. Above the Néel temperature the measurements have not been extended to high enough temperatures to show whether a hyperbola-like curvature, as found for ferrimagnetics, occurs here. From the fact that the tangent to the curve at high temperatures must intersect the T-axis below 0 °K, because all interactions are negative, it may be deduced that such a curvature indeed occurs.

It may be noted that $KFe_{11}O_{17}$ is not an ordinary antiferromagnetic, because inside fairly large regions (viz. the spinel layers) the antiferromagnetism is non-compensated, so that the magnetic behaviour may well be different from that of other antiferromagnetics.

We cannot at present account for the practically linear slope of the σ-T curve of $BaFe_{12}O_{19}$ (fig. 15, curve I).

A theoretical treatment like Néel has given for a lattice containing two sublattices, in order to evaluate the various interaction constants, is very difficult, as the $BaFe_{12}O_{19}$ lattice contains five crystallographically different sublattices [78]). Even if only those interactions involving shortest distances Me-O are taken into account, there are still six different interactions.

We wish to draw attention to a difference beween the $BaFe_{12}O_{19}$ and spinel structures that may have a bearing on this problem.

We have seen (section 2.3.4) that the geometry of the spinel lattice is such that the *AB* interaction is predominant with respect to the *AA* and *BB* interactions.

In $BaFe_{12}O_{19}$ one of the interactions that do not determine the orientation of the ionic moments is probably still fairly strong: the interaction between the sublattices ⊙ and ◍ ([78]), part II, fig. 2*a*), which have parallel ionic moments as a result of the predominant (negative) interactions ⊙ - ○ and ● - ◍ , must be fairly strong, since the angle ⊙ - oxygen - ◍ is approximately 125°.

Néel's simple theory for one type of magnetic ion distributed amongst two sublattices shows (see fig. 8) that anomalous σ-T curves (including practically linear ones, which occur between types *f* and *g*), occur in a wider range of x_a/x_b, as $|\beta|$ is larger and $|\alpha|$ smaller (or vice versa).

It may be suggested that the existence of one strong "competing" interaction in $BaFe_{12}O_{19}$ causes the linear curve to occur for full occupation by magnetic ions of all sublattices.

5.2.3. Application to $BaFe_2^{II}Fe_{16}^{III}O_{27}$

Another compound has been reported [78]) with an analogous crystal structure, viz. $BaFe_2^{II}Fe_{16}^{III}O_{27}$, or $BaO.2FeO.8Fe_2O_3$, or $BaFe_{12}O_{19}.2Fe_3O_4$. The crystal structure, which was determined by Braun [79]), differs from that of $BaFe_{12}O_{19}$ mainly in that the spinel layer is thicker: two formula units $Fe^{II}Fe_2^{III}O_4$ are inserted in each spinel "block" in the unit cell (see [78]) part III, fig. 2*c*).

The saturation magnetization of this compound has been measured on a single crystal, prepared by Wijn by a high-frequency melting technique described elsewhere [80]).

The saturation moment found is about $n_B = 48$ per unit cell *), whereas we calculated $n_B = 56$, assuming the Fe^{2+} ions to occupy octahedral sites inside the spinel blocks i.e. for an arrangement $\underrightarrow{20\,Fe^{3+}}\ \underrightarrow{4Fe^{2+}}\ \underleftarrow{12Fe^{3+}}$.

Other antiparallel arrangements for which n_B is nearer to 48 (e.g. 44) are very unlikely.,

*) Measurements at liquid-hydrogen temperature and in high fields are so far lacking.

REFERENCES.

71) H. A. Kramers, Physica **1**, 182-192, 1934.
72) A. Burdese, Ric. Sci. **22**, 259-264, 1952.
73) J. Phys. Radium **12**, 237-238, 1951.
74) E. J. W. Verwey, P. B. Braun, E. W. Gorter, F. C. Romeijn and J. H. van Santen, Z. phys. Chem. **198**, 6-22, 1951.
75) V. Adelsköld, Arkiv Kemi, Min. Geol. **12A**, No 29, 1-9, 1938.
76) L. G. Berry, Amer. Min. **36**, 512-514, 1951.
77) C. A. Beevers and M. A. S. Ross, Z. Kristallogr. **97**, 57-66, 1937.
78) J. J. Went, G. W. Rathenau, E. W. Gorter and G. W. van Oosterhout, Philips tech. Rev. **13**, 194-208, 1952.
79) P. B. Braun, Nature **170**, 708, 1952.
80) H. P. J. Wijn, Nature **170**, 707, 1952.

6. SATURATION MOMENT AND CRYSTAL CHEMISTRY OF FERRIMAGNETIC SPINELS CONTAINING TITANIUM

6.1. Introduction to the Sections 6-8

The investigations to be reported in sections 6, 7 and 8 have been started in order to obtain a mixed-crystal series in which the difference of the sublattice saturation magnetizations at 0 °K, $m_b - m_a$, changes sign. Our discussion of Néel's theory (section 2.2.1) shows that for compositions near that for which $m_b - m_a = 0$ anomalous σ-T curves may be expected.

By replacing in an inverse ferrite $Fe^{3+}[Me^{2+}Fe^{3+}]O_4$ the ferric ion in the B position completely or partly by a non-magnetic ion, or by a magnetic ion with a smaller magnetic moment, the saturation moment is lowered, and a reversal in sign of $m_b - m_a$ might in principle be brought about in this way.

Supposing that the distribution of the other ions remains unaltered, and that all moments in the B position are antiparallel to all those in the A position, replacement of the ferric ion in the B position will give a change in saturation moment which can be simply calculated. The ferric ion in the B position might be replaced in the following ways:
(1) Substitution of 1 Al^{3+} for 1 Fe^{3+} would for the above supposition give $m_b - m_a = m_{Me^{2+}} - 5$, and thus give reversal if the moment of the divalent ion $m_{Me^{2+}} < 5$. Aluminium is known, however, not to have a great preference for sixfold with respect to fourfold coordination (cf. the silicates and $Al[Li_{0.5}Al_{1.5}]O_4$) *). Moreover it was known to us that a miscibility gap occurs in the system $MgFe_2O_4$-$MgAl_2O_4$ (section 1.2, ref. [7])). In view of the large difference in cell edge between the ferrites and the corresponding aluminates this might have been a very general phenomenon. For these reasons this substitution was not the first to be investigated.

The system $NiFe_2O_4$-$NiAl_2O_4$, as well as the systems $MgFe_2O_4$-$MgAl_2O_4$ and $Fe^{II}Fe_2O_4$-$Fe^{II}Al_2O_4$, investigated by other authors, are discussed in section 8.
(2) Substitution of 1 Cr^{3+}, which has a strong preference for sixfold coordination, for 1 Fe^{3+}, gives $m_b - m_a = m_{Me^{2+}} - 2$, assuming $m_{Cr^{3+}} = 3$, and would thus give reversal in sign of $m_b - m_a$ if $m_{Me^{2+}} < 2$. By substituting Cr^{3+} for Fe^{3+} in Mg ferrite or Cu ferrite, therefore, one might get such a reversal; these ferrites are, however, already partly normal. $Fe[Li_{0.5}Fe_{1.5}]O_4$ has a completely inverse arrangement, however, and thus, with the above suppositions, replacement of 1·25 Fe^{3+} by 1·25 Cr^{3+} gives $m_b - m_a = 0$, and replacement of $>1{\cdot}25$ Fe^{3+} by $>1{\cdot}25$ Cr^{3+} reversal of $m_b - m_a$. This system will be reported upon in section 7.
(3) Substitution of $0{\cdot}5\ Me^{2+} + 0{\cdot}5\ Ti^{4+}$ for Fe_B^{3+} would, with the above suppositions, give $m_b - m_a = 1{\cdot}5\ m_{Me^{2+}} - 5$ and thus reversal of $m_b - m_a$ for $m_{Me^{2+}} \leqslant 3{\cdot}33$, i.e. for $Me^{2+} = Ni^{2+}$ (or Cu^{2+} or Mg^{2+}). The system with $Me^{2+} = Ni^{2+}$ is one of the systems reported upon in section 6.

It will be seen, however, that neither Al^{3+} nor Ti^{4+} occupy octahedral sites only, and that substitution of Cr^{3+} for Fe^{3+} alters the distribution of the other cations.

In the first system to be described in the present section 6 we have replaced 1 Fe^{3+} in $Fe[NiFe]O_4$ by $(0{\cdot}5\ Ni^{2+} + 0{\cdot}5\ Ti^{4+})$. Nickel is known to have a strong preference for sixfold coordination: nickel titanate,

*) Scandium has, but is very expensive.

Ni_2TiO_4, does not exist [81] [82] *). In another series, viz. $Zn_{2-a}Ni_aTiO_4$, investigated by Birnbaum and Scott [81], the spinel phase extends only up to $a = 1{\cdot}0$, which suggests that Ni^{2+} and Ti^{4+} will occupy octahedral sites only, corresponding to a formula $Zn[NiTi]O_4$ for $a = 1$. For this reason we have originally extended the series $Ni_{1+a}Fe_{2-2a}Ti_aO_4$, nickel ferrite-nickel titanate, only up to $a = 0{\cdot}5$, i.e. to the composition $Ni_{1{\cdot}5}FeTi_{0{\cdot}5}O_4$.

Materials with $a = 0{\cdot}60$, $0{\cdot}70$, $0{\cdot}75$ and $0{\cdot}80$ have since also been prepared: the X-ray diagrams of these preparations show reflexions of an ilmenite phase ($NiTiO_3$), with intensities increasing in the above order, next to the spinel pattern, and possibly NiO reflexions, which, however, coincide with strong spinel reflexions. This behaviour is the same as that found in the series $Zn_{2-a}Ni_aTiO_4$ for $a > 1$ [81]) and shows up the instability of Ni_2TiO_4 even in mixed crystals.

Two more series of mixed crystals have been investigated in which with the above suppositions m_b—m_a would change sign. These systems, $Ni_{1{\cdot}5}FeTi_{0{\cdot}5}O_4$-$NiZn_{0{\cdot}5}FeTi_{0{\cdot}5}O_4$ **) and $Ni_{1{\cdot}5}FeTi_{0{\cdot}5}O_4$-$Mn_{1{\cdot}5}FeTi_{0{\cdot}5}O_4$, are reported upon in sections 6.3 and 6.4 respectively.

6.2. The system $Ni^{II}_{1+a}Fe^{III}_{2-2a}Ti^{IV}_aO_4$ ($NiFe_2O_4$-$Ni_{1{\cdot}5}FeTi_{0{\cdot}5}O_4$)

6.2.1. Experimental

Materials with the above general formula were prepared with $a = 0$, $0{\cdot}1$, $0{\cdot}2$, $0{\cdot}3$, $0{\cdot}4$ and $0{\cdot}5$.

These materials were prepared from
Fe (C 0·03 %),
Ni (Si 0·02 %, Co 0·01$_0$ %, Pb 0·01 %),
TiO_2 (Si 0·13 %, Fe 0·02$_5$ %, Al 0·01 %, Mg 0·01 %),
by method (B), pref. 600 °C until complete decomposition of the nitrates is obtained, milling, pref. 4 h 1000 °C, remilling, sint. 4 h 1200 °C in O_2.

Two series of samples were prepared:
(1) cooled slowly from 1200 °C in O_2 and annealed in O_2 at low temperatures (3 h 800 °C, 7 h 700 °C, 30 h 600 °C);
(2) quenched from 1200 °C by dropping rapidly into a sodium-chloride solution, which is afterwards rinsed out with boiling distilled water.

Chemical analysis: no detectable amounts of Fe^{2+} were present in either series.

X-ray diffraction patterns obtained on a Norelco High-angle X-ray Diffractometer showed the preparations to be pure spinels, but yielded

*) Unpublished observation by the author for various firing temperatures.
**) Here m_b—m_a would change sign if an additional supposition is made, viz. that Zn^{2+} occupies tetrahedral sites only.

no data as regards ionic distribution, which fact is due to the small difference in scattering powers of the ions present. Saturation vs temperature curves were measured for all preparations *). The saturation moments in Bohr magnetons are given in fig. 16*a* and in table X. The Curie temperatures (Θ) for all samples and the cell edges for the annealed preparations only, are also given in the table.

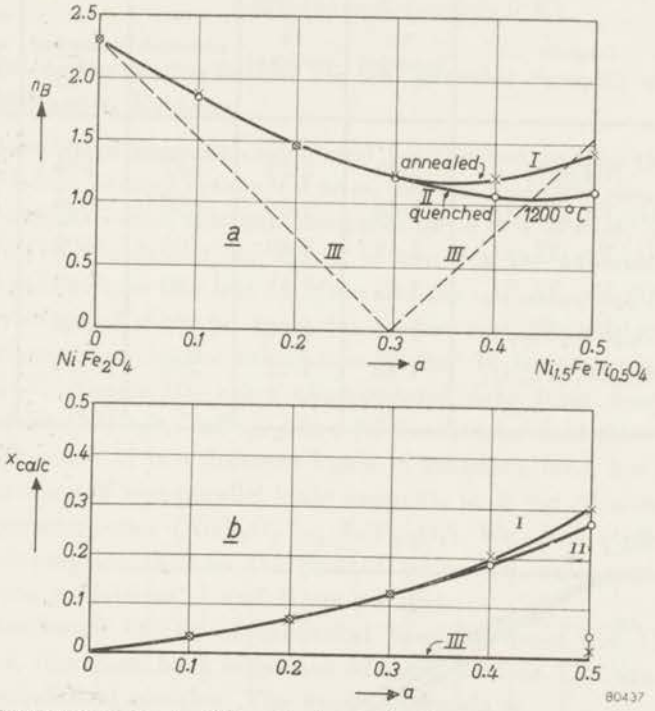

Fig. 16*a*. Saturation moments of the mixed-crystal series $Ni_{1+a}Fe_{2-2a}Ti_aO_4$, for $a = 0$ - 0·5. Curve I: annealed samples; curve II: samples quenched from 1200 °C; line III: saturation moments calculated for all Ti^{4+} and Ni^{2+} ions in the octahedral position.
b. Amount of Ti^{4+} ions in the tetrahedral position per formula unit (x), calculated from the saturation moments shown in fig. 16*a*, assuming the Ni^{2+} ions to occupy octahedral sites throughout the series.
Curve I: annealed samples; curve II: samples quenched from 1200 °C; line III: the line $x = 0$, for which line III of fig. 16*a* was drawn.

The reduced saturation magnetization vs temperature (i.e. $\sigma_T/\sigma_{T=0}$ vs T/Θ) curves for the annealed preparations are given in fig. 17. Mr H. G. Beljers has kindly measured the effective *g*-factor (g_{eff}) of annealed $Ni_{1\cdot5}FeTi_{0\cdot5}O_4$ for us by the ferromagnetic resonance method at 3·18 and 1·24 cm wavelengths on spheres of about 0·5 mm diameter.

*) Fields up to 5900 oersteds were used, also at 20 °K.

TABLE X

Saturation moments, Curie temperatures and cell edges for the series $Ni^{II}_{1+a}Fe^{III}_{2-2a}Ti^{IV}_{a}O_4$

Ti content a	formula	n_B annealed	n_B quenched	Θ annealed (°C)	Θ quenched (°C)	cell edge annealed Å
0	$NiFe_2O_4$	2·29	2·29	585	585	8·337
0·1	$Ni_{1·1}Fe_{1·8}Ti_{0·1}O_4$	1·88	1·85	550	550	$8·337_5$
0·2	$Ni_{1·2}Fe_{1·6}Ti_{0·2}O_4$	1·49	1·48	500	500	8·338
0·3	$Ni_{1·3}Fe_{1·4}Ti_{0·3}O_4$	1·25	1·23	440	440	$8·338_5$
0·4	$Ni_{1·4}Fe_{1·2}Ti_{0·4}O_4$	1·24	1·10	375	356	8·339
0·5	$Ni_{1·5}Fe_{1·0}Ti_{0·5}O_4$	1·45	1·12	293	265	—

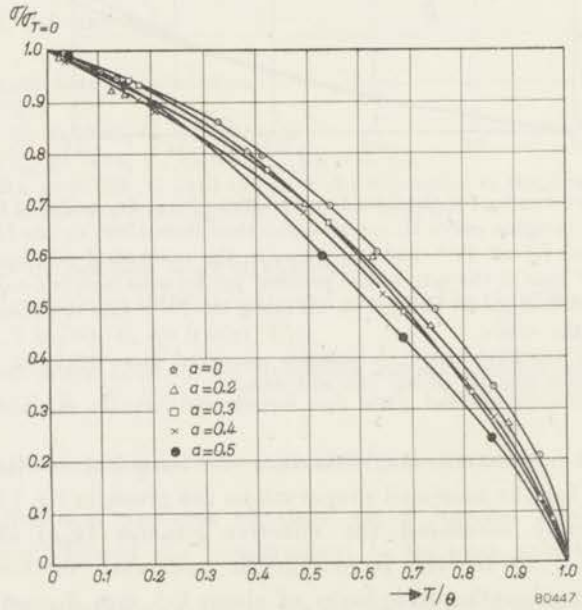

Fig. 17. Reduced saturation-magnetization vs temperature (σ/σ_0 vs T/Θ) curves for the mixed-crystal series $Ni_{1+a}Fe_{2-2a}Ti_aO_4$.

The results are

$Ni_{1.5}FeTi_{0.5}O_4$ (annealed)

wavelength	temperature	g_{eff}
1·24 cm	300 °K	2·70-2·71
3·18 cm	293 °K	2·73
3·18 cm	83 °K	2·85
	(extrapolated towards 0°K)	2·90

6.2.2. Discussion of the Results for the Annealed Samples and Neutron-Diffraction Evidence

The saturation moments calculated for the assumption that all Ni^{2+} and Ti^{4+} ions occupy octahedral sites, and for mutually completely antiparallel orientation of the ionic moments on A and B sites, are indicated in fig. 16*a* by the dashed line III. It is seen that the experimental curves deviate widely from this line *). Moreover the σ-T curves of the compositions investigated show no anomalous behaviour. Obviously one of the assumptions made in the calculation of line II is incorrect.

Dr K. F. Niessen [83]), using experimental data from another mixed-crystal series ($NiFe_2O_4$-$ZnFe_2O_4$) in a Néel molecular-field theory, extended for the presence of two different kinds of magnetic ions, has shown that the occurrence of non-parallel ionic moments in B (or A) sites is unlikely in the present series ($NiFe_2O_4$-$Ni_{1.5}FeTi_{0.5}O_4$). We shall stick, therefore, to our assumption that in the present series the ionic moments inside each of the sublattices A and B are parallel.

The deviations of the experimental moments from line III must be explained, therefore, by a migration of some Ni^{2+} or Ti^{4+} ions, or both, to the tetrahedral position. The general formula is

$$Ni_y\, Ti_x\, Fe_{1-x-y}\, [Ni_{1+a-y}\, Fe_{1-2a+x+y}\, Ti_{a-x}]\, O_4\,, \qquad (6.1)$$

for which for antiparallel moments in A and B positions

$$n_B = |m_b - m_a|\,,$$

while

$$m_b - m_a = 2{\cdot}3 - 7{\cdot}7a + 10x + (7{\cdot}7 - p)y. \qquad (6.2)$$

In this equation $p = (g_{Ni^{2+}})_A$, the g-factor of Ni^{2+} in the A position **).

*) Except for $a = 0{\cdot}5$, where, moreover, a cation distribution $Fe[Ni_{1.5}Ti_{0.5}]O_4$ a priori seemed likely because of the possibility of long-range order of the $Fe[Li_{0.5}Fe_{1.5}]O_4$ type.

**) In view of the difference between the crystalline electric fields in the A and B position $(g_{Ni^{2+}})_A$ will be different from (and presumably higher than) $(g_{Ni^{2+}})_B$. Dr J. S. Smart (private communication, to be published in Phys. Rev.) uses a value $(g_{Ni^{2+}})_A = 3{\cdot}5$, obtained from susceptibility measurements on $NiAl_2O_4$.

From the experimental n_B values of table X we obtain, using this formula

$$\text{for } a = 0{\cdot}1,\ 0{\cdot}2,\ 0{\cdot}3,\ 0{\cdot}4 \text{ and } 0{\cdot}5$$

$$10x + (7{\cdot}7 - p)y = 0{\cdot}35,\ 0{\cdot}73,\ 1{\cdot}26,\ 2{\cdot}02 \text{ and } 3{\cdot}00 \text{ or } 0{\cdot}10 \text{ respectively.}$$

For $a = 0{\cdot}5$ there are two solutions: the second figure indicates the solution for which $m_b - m_a < 0$.

There is ample evidence that it is mainly Ti^{4+} rather than Ni^{2+} ions that migrate to the tetrahedral position:

(1) Niessen [84]) has calculated, in a manner indicated above, that the Curie temperatures given in table X can be accounted for only by assuming an increasing migration of Ti^{4+} ions to the A sites with increasing a *).

(2) The value of g_{eff}, extrapolated towards $T = 0$ °K may be used together with n_B to determine the cation distribution, using formula (4.6) for g_{eff}. Using the values for $Ni_{1{\cdot}5}FeTi_{0{\cdot}5}O_4$ ($a = 0{\cdot}5$) we have

$$n_B = \pm\,[-1{\cdot}55 + 10x + (7{\cdot}7 - p)y] = 1{\cdot}45$$

and

$$g_{eff} = \pm\left(\frac{n_B}{-1 + 5x + 3y}\right) = 2{\cdot}90,$$

which equations give only one physically possible solution:

$$x = 0{\cdot}30, \qquad y = 0.$$

This means that only (or, in view of the uncertainty of the extrapolation of g_{eff} towards 0 °K, practically only) Ti^{4+} ions migrate to the tetrahedral position and that $m_b - m_a > 0$.

We wish to draw attention to the fact that generally for ferrimagnetics containing two different kinds of magnetic ions, the cation distribution may be calculated from g_{eff} and n_B, provided the g-factors of the ions are known and sufficiently different, and provided the ionic moments inside each lattice position are parallel [85]) **).

Although theory cannot yet account for details such as the frequency dependence of the effective g-factor, we feel justified in using g_{eff} in the above manner to determine the approximate cation distribution.

(3) Neutron diffraction patterns, kindly made for us by Dr C. G. Shull ***) for the annealed preparations with $a = 0$, 0·3 and 0·5 show a regular

---

*) This result was obtained before the following experimental evidence, given sub (2) and (3), was available.

**) J. S. Smart has independently used this method for determining the cation distribution in the series $NiFe_2O_4$-$NiAl_2O_4$ (see section 8) (private communication from Dr Smart, to be published Phys. Rev). For non-parallel ionic moments inside one lattice position see section 6.3.2.

***) The author is indebted to Dr Shull for making these measurements for him.

decrease of the intensity of the 220 reflexion (structure factor $= 8f_{tetr}$), which points to an increasing amount of Ti^{4+} in the A sites in this order, in view of the very small neutron scattering cross-section of the Ti nucleus.

A comparison of the experimental intensities of the neutron diffraction pattern of $Ni_{1\cdot5}FeTi_{0\cdot5}O_4$, with those calculated for the distribution

$$Fe_{0\cdot7}Ti_{0\cdot3}[Ni_{1\cdot5}Fe_{0\cdot3}Ti_{0\cdot2}]O_4 \quad , \qquad (6.3)$$

taking into account the magnetic contribution to these intensities, will be given elsewhere.

In view of the above evidence we feel justified in assuming $y \approx 0$ and calculating x from the saturation moments for the whole series of mixed crystals. The values obtained are given in fig. 16*b*. The distribution in the annealed samples is very near to one in which Ni^{2+} occupies the octahedral position and Fe^{3+} and Ti^{4+} are distributed at random amongst the remaining sites, i.e.

$$Fe_{0\cdot667}Ti_{0\cdot333}[Ni_{1\cdot5}Fe_{0\cdot333}Ti_{0\cdot167}]O_4.$$

The presence of Ti^{4+} ions in tetrahedral coordination is rather unexpected. So far the only indication of the occurrence of Ti^{4+} ions in tetrahedral coordination to our knowledge is the incorporation of Ti^{4+} activator ions in SiO_2 and Zn_2SiO_4 phosphors [86]): in the structures of the latter compounds the cations occur in tetrahedral coordination only.

J. S. Smart *) has shown for another system of ternary spinels ($NiFe_2O_4$-$NiAl_2O_4$) that in the two Boltzmann distribution formulae of the type of formula (1.1.) of section 1.2.6 the values of the energies of interchange of two cations between the two crystallographic positions E can be chosen in such a way that the theoretical cation distribution curves coincide with the experimental ones. These curves are of the same type as those found in the present system for the annealed and quenched samples (fig. 16*b*).

This suggests that our distribution curves can be qualitatively accounted for without taking into account the occurrence of short-range order. We shall see, however, that the decrease of n_B on quenching cannot be accounted for without the influence of short-range order.

6.2.3. **Discussion of the Results for the Quenched Samples**

The saturation moments and the Curie temperatures for the quenched samples show a decrease with respect to those for the annealed samples near $a = 0\cdot5$.

*) See footnote p. 72.

Quenching generally results in the preservation of a more random distribution of the cations amongst A and B sites. Formula (6.2) shows that an increase of y gives an increase of n_B, and even for an arrangement in which the Fe^{3+} and Ti^{4+} ions are kept distributed about at random amongst the sites not occupied by Ni^{2+}, i.e. for $x \approx (1-y)a/(2-a)$, the n_B values calculated are higher than the experimental values for the annealed samples. The saturation moment alone, therefore, leads to the conclusion that quenching primarily results in a decrease of x, and thus in a *less* statistical distribution of Ti^{4+} and Fe^{3+} ions amongst the available sites. This paradox is removed only by assuming that the Ti^{4+} ions have some preference for the B sites with respect to the Fe^{3+} ions, which is still noticeable in the quenched sample ($x = 0{\cdot}27$). During slow cooling entropy alone would cause more Ti^{4+} ions to migrate to the B sites, but in fact more Ti^{4+} then move to the A sites ($x = 0{\cdot}30$), presumably because the gain in short-range-order energy of Ti^{4+} and Fe^{3+} ions in the A sites outweighs the combined effect of entropy and any loss of short-range order in the B sites.

Our knowledge of the various energy terms involved is too small to account for this effect.

6.3. The system $Ni^{II}_{1.5-a}Zn^{II}_{a}Fe^{III}Ti^{IV}_{0.5}O_4$ ($Ni_{1.5}FeTi_{0.5}O_4$-$NiZn_{0.5}FeTi_{0.5}O_4$)

6.3.1. Experimental

Materials with the above general formula were prepared with $a = 0$ *), 0·1, 0·2, 0·3, 0·4 and 0·5.

The preparation was carried out in the same manner as for the materials described in the preceding system (6.2); ZnO (AnalaR) was used as an additional raw material.

Two series of samples were prepared, either annealed at low temperatures, or quenched from 1200 °C, like in section 6.2. Chemical analysis showed no detectable amounts of Fe^{2+} in either series.

The X-ray diffraction patterns obtained on a Norelco X-ray Diffractometer showed the preparations to be pure spinels; no data as regards ionic distribution could be obtained. The saturation moments **) in Bohr magnetons are given in fig. 18*a* and in table XI; the Curie temperatures for all samples and the cell edges for the annealed preparations only, are also given in table XI.

The reduced saturation vs temperature ($\sigma_T/\sigma_{T=0}$ vs T/Θ) curves for the annealed preparations are given in fig. 19. For the annealed sample of $NiZn_{0.5}FeTi_{0.5}O_4$ the effective g-factor was measured by Mr H. G. Beljers.

*) This is the preparation of the preceding series with $a = 0{\cdot}5$.

**) Fields up to 5900 oersteds were used, also at 20 °K.

TABLE XI

Saturation moments, Curie temperatures and celle edges for the series $Ni^{II}_{1\cdot5-a}Zn^{II}_{a}Fe^{III}Ti^{IV}_{0\cdot5}O_4$

Zn content a	formula	n_B annealed	n_B quenched	Θ annealed (°C)	Θ quenched (°C)	cell edge annealed (Å)
0	$Ni_{1\cdot5}FeTi_{0\cdot5}O_4$	1·44	1·12	293	265	—
0·1	$Ni_{1\cdot4}Zn_{0\cdot1}FeTi_{0\cdot5}O_4$	1·02	1·04	267	250	8·348
0·2	$Ni_{1\cdot3}Zn_{0\cdot2}FeTi_{0\cdot5}O_4$	1·07	1·34	265	235	8·355
0·3	$Ni_{1\cdot2}Zn_{0\cdot3}FeTi_{0\cdot5}O_4$	1·32	$1\cdot52_5$	264	220	8·365
0·4	$Ni_{1\cdot1}Zn_{0\cdot4}FeTi_{0\cdot5}O_4$	1·73	1·82	240	195	8·372
0·5	$NiZn_{0\cdot5}FeTi_{0\cdot5}O_4$	2·1	2·1	225	172	8·382

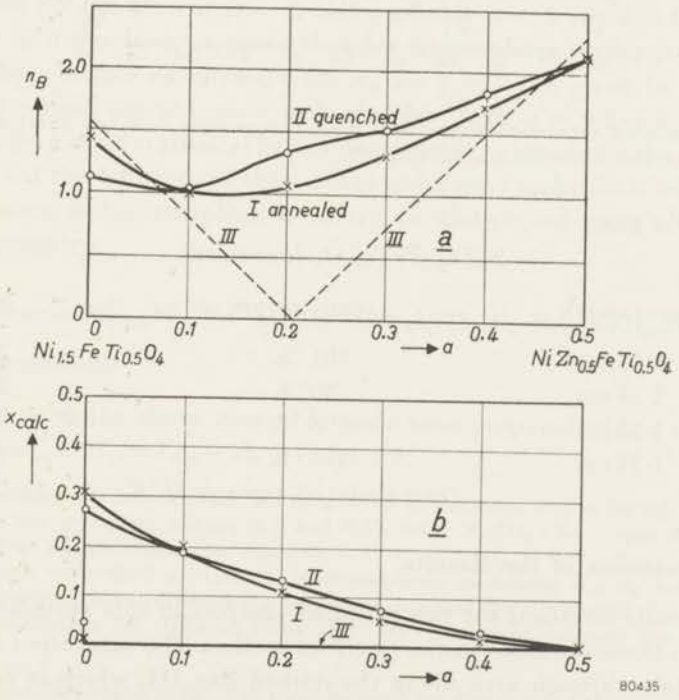

Fig. 18*a*. Saturation moments of the mixed-crystal series $Ni_{1\cdot5-a}Zn_aFeTi_{0\cdot5}O_4$, for $a = 0$ - 0·5. Curve I: annealed samples; curve II: samples quenched from 1200 °C; line III: saturation moments calculated for all Ti^{4+} and Ni^{2+} ions in the octahedral position and all Zn^{2+} ions in the tetrahedral position.

b. Amount of Ti^{4+} ions in the tetrahedral position per formula unit (x), calculated from the saturation moments shown in fig. 18*a*, assuming the Zn^{2+} ions to occupy tetrahedral sited and the Ni^{2+} ions octahedral sites throughout the series.

Curve I: annealed samples; curve II: samples quenched from 1200 °C; line III: the line $x = 0$ for which line III of fig. 18*a* was drawn.

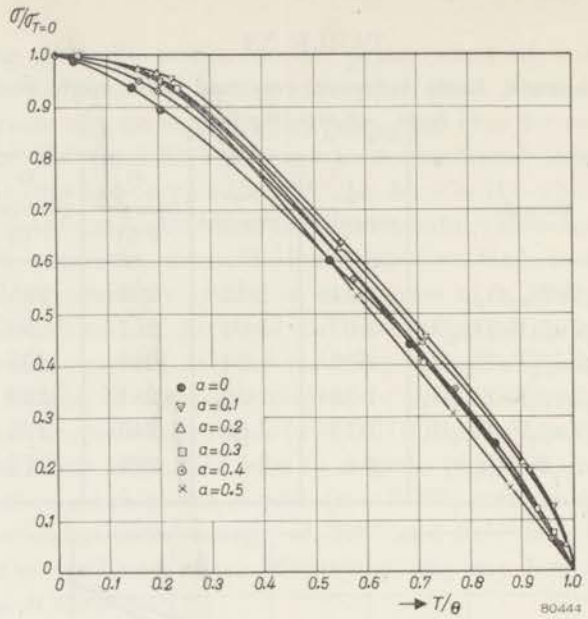

Fig. 19. Reduced saturation-magnetization vs temperature (σ/σ_0 vs T/Θ) curves for the mixed-crystal series $Ni_{1\cdot5-a}Zn_aFeTi_{0\cdot5}O_4$.

The results are

$NiZn_{0\cdot5}FeTi_{0\cdot5}O_4$ (annealed)

wavelength	temperature	g_{eff}
3·18 cm	301 °K	2·33
3·24 cm	90 °K	2·44
1·24 cm	298 °K	2·19
1·24 cm	143 °K	2·19
	(extrapolated towards 0 °K	≈2·19

6.3.2. **Discussion of the Results**

The results obtained for the annealed samples in this system are very similar to those obtained in the previous section. The saturation moments do not pass through zero along the dashed line III, which is calculated for Zn^{2+} in tetrahedral sites and Ni^{2+} and Ti^{4+} in octahedral sites. None of the materials investigated show anomalous σ-T curves (fig. 19).

This result is understood from the fact that for $Ni_{1\cdot5}FeTi_{0\cdot5}O_4$, as we have seen, $m_b > m_a$. We shall now try to deduce the cation distributions from the experimental data. In view of the fact that the amount of Fe^{3+} ions in the A sites for $a = 0\cdot5$ is only about 0·5, we have to reckon with the possibility of non-parallel ionic moments inside the B position.

The general formula of $NiZn_{0\cdot5}FeTi_{0\cdot5}O_4$ ($a = 0\cdot5$) is represented by

$$(Zn + Ti)_{x'}Ni_yFe_{1-x'-y}[Ni_{1-y}Fe_{x'+y}(Zn + Ti)_{1-x'}]O_4.$$

The usual equation for n_B and g_{eff} for parallel ionic moments in the B position yield one physically possible solution for the annealed sample, viz. $x' = 0\cdot45$, $y = 0\cdot07$ (for $(g_{Ni^{2+}})_A = 3\cdot5$). As the simultaneous occurrence of appreciable amounts of Ni^{2+} ions in A sites and of Zn^{2+} ions in B sites in an annealed sample may be ruled out as being unlikely from every crystal-chemical point of view, another arrangement with not quite parallel moments in the B position, i.e. $x' \approx 0\cdot5$ and $y = 0$, seems more likely *). It may be noted that, unlike the saturation moments, the Curie temperatures for the quenched and annealed samples are different, so that the cation distributions probably are not quite the same.

The amount of Ti^{4+} ions in the A position, which we shall denote by x, is $x = 0\cdot30$ for Zn content $a = 0$, and probably $x \approx 0$ for $a = 0\cdot5$, both with $y = 0$; it has been assumed that for intermediate compositions also $y \approx 0$. The x values calculated from n_B for $y = 0$ are given in fig. 18*b*.

The n_B values for the quenched samples with $a = 0\cdot2$-$0\cdot4$ may be explained by a more statistical cation distribution, whereas for the material with $a = 0\cdot5$ the influence of short-range order may make itself felt again.

The system is too complicated to try to understand more about the crystal chemistry.

6.4. The System $Ni^{II}_{1\cdot5-a}Mn^{II}_aFe^{III}Ti^{IV}_{0\cdot5}O_4$ ($Ni_{1\cdot5}FeTi_{0\cdot5}O_4$-$Mn_{1\cdot5}FeTi_{0\cdot5}O_4$)

6.4.1. Experimental

Materials with the above general formula were prepared with $a = 0$ **), $0\cdot2$, $0\cdot4$, $0\cdot57_5$, $0\cdot67_5$, $0\cdot77_5$, $0\cdot95$, $1\cdot1$ and $1\cdot5$.

The preparation of the materials was carried out in the same way as for the materials described in the preceding section (6.2 and 6.3), using $MnCO_3$ (Na < approx. 0·1 %, Mg 0·01 %) as an additional raw material.

The samples were fired at 1200 °C in atmospheres containing N_2, H_2 and CO_2 in different proportions: X-ray diffraction patterns and chemical analysis showed that preparations with different a, i.e. different ratios Mn^{2+}/Ni^{2+}, required different atmospheres.

---

*) For the case that angles $(180° - 2\psi)$ occur between the directions of the ionic moments inside the B sublattice, we read formula (4.5) in such a way that $(M_{total})_B$ and $(M_{spin})_B$ are the *resultant* moments of the B sublattice, i.e. we use

$$n_B = \left| \sum_i (x_i g_i S_i)_A - \sum_i (x_i g_i S_i)_B \sin\psi \right| , \qquad (6.3)$$

$$g_{eff} = \left| \frac{n_B}{\sum_i (x_i S_i)_A \quad - \sum_i (x_i S_i)_B \sin\psi} \right| . \qquad (6.4)$$

**) This is the preparation of section 6.2 with $a = 0\cdot5$.

Adjustment of the oxygen content was carried out by heating for 3 h at 1100 °C fired rods with known oxygen deficit in sealed evacuated quartz tubes which also contained an amount of BaO_2 calculated to give off just the amount of O_2 necessary to oxidize the rods to the correct composition.

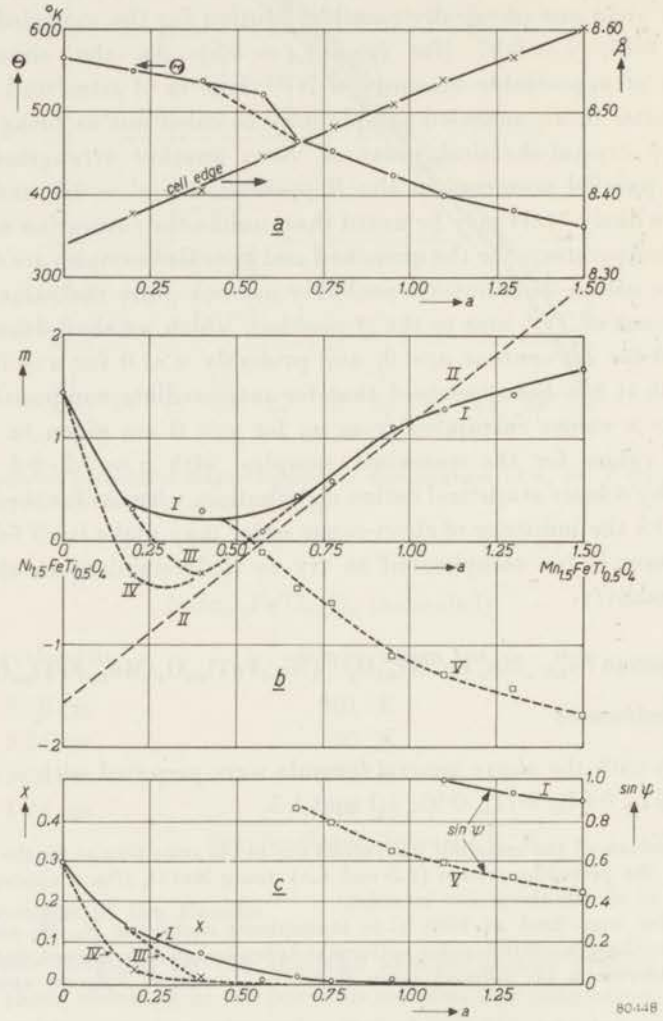

Fig. 20. Properties of the mixed-crystal series $Ni_{1.5-a}Mn_aFeTi_{0.5}O_4$.
a. Curie temperature Θ (°K, left-hand scale) and cell edges (Å, right-hand scale).
b. Saturation moments m; the sign of m is not known with certainty.
Curve I: most probably curve; line II: saturation moments calculated for all Ti^{4+} and Ni^{2+} ions in octahedral sites, without angles between the ionic moments inside one of the sublattices; curves III, IV, V: other possible curves.
c. Amount of Ti^{4+} ions in the tetrahedral position per formula unit (x) for the cases I, III and IV (left-hand scale).
Sin ψ, for angles $180° - 2\psi$ occurring between the directions of the ionic moments in B positions for the cases I and V (right-hand scale).

The preparations for which the measurements reported upon below were carried out contained the following amounts of excess *) oxygen:

a =	0·2	0·4	0·575	0·675	0·775	0·95	1·1	1·3	1·5
oxygen, wt %	0·04	0·11	0·04	−0·04	0·06	0·05	$-0{\cdot}01_5$	0·00	−0·1

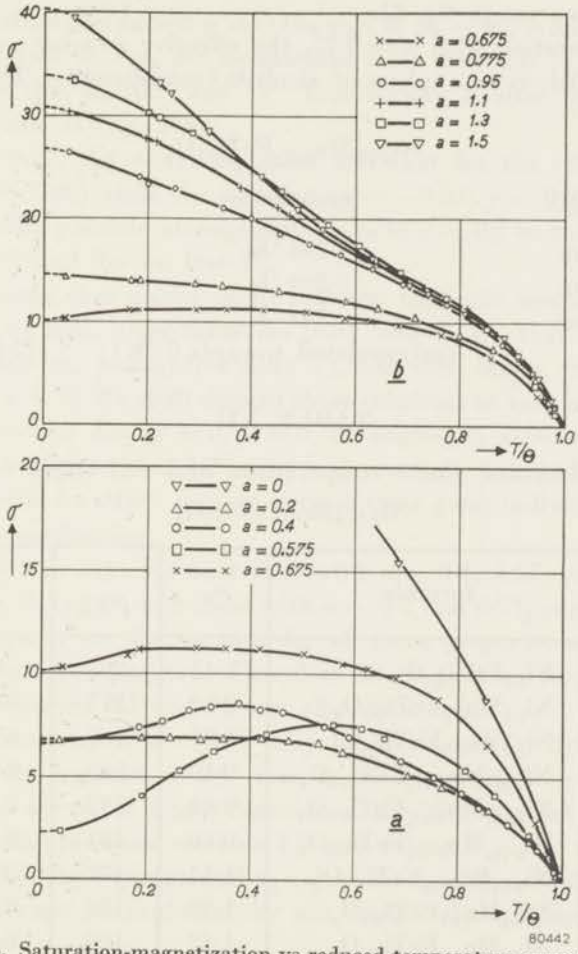

Fig. 21 *a* and *b*. Saturation-magnetization vs reduced temperature curves for the system $Ni_{1\cdot5-a}Mn_aFeTi_{0\cdot5}O_4$.

X-ray diffraction patterns obtained with Fe $K\alpha$ radiation on a Norelco X-ray Diffractometer showed the preparations to be pure spinels. No data on the cation distribution could be obtained from these diffraction patterns.

Saturation-magnetization measurements were carried out using fields up to 6000 oersteds down to 77 °K; at 77 and 20 °K measurements were

*) An oxygen deficit is indicated by a minus sign.

made in fields up to 23000 oersteds by Mr P. Jongenburger by a method to be described elsewhere by him.

The saturation moments, the Curie temperatures and the cell edges are shown in figs 20*a* and *b* and in table XII.

The saturation-magnetization vs temperature measurements are given as σ vs T/Θ curves in fig. 21.

For the preparation with $a = 0{\cdot}77_5$ the effective *g*-factor was measured by Mr H. G. Beljers on a sphere of about 0·5 mm diameter. The results are

$Ni_{0{\cdot}72_5}Mn_{0{\cdot}77_5}FeTi_{0{\cdot}5}O_4$

wavelength	temperature	g_{eff}
$1{\cdot}25_5$ cm	293 °K	2·58
$1{\cdot}25_5$ cm	209 °K	2·68
$1{\cdot}25_5$ cm	143 °K	2·75
	(extrapolated towards 0 °K)	(2·80-)2·88

TABLE XII

Saturation moments, Curie temperatures and cell edges for the series $Ni_{1{\cdot}5-a}Mn_aFeTi_{0{\cdot}5}O_4$

Mn content *a*	formula	n_B	Θ (°C)	cell edge (Å)
0	$Ni_{1{\cdot}5}FeTi_{0{\cdot}5}O_4$	1·45	293	—
0·2	$Ni_{1{\cdot}3}Mn_{0{\cdot}2}FeTi_{0{\cdot}5}O_4$	0·32	277	8·3752 ± 10
0·4	$Ni_{1{\cdot}1}Mn_{0{\cdot}4}FeTi_{0{\cdot}5}O_4$	0·30	265	8·4033 ± 4
$0{\cdot}57_5$	$Ni_{0{\cdot}92_5}Mn_{0{\cdot}57_5}FeTi_{0{\cdot}5}O_4$	0·10	249	8·4456 ± 10
$0{\cdot}67_5$	$Ni_{0{\cdot}82_5}Mn_{0{\cdot}67_5}FeTi_{0{\cdot}5}O_4$	$0{\cdot}44_5$	192	8·4667 ± 10
$0{\cdot}77_5$	$Ni_{0{\cdot}72_5}Mn_{0{\cdot}77_5}FeTi_{0{\cdot}5}O_4$	0·60	181	8·4834 ± 4
0·95	$Ni_{0{\cdot}55}Mn_{0{\cdot}95}FeTi_{0{\cdot}5}O_4$	1·11	152	8·5096 ± 7
1·1	$Ni_{0{\cdot}4}Mn_{1{\cdot}1}FeTi_{0{\cdot}5}O_4$	1·28	126	8·5412 ± 7
1·3	$Ni_{0{\cdot}2}Mn_{1{\cdot}3}FeTi_{0{\cdot}5}O_4$	1·42	109	8·5691 ± 10
1·5	$Mn_{1{\cdot}5}FeTi_{0{\cdot}5}O_4$	1·68	89	8·6025 ± 10

6.4.2. **Discussion of the Results**

The general formula of this mixed-crystal series is

$$Ti_xNi_y(Fe^{III} + Mn^{II})_{1-x-y}\,[Ni_{1{\cdot}5-a-y}(Fe^{III} + Mn^{II})_{a+x+y}Ti_{0{\cdot}5-x}]\,O_4\ ^*).$$

*) Since $m_{Mn^{2+}} = m_{Fe^{3+}} = 5$ an interchange of Mn^{2+} and Fe^{3+} between *A* and *B* sites does not influence n_B.

As long as the ionic moments in the A and B sublattices are antiparallel, the saturation moment will be

$$n_B = |m_b - m_a|;$$

in the present case

$$m_b - m_a = -1{\cdot}55 + 2{\cdot}7a + 10x + (7{\cdot}7 - p)y \quad . \qquad (6.5)$$

For all values of a except $a = 0$ the sign of $m_b - m_a$ is unknown.

The values of $m_b - m_a$ for antiparallel ionic moments in A and B sites, for the case that all Ni^{2+} and Ti^{4+} ions occupy B sites, are represented by dashed line II (fig. 20*b*).

For $a = 0{\cdot}77_5$ the above equation and that for the effective g-factor (using $g_{eff} = 2{\cdot}88$) yield one solution ($x = -0{\cdot}02$; $y = 0{\cdot}02$) that is near to a physically possible arrangement ($x \approx 0$; $y \approx 0$); in this case $m_b - m_a$ is positive *) and lies on line II.

If we assume that angles occur between the ionic moments inside the B position we find, using formulae (6.3) and (6.4), that solutions exist for which $m_b - m_a$ is negative (line V), but with larger values of y, e.g. $y \approx 0{\cdot}2$ for $x \approx 0$. We shall discard these solutions as very much less likely than the previous one ($x \approx 0$, $y \approx 0$, no angles) in view of the fact that $y = 0$ for $a = 0$, and that Ni^{2+} ions will certainly not be driven from the octahedral sites by Mn^{2+} ions, in view of their great individual preference for sixfold coordination.

From the fact that the materials with $a = 0{\cdot}4$, $0{\cdot}57_5$ and $0{\cdot}67_5$ show curves of fig. 8, type *c*, and those with $a = 0{\cdot}2$ and $0{\cdot}77_5$ curves practically of fig. 8, type *b*, we deduce that for all these preparations $m_b - m_a$ has the same sign, i.e. positive. Therefore m is positive for the complete system, and curves III and IV are also discarded.

The n_B values up to $a = 0{\cdot}95$ may be accounted for by a continuous decrease of the amount of Ti^{4+} ions in the tetrahedral position (x) (see fig. 20*c*). The curve for x as a function of the Ni^{2+} content has the same shape as in the previous sections 6.2 and 6.3.

The fact that the experimental n_B values for $a = 1{\cdot}1$ - $1{\cdot}5$ fall below line II must in our view be explained by not completely antiparallel A and B moments.

The Curie temperatures show a break near $a = 0{\cdot}57_5$ but from the saturation moment we deduced that this preparation has less Ti^{4+} ions in the tetrahedral position than the value lying on the smooth line I drawn through the other points: this would explain a Curie temperature for this preparation higher than the value lying on the smooth dashed line I through the other points.

*) The fact that no physically possible solution is found is not surprising in view of the sensitivity of n_B to slight variations in e.g. x; the measurements of n_B and g_{eff} have been carried out on different parts of the same sample so that very slight inhomogeneities, i.e. differences in the average value of x of the order of $\pm 0{\cdot}01$, might cause such a small shift in values.

The cell edges vary practically linearly from $a = 0$ to $a = 1{\cdot}5$, although the amount of Ti^{4+} in the A sites does not vary linearly with a. The same behaviour can be observed in the two previous mixed-crystal systems (sections 6.2 and 6.3); it seems that the interchange of Ti^{4+} and Fe^{3+} between the A and B positions does not noticeably affect the cell edge.

The Mn^{2+}-Fe^{3+} distribution amongst the two sublattices cannot be deduced from the available data.

Though one type of anomalous σ-T curve occurs in the present system, no change of sign of $m_b - m_a$ has been found.

REFERENCES

[81]) H. Birnbaum and R. K. Scott, J. Amer. chem. Soc. **72**, 1398-1399, 1950.
[82]) N. W. Taylor, Z. phys. Chem. **9B**, 241-264, 1930.
[83]) K. F. Niessen, private communication.
[84]) K. F. Niessen, Physica **19**, 1127-1132, 1953.
[85]) E. W. Gorter, Nature **173**, 123-124, 1954.
[86]) F. A. Kröger, Some Aspects of the Luminescence of Solids, Elseviers Publishing Co Inc., Amsterdam-New York 1948, p. 158-160.

7. FERRIMAGNETIC OXIDES CONTAINING CHROMIUM: THE SYSTEM $Li_{0.5}Fe^{III}_{2.5-a}Cr^{III}_{a}O_4$ ($Li_{0.5}Fe_{2.5}O_4$-$Li_{0.5}Fe_{0.5}Cr_2O_4$)

7.1. Experimental

A series of materials with the general composition $Li_2O.(5-2a)Fe_2O_3.2aCr_2O_3$ was prepared with $a = 0$, 0·50, 0·75, 1·00, 1·25, 1·50, 1·60, 1·70, 2·00 and 2·50.

The materials were prepared from
Fe (Ni $0{\cdot}01_6$ %),
CrO_3 (Ca<appr. 0·2 %, Cu $0{\cdot}01_2$ %, Si 0·01 %),
Li_2CO_3 (Mg and Ca 0·02 %, Fe, Al and Si 0·01 %).
A Cr^{III} nitrate solution was prepared by dissolving the CrO_3 in water and reducing with ethanol at 40 °C; after leaving overnight the gelatinous mass was dissolved in concentrated HNO_3. To a mixed Fe^{III}-Cr^{III} nitrate solution excess ammonia was added; after boiling the precipitate was filtered, washed well to remove NH_4NO_3, dried in vacuo and slowly heated to 500 °C. The mixed crystal oxides with the formula $Fe_{2-0{\cdot}8a}Cr_{0{\cdot}8a}O_3$ were milled in an agate Bloch-Rossetti mill with Li_2CO_3 under benzene. The mixture was dried and heated for 2 h at 700 °C in an atmosphere of equal volumes CO_2 and O_2. After remilling, bars and disks were pressed from the resulting powder and sintered for 2 h at 1150 °C in O_2 and cooled slowly. By this method of preparation undue loss of Li_2O by evaporation was avoided.

$Li_{0.5}Fe_2Cr_{0.5}O_4$ ($a = 0{\cdot}5$) was also prepared by an alternative method: 1 Li_2CO_3 and 1 Cr_2O_3 were milled in an agate ball mill under benzene, dried and heated for 2 h at 1100 °C in O_2. The resulting powder showed no X-ray diffraction lines of Li_2O, Li_2CO_3, Cr_2O_3 or spinel and is probably a compound $LiCrO_2$. This material was mixed with Fe_2O_3 in the required proportion, milled, dried and fired at 1150 °C in O_2.

A study of the X-ray diffraction patterns obtained on a Norelco High-angle X-ray Diffractometer [85]) showed that a spinel $Li_{0.5}Cr_{2.5}O_4$ is not formed: the preparation with $a = 2{\cdot}5$ showed practically only Cr_2O_3 lines *). Some additional weak reflexions were probably those of $LiCrO_2$.

The other preparations prepared as described above were pure spinels except that with $a = 2{\cdot}00$ which showed weak Cr_2O_3 reflexions.

A pressed disk of the unsintered material with $a = 2{\cdot}00$ was now embedded in slabs pressed from the same material in order to maintain a suitable Li_2O vapour pressure, and sintered in the same way as indicated above. The Cr_2O_3 lines had now become much weaker (for details see [85])).

The distribution of the Li^+ ions in the mixed-crystal series $Li_{0.5}Fe_{2.5}O_4$-$Li_{0.5}Fe_{0.5}Cr_2O_4$ was determined by Braun [85]). His results are reproduced in fig. 22*b*.

Annealing the preparations for a long period at low temperatures (24 h at 500 °C, 96 h at 450 °C) did not change the diffraction patterns at all. The measurements of the magnetic properties were made on the samples that were only cooled slowly.

*) A report that "$Li_{0.5}Cr_{2.5}O_4$ is non-cubic" [86]) should be read: there is no cubic $Li_{0.5}Cr_{2.5}O_4$.

The preparation $Li_{0.5}Fe_2Cr_{0.5}O_4$ ($a = 0.5$) showed the same superstructure lines as $Fe[Li_{0.5}Fe_{1.5}]O_4$; the preparation $Li_{0.5}Fe_{0.5}Cr_2O_4$ ($a = 2$) showed a new superstructure (1 Li^+ : 1 Fe^{3+} in the tetrahedral position) already described in section 1.2.3 [85]). A beginning of this long-range order was detectable in the preparation with $a = 1.6$.

The relative distribution of the Fe^{3+} and Cr^{3+} ions cannot be determined by X-ray diffraction. The fact that a spinel $Li_{0.5}Cr_{2.5}O_4$ is not formed, and the migration of all Li^+ to the tetrahedral position as a is increased

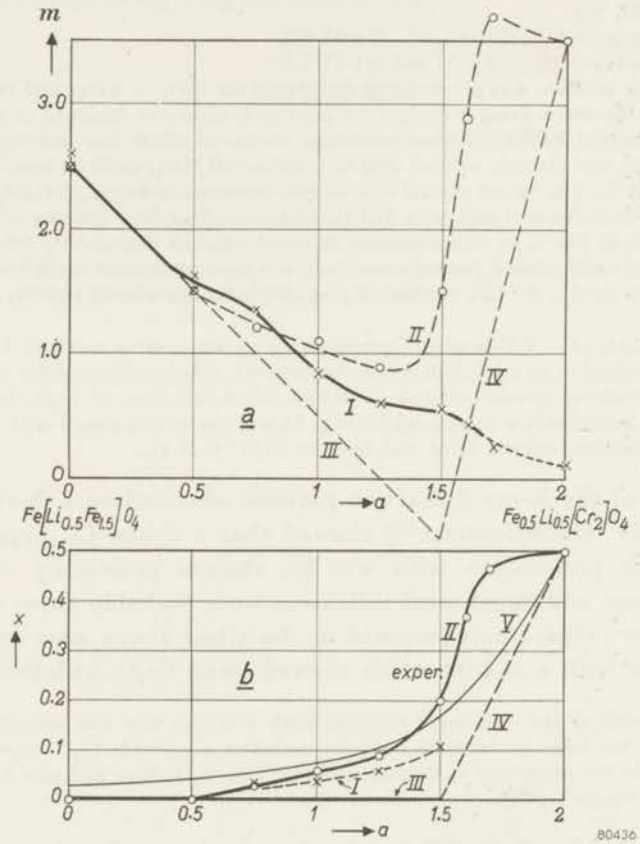

Fig. 22*a*. Saturation moments for the system $Li_{0.5}Fe_{2.5-a}Cr_aO_4$.
Curve I: experimental values; curve II: values calculated from the cation distribution determined by X-ray diffraction (fig. 22*b*, curve II); line III: values calculated for all Li^+ and Cr^{3+} ions in octahedral sites; line IV: values calculated for all Fe^{3+} ions in tetrahedral sites.
b. Amount of Li^+ ions in tetrahedral sites per formula unit (x) for the system $Li_{0.5}Fe_{2.5-a}Cr_aO_4$ $(Fe_{1-x}Li_x[Li_{0.5-x}Fe_{1.5+x-a}Cr_a]O_4)$.
Curve II: experimental values obtained by X-ray diffraction; curve I: values calculated from the saturation moments (fig. 22*a*, curve I); lines III and IV: values for which lines III and IV in fig. 22*a* were obtained, for all Cr^{3+} ions in octahedral sites.
Curve V: calculated distribution curve (see text).

to 2·0, however, clearly point to the presence of Cr^{3+} ions in the octahedral sites only.

Saturation vs temperature curves were measured for all preparations of the mixed-crystal series. Fig. 23 shows the reduced saturation magnetizations (σ/σ_0) against the reduced temperatures T/Θ. It is seen that here for several preparations anomalous σ-T curves occur of Néel's type (N) (see fig. 8, curve e) which have a compensation temperature T_{comp} for which $\sigma = 0$ [89]). In fig. 23 we have drawn the saturation magnetizations below and above the compensation temperature with different sign, although saturation measurements of course only give the absolute value of the spontaneous magnetization. In order to show that the spontaneous magnetization does change sign at T_{comp} we have measured the remanent induction (B_r) for $Li_{0.5}Fe_{1.25}Cr_{1.25}O_4$ in the absence of a magnetic field,

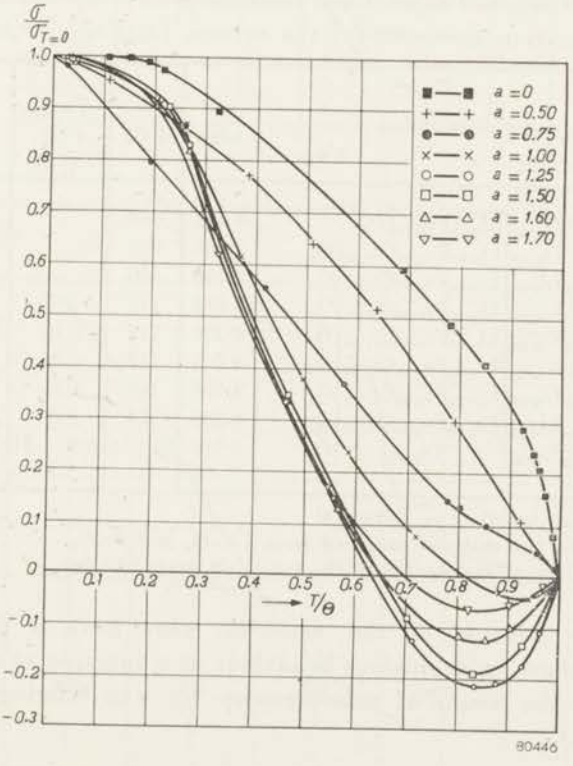

Fig. 23. Reduced saturation-magnetization vs temperature (σ/σ_0 vs T/Θ) curves for the system $Li_{0.5}Fe_{2.5-a}Cr_aO_4$. For clarity's sake the values of σ/σ_0 below and above the compensation temperature ($\sigma = 0$) have been drawn with different sign, although the measurements only determine the absolute values. More measuring points are shown in ref. [88b]).

perpendicularly to the earth's magnetic field. Fig. 25 shows that the remanent magnetization indeed changes sign at T_{comp}.

For $Li_{0.5}Fe_{0.5}Cr_2O_4$ ($a = 2.0$) σ was found to decrease almost linearly from $\sigma = 1$ $cgs_{magn} \cdot cm^3/g$ at appr. 100 °K to $\sigma \approx 0$ at the Curie temperature. Measurements of the remanent magnetization, however, clearly revealed a compensation temperature. The cause of this seeming paradox it discussed in section 8.2.4 for mixed crystals $NiFe_2O_4$-$NiAl_2O_4$.

The saturation moments (in Bohr magnetons) are given in fig. 22*a*, curve I, and in table XIII.

The Curie temperatures (Θ) and compensation temperatures (T_{comp}) are given in fig. 24 and in table XIII. Braun's values for the cell edges are also given in table XIII.

TABLE XIII

Cation distributions, cell edges, Curie temperatures, compensation temperatures and saturation moments for the system $Li_{0.5}Fe_{2.5-a}Cr_aO_4$.

Cr content a	ionic distribution	cell edge	Θ (°C)	T_{comp} (°C)	n_B
0	$Fe_{1.00}[Li_{0.50}Fe_{1.50}]O_4$	8.331	680		2.47; 2.60 *)
0.50	$Fe_{1.00}[Li_{0.50}Fe_{1.00}Cr_{0.50}]O_4$	8.306	500		1.62; 1.50 **)
0.75	$Fe_{0.98}Li_{0.02}[Li_{0.48}Fe_{0.77}Cr_{0.75}]O_4$	8.296	410		1.35
1.00	$Fe_{0.94}Li_{0.06}[Li_{0.44}Fe_{0.56}Cr_{1.00}]O_4$	8.292	315	205	0.84
1.25	$Fe_{0.91}Li_{0.09}[Li_{0.41}Fe_{0.34}Cr_{1.25}]O_4$	8.290	214	+38	0.61
1.50	$Fe_{0.80}Li_{0.20}[Li_{0.30}Fe_{0.20}Cr_{1.50}]O_4$	8.287	119	−16	0.55
1.60	$Fe_{0.64}Li_{0.36}[Li_{0.14}Fe_{0.26}Cr_{1.60}]O_4$	8.288	167	+11	0.42
1.70	$Fe_{0.54}Li_{0.46}[Li_{0.04}Fe_{0.26}Cr_{1.70}]O_4$	8.290	155	+20	0.22
2.00	$Fe_{0.50}Li_{0.50}[Cr_{2.00}]O_4$	8.288	80±16	+37±15 ***)	0.10

*) For material described in section 4.
**) Obtained for the material prepared from $LiCrO_2$ and Fe_2O_3.
***) Obtained from measurements of the remanent magnetization.

The effective *g*-factor of the materials that have a compensation temperature show an anomalous behaviour as a function of temperature. Fig. 25 shows the results of measurements by Van Wieringen [87]) [88a]) on $Li_{0.5}Fe_{1.25}Cr_{1.25}O_4$.

7.2. Discussion of the Magnetic Measurements

7.2.1. Saturation Moments

The distribution of the Li^+ ions being known, and assuming the Cr^{3+} ions to occupy octahedral sites only, the saturation moments can be

calculated for complete antiparallelism between the ionic moments in A and B sites respectively. The moments thus calculated (with for Cr^{3+}: $g = 2$, $S = 3/2$) are represented by the dashed curve II in fig. 22*a*. For $0 \leqslant a \leqslant 1{\cdot}25$

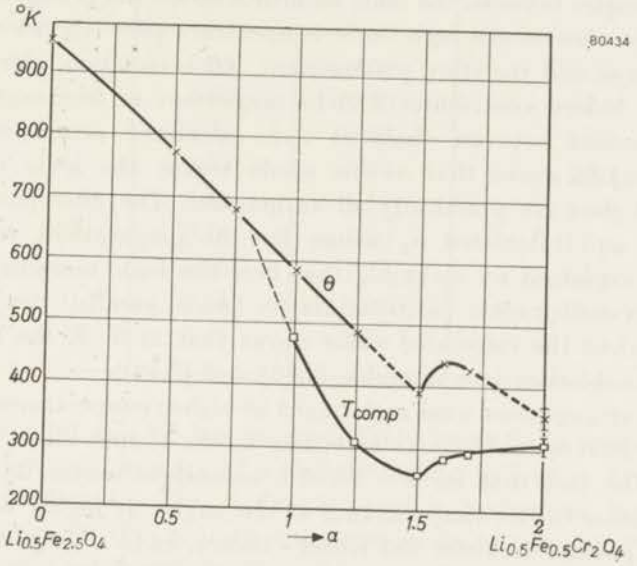

Fig. 24. Curie temperatures (Θ) and compensation temperatures (T_{comp}) for the system $Li_{0{\cdot}5}Fe_{2{\cdot}5-a}Cr_aO_4$.

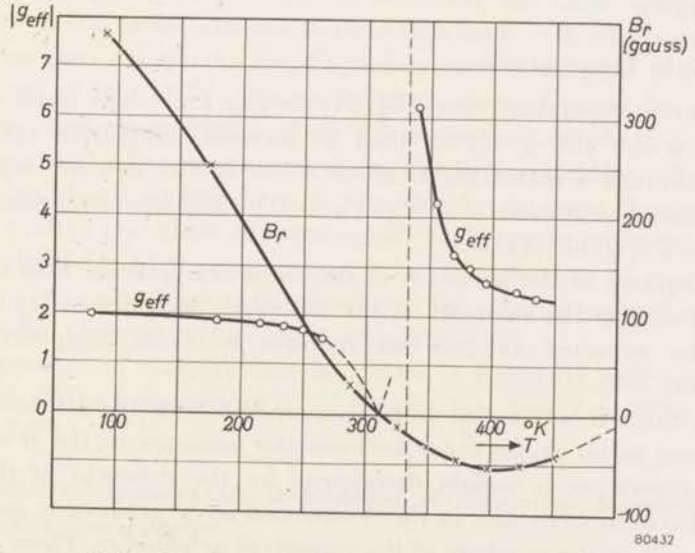

Fig. 25. Remanent induction ($B_r = 4\pi I_r$, right-hand scale) of $Li_{0{\cdot}5}Fe_{1{\cdot}25}Cr_{1{\cdot}25}O_4$ as a function of temperature: a change of sign is shown. Effective g-factor (g_{eff}, left-hand scale) of $Li_{0{\cdot}5}Fe_{1{\cdot}25}Cr_{1{\cdot}25}O_4$ measured by Van Wieringen [87]). A hyperbolic curve according to formula (4.5) is shown.

the observed and calculated moments are practically equal. We have seen there is indirect X-ray evidence that the Cr^{3+} ions occupy octahedral sites only. The moment of $Li_{0.5}Fe_2Cr_{0.5}O_4$ ($a = 0.5$), for which the occurrence of angles between the ionic moments inside the B sublattice is very unlikely in view of the high Curie temperature (500 °C), which indicates a very large and therefore predominant AB interaction, shows that the Cr^{3+} ion indeed contributes 3 Bohr magnetons in ferrimagnetism. The fair agreement between observed and calculated saturation moments for $0 \leqslant a \leqslant 1.25$ shows that in this whole region the ionic moments in A and B sites are practically all antiparallel. The discrepancy between observed and calculated n_B values for the preparations with $a > 1.25$ must be explained by assuming that here the ionic moments inside one of the crystallographic positions are no longer parallel: the fact that m is lower than the calculated value shows that at 0 °K the angles occur in the B sublattice (see formulae (2.18) and (2.19)).

If this arrangement were maintained at higher temperatures, no anomalous σ-T curves could occur according to the simple theory (see section 2.2.2). The fact that for $a = 1.6$-2.0 anomalous curves do occur must be due either to the disappearance of the angles at higher temperatures, which is possible in Yafet and Kittel's theory, or to a temperature dependence of γ_2, whereby $\gamma_2 = -1$ at T_{comp}. A temperature dependence of the ratios of the interactions has so far been introduced into theory only by Smart [92]).

7.2.2. **Curie Temperatures**

The Curie temperature curve (fig. 24) shows a practically linear decrease between $a = 0$ and $a = 1.50$, then an increase, decreasing again after passing through a maximum at about $a = 1.6$. The unit-cell edges show a small decrease between $a = 0$ and $a = 1.50$, and increase again slightly near $a = 2.0$ (table XIII).

The anomaly in the variation of the Curie temperature with a cannot be attributed to this anomaly in the cell edges, as a decreasing cell edge would be expected to give an increase in Curie temperature and vice versa.

When the AB interaction is large compared with the BB interaction, i.e. as long as no angles occur between the moments in the B sites, the Curie temperature is mainly determined by the strengths of the interactions between ferric ions in the A sites and ferric or chromic ions in the B sites, and on the numbers of the respective neighbours. These numbers of neighbours are proportional to the products of the numbers of ions in each lattice site per formula unit. These products, taken from table XIII, column 2, are given in table XIV.

TABLE XIV

Cr content a \ product	$Fe_A.Fe_B$ (1)	$Fe_A.Cr_B$ (2)	$Fe_A.(Fe_B + Cr_B)$ (3)
0	1·50	0·00	1·50
0·50	1·00	0·50	1·50
0·75	$0·75_5$	$0·73_5$	1·49
1·00	$0·52_5$	0·94	$1·46_5$
1·25	0·31	$1·13_5$	$1·44_5$
1·50	0·16	1·20	1·36
1·60	$0·16_5$	$1·02_5$	1·19
1·70	0·14	0·92	1·06
2·00	0·00	1·00	1·00

The material with $a = 0·5$ has an appreciably lower Curie temperature than that with $a = 0$, in spite of a slightly smaller cell edge. From the fact that the product $Fe_A.(Fe_B + Cr_B)$ is equal in both cases, it follows that the interaction Fe_A-Fe_B is much stronger than the interaction Fe_A-Cr_B.

This can account only partly for the sudden rise of the Curie temperature for $a > 1·5$ (fig. 24), since the figures in table XIV, column 1, show an irregularity but not a rise for $a > 1·5$. Moreover the Curie temperature for $a = 2·00$ is still more than one third of that for $a = 0$, whereas neglect of all interactions except the Fe_A-Fe_B interaction would give $\Theta = 0$ °K.

The figures of table XIV, column 3 show a sharp decrease for $a > 1·5$, which shows that consideration of all AB interactions accounts even less for the rise in the Curie temperatures there. The BB interactions will, therefore, play an important rôle here: it was already apparent from the n_B values for $a > 1·25$ that these BB interactions could not be neglected there. Only a molecular-field theory, extended for the presence of two kinds of magnetic ions, like Niessen has developed for other cases, will be able to account for these anomalies more quantitatively.

The compensation temperatures also show a minimum near $a = 1·5$. A discussion of the behaviour of T_{comp}/Θ as a function of a will be given in section 7.2.3.

7.2.3. Anomalous Temperature Dependence of Saturation Magnetization and Effective g-factor

We have seen in section 2.2 that for a ferrimagnetic spinel containing one kind of magnetic ion, a σ-T curve of Néel's type (N) (fig. 8, type e) occurs for x_a/x_b between 1 and $(1 + \beta)/(1 + \alpha)$.

Since in this case $|\alpha|$ and $|\beta|$ are small against 1 in view of the geometry of the spinel lattice, the occurrence of this type of curve, as well as of the other anomalous curves, is restricted to a narrow range of compositions. This means that T_{comp} will change from 0 °K to the Curie temperature for a small change in composition.

In the present system T_{comp} is not strongly dependent on composition above $a \approx 1{\cdot}25$, where it passes through a minimum. This is connected with
(1) the anomaly in the Curie temperature curve, which has been discussed in section 7.2.2;
(2) the minimum occurring in the ratio T_{comp}/Θ.

Fig. 8 showed that generally a curve of Néel's type (N) (fig. 8, curve e) will occur in a range of mixed crystals bounded by two materials, showing σ-T curves of the types d and f respectively, i.e. T_{comp}/Θ will then range from 0 to 1. Fig. 23 shows that in the present system the quotient $T_{comp}/\Theta = 1$ for a Cr content a slightly above 0·75, decreases up to the composition $a = 1{\cdot}25$ but then increases again.

This peculiar behaviour is primarily due to the sudden migration of Li^+ to the tetrahedral position, which prevents the saturation moment from passing through zero along dashed line III in fig. 22a, calculated for the case that both Li^+ and Cr^{3+} would be situated in octahedral sites.

A theory for the occurrence of compensation temperatures extended for the presence of two kinds of magnetic ions has been given by K. F. Niessen [90]).

A magnetized rod of a material having a compensation temperature, suspended in a weak horizontal magnetic field (smaller than the coercive force), e.g. above a permanent magnet made from "Ferroxdure" *) will turn about on heating through the compensation temperature. This very simple experiment is the first visual demonstration of the existence of non-compensated antiferromagnetism, or ferrimagnetism.

A practical result of the fact that T_{comp} in the system does not not vary strongly with composition, is to make the value of T_{comp} less sensitive to the exact composition and homogeneity of the preparation than would be the case if the phenomenon occurred only in a narrow range of compositions. Therefore it is easy to prepare a material for this experiment with T_{comp} conveniently situated, i.e. slightly above room temperature (viz. $Li_{0{\cdot}5}Fe_{1{\cdot}25}Cr_{1{\cdot}25}O_4$).

The effective g-factor for this type of material measured against temperature shows a hyperbolic behaviour, which is in accordance with the formula

$$g_{eff} = 2 \cdot \frac{(M_{total})_A - (M_{total})_B}{(M_{spin})_A - (M_{spin})_B}. \qquad (4.5)$$

This formula gives $g_{eff} = 0$ for T_{comp}, but the denominator becomes zero at a slightly different temperature, giving $g_{eff} = \pm \infty$.

*) A permanent-magnet material with high coercive force with the approximate composition $BaFe_{12}O_{19}$ [91]).

7.3. Discussion of the Cation Distribution

The three mixed-crystal series of section 6 gave x vs a curves (figs 16*b*, 18*b* and 20*c*) of a type that must be considered to be normal in ternary or multiple spinels. This means that in the simple Boltzmann expressions as used by Néel and Smart the energies of interchange of two cations between the two lattice positions are usually not very large, and that we must keep in mind that the ionic distributions found in practice are frozen in and dependent on the cooling rate.

In the present system the presence of all Li^+ ions in the tetrahedral position in $Li_{0.5}Fe_{0.5}[Cr_2]O_4$ is easily understood from the very strong preference of the Cr^{3+} ions for sixfold coordination.

If we assume that for Li_A^+-Cr_B^{3+} the interchange energy is very large, but for Li_B^+-Fe_A^{3+} small, then the stability of the inverse arrangement in $Fe[Li_{0.5}Fe_{1.5}]O_4$ is due to the 1:3 order in the octahedral position. A replacement of Fe^{3+} by Cr^{3+} in this material is not expected to alter the factors determining the *most stable* Me^+-Me^{3+} distribution (a, u, order energy, etc.) to any great extent, so that the most stable distribution for $a = 1{\cdot}5$ is still $Fe[Li_{0.5}Cr_{1.5}]O_4$.

The fact that in this material 0·20 Li^+ is found in the tetrahedral sites is due to the strong preference of Cr^{3+} for the B sites, which alters the Li^+-Fe^{3+} distribution frozen in amongst the remaining sites.

When the interchange energy Li_A^+-Cr_B^{3+} is taken $E = \infty$, and the other interchange energy Li_A^+-Fe_B^{3+} adjusted to make the theoretical distribution curve coincide with Braun's experimental curve for $a = 1$-$1{\cdot}5$ (fig. 22*b*) a curve like the drawn curve (V) is obtained *). The fact that for $a = 0$-$0{\cdot}75$ and $a = 1{\cdot}6$-$1{\cdot}7$ the experimental values of x are nearer to 0 and 0·5 respectively than the theoretical values clearly points to the influence of short-range order in the A or B position respectively. It is clear that in the region $a = 1$-$1{\cdot}5$ short-range order cannot be neglected, but here the order energies gained in both sublattices presumably compensate each other [85]).

*) The author is indebted to Dr J. S. Smart for a discussion on this subject and for performing this calculation.

REFERENCES

85) P. B. Braun, Physica, forthcoming.
86) E. Kordes and E. Röttig, Z. anorg. Chem. **264**, 34-47, 1951.
87) J. S. van Wieringen, Phys. Rev. **90**, 488, 1953.
88a) H. G. Beljers and J. S. van Wieringen, Physica, forthcoming.
88b) E. W. Gorter and H. A. Schulkes, Physica, forthcoming.
89) E. W. Gorter and J. A. Schulkes, Phys. Rev. **90**, 487-488, 1953.
90) K. F. Niessen, Physica **19**, 445-450, 1953.
91) J. J. Went, G. W. Rathenau, E. W. Gorter and G. W. van Oosterhout, Philips tech. Rev. **13**, 194-208, 1952.
92) J. S. Smart, Phys. Rev. **90**, 55-58, 1953.

8. FERRIMAGNETIC SPINELS CONTAINING ALUMINIUM

8.1. Discussion of Data Published on the Systems $Fe^{II}Fe^{III}_{2-a}Al_aO_4$ and $MgFe^{III}_{2-a}Al_aO_4$

A small part of the system ferrous ferrite-ferrous aluminate, $Fe^{II}Fe^{III}_{2-a}Al_aO_4$, has been studied by Guillaud and Michel [93] [94] for $a = 0$-$0{\cdot}2$.

The saturation moments found for four preparations with increasing a decreased linearly, and very nearly had the values $n_B = 4-3a$.

Guillaud [94] assumes that either of the following two ionic distributions occurs:

(1) Al^{3+} gradually replaces Fe^{3+} in the octahedral position;

(2) Al^{3+} gradually replaces Fe^{2+} in the octahedral position, an equal amount of Fe^{3+} ions in the tetrahedral position becoming Fe^{2+} ions.

He states that the results, therefore, conform with Néel's theory, i.e. can be accounted for by these ionic distributions when the additional assumption is made that the ionic moments in A and B sites are completely antiparallel, which latter assumption is here undoubtedly justified.

The general formula is

$$Fe^{II}_yAl_xFe^{III}_{1-x-y}\,[Fe^{II}_{1-y}Fe^{III}_{1-a+x+y}Al_{a-x}]\,O_4, \tag{8.1}$$

for which, taking $g_{Fe^{2+}} = 2$, we find the saturation moment

$$n_B = |m_b - m_a| \quad \text{and} \quad m_b - m_a = 4-5a+10x+2y. \tag{8.2}$$

Guillaud's first assumption, i.e. $x = 0$, $y = 0$, would give $n_B = 4-5a$, and is therefore incorrect.

This does not mean, however, that his second assumption is the correct one, because there is yet another cation distribution that can account for the experimental data, viz. $x = 0{\cdot}2a$, $y = 0$. The latter distribution seems more likely for the following reasons:

(1) If all Al^{3+} ions occupy B sites and the interchange energy Fe^{3+}_A-Fe^{2+}_B is not exceptionally small, it may be expected that this interchange, which is only an electron transfer, is so easy that at low temperatures the most stable distribution is practically obtained, i.e. with the Fe^{2+} ions in B sites like in Fe_3O_4.

(2) For $Fe^{II}Fe^{III}AlO_4$ ($a = 1$), the large decrease of the conductivity on annealing [95], as well as the X-ray pattern [96], point to a formula

$$Fe^{III}_{1-x}Al_x\,[Fe^{II}Fe^{III}_xAl_{1-x}]\,O_4,$$

with $x \leqslant 0{\cdot}1$.

We therefore expect that also for $0{\cdot}04 < a < 0{\cdot}2$ a small part of the Al^{3+} ions is found in tetrahedral sites, rather than part of the Fe^{2+} ions.

The system $MgFe_{2-a}Al_aO_4$ has been investigated by Jones and Roberts [97]: contrary to Dr G. H. Jonker [98]) they do not find a miscibility gap. We can only account for this discrepancy by supposing that their preparations *) were cooled more rapidly after sintering. The saturation moments (values at 20 °K) are reproduced in fig. 26*a*.

The general formula for these materials is

$$Mg_xAl_yFe_{1-x-y}[Mg_{1-x}Al_{a-y}Fe_{1-a+x+y}]O_4. \qquad (8.3)$$

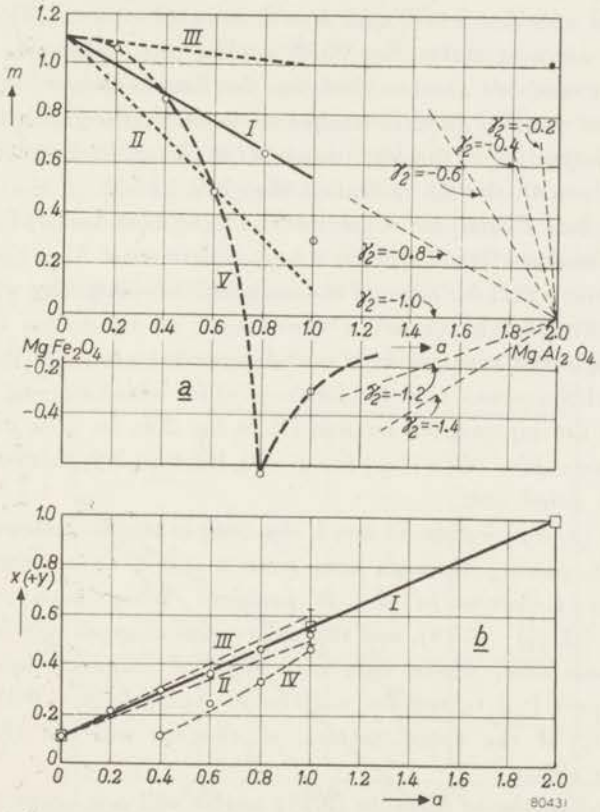

Fig. 26*a*. Saturation moments in the system $MgFe_{2-a}Al_aO_4$ (Jones and Roberts).
The experimental points lie around line I and between lines II and III. Curve V: a hypothetical curve through the experimental points, for which m changes sign as a result of angles in the B sites.
The lines indicated by $\gamma_2 = -0{\cdot}2$ - $\gamma_2 = -1{\cdot}4$ are derived from (2.19) for the cation distribution of line I of fig. 26*b*.
b. The values of $x+y$, presumably of x, in the formula

$$Mg_xAl_yFe_{1-x-y}[Mg_{1-x}Al_{a-y}Fe_{1-a+x+y}]O_4,$$

derived from the saturation moments.
Lines I, II and III correspond to those of fig. 26*a*. Line IV: alternative values for completely antiparallel moments in A and B positions.
□ — □: values determined by neutron diffraction (Bacon and Roberts).

*) Prepared by a method so far not published (see ref. in [97])).

Assuming with the authors complete antiparallelism of the ionic moments in the A and B positions,

$$n_B = |m_b - m_a| \quad \text{and} \quad m_b - m_a = 10(x+y) - 5a. \tag{8.4}$$

The values of $(x+y)$ thus calculated from the experimental n_B values are given in fig. 26*b*. The points scatter around a straight line I through $(x+y=1;\ a=2)$, for which $x+y = 0{\cdot}11 + 0{\cdot}44_5 a$, and lie between lines II and III, for which $x+y = 0{\cdot}11 + (0{\cdot}44_5 \pm 0{\cdot}04_5)\,a$.

The values of x for $a=0$ and $a=2$ were determined by Bacon and Roberts by neutron diffraction [99] [100a]), like the value of $(x+y)$ for $a=1$ *): the authors assume that in the latter case $y=0$, and that the Al^{3+} ions remain in the octahedral position throughout the series, i.e. that the migration of the Mg^{2+} ions to the tetrahedral position proceeds about linearly with the Al content a (fig. 26*b*, line I).

The scattering of the points around line I (figs 26*a* and *b*) is due, according to the authors [97]), to different heat treatments.

The possibility that for some of the materials m is negative will be briefly considered. This might occur in two ways:

(1) For completely antiparallel A and B moments, for $a = 0{\cdot}4$-$1{\cdot}0$ equation (8.4) yields a second solution for $(x+y)$ for which $m_b - m_a$ is negative: these values are represented by line IV in fig. 26*b*. In view of the unambiguity of the values of $(x+y)$ for $a = 0$, $0{\cdot}2$ and $2{\cdot}0$, this solution may, however, be ruled out.

(2) For the $(x+y)$ values of line I (fig. 26*b*) m might decrease along line V (fig. 26*a*), passing through zero near $a = 0{\cdot}7$, as a result of angles between the moments in the B position. When such angles occur, $m = -m_a(1 + 1/\gamma_2)$ (2.19), and this expression changes sign for $\gamma_2 = -1$. In the present case, where only one type of magnetic ion is present, we may expect $|\gamma_2|$ to remain well below unity (e.g. $< 0{\cdot}3$) in view of the geometry of the spinel lattice, so that m will not change sign in this manner either.

In fact, according to formula (2.19) angles will not occur at all in the whole system $MgFe_2O_4$-$MgAl_2O_4$ as long as $|\gamma_2| < 0{\cdot}8$.

8.2 The system $Ni^{II}Fe^{III}_{2-a}Al^{III}_a O_4$ ($NiFe_2O_4$ - $NiFeAlO_4$)

8.2.1. Experimental

A series of mixed crystals $NiFe_{2-a}Al_aO_4$ were prepared with $a = 0$, $0{\cdot}25$, $0{\cdot}45$, $0{\cdot}50$, $0{\cdot}62_5$, $0{\cdot}66$, $0{\cdot}68$, $0{\cdot}68_6$, $0{\cdot}68_8$, $0{\cdot}70$, $0{\cdot}75$ and $1{\cdot}00$.

*) The latter data has recently been confirmed by X-ray diffraction [100b]).

These materials were prepared from
Ni (Si 0·02 %, Co $0{\cdot}01_8$ %, Pb 0·01 %),
Fe (C 0·03 %),
Al (Si $0{\cdot}01_3$ %, Cr $0{\cdot}01_5$ %, Pb appr. 0·01 %, Ti $0{\cdot}01_3$ %), by method (B), pref. 2 h 700 °C in O_2, sint. 2 h 1350 °C in O_2.

Three series of samples were prepared:
(1) cooled slowly from 1350 °C (only for $a = 0{\cdot}66$ - $0{\cdot}75$);
(2) annealed 16 h 1250 °C, 16 h 1150 °C, 16 h 1000 °C, 45 h 600 °C, cooling rate between and below these temperatures about $^1/_4$ °C/min;
(3) quenched from 1350 °C (only for $a = 0$ - $0{\cdot}62_5$ and $0{\cdot}75$ - $1{\cdot}00$).
Analysis: Fe^{2+} content $<0{\cdot}1$ %.

X-ray diffraction patterns obtained on a Norelco X-ray Diffractometer showed all preparations to be pure spinels. No attempt was made to obtain information from the observed intensities about the cation distribution.

Saturation magnetizations were measured using fields up to 9000 oersteds down to 77 °K; at 77 and 20 °K measurements were made in fields up to 23000 oersteds by Mr P. Jongenburger. The saturation moments for the annealed and quenched samples are shown in fig. 27 and in table XV. The reduced σ-T curves ($\sigma/\sigma_{T=0}$ vs T/Θ) of the annealed samples for $a = 0$ - $0{\cdot}62_5$ and $0{\cdot}75$ - $1{\cdot}0$ are given in fig. 28 *). For $a = 0{\cdot}66$ - $0{\cdot}75$ the σ-T curves are shown in fig. 29*a-e* **). The Curie temperatures and the cell edges of the annealed samples are also given in table XV.

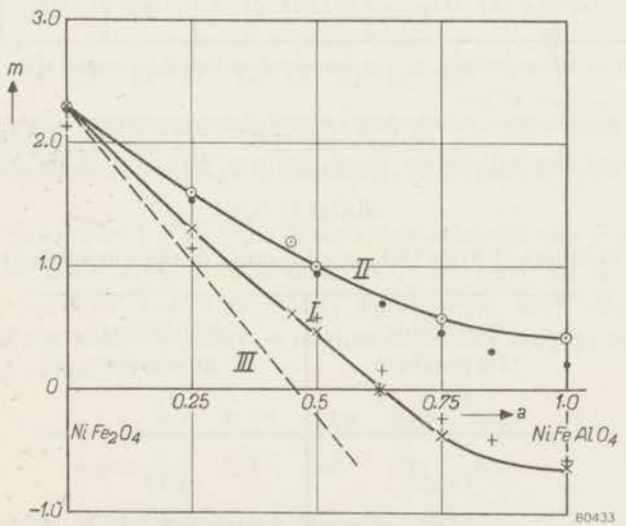

Fig. 27. Saturation moments (m) of the mixed-crystal series $NiFe_{2-a}Al_aO_4$ between $a = 0$ and $a = 1{\cdot}0$.
Curve I: Experimental values for annealed samples; × — ×: own measurements; + — +: measurements by Maxwell and Pickart. Curve II: Experimental values for quenched samples; ○ — ○: own measurements on samples quenched from 1350 °C; • — •: measurements by Maxwell and Pickart on samples quenched from 1420 °C. Curve III: values calculated for all Ni^{2+} and all Al^{3+} ions in the octahedral position.

*) These experiments were carried out by Mr F. Herbschleb.
**) These experiments were carried out by Mr J. A. Schulkes.

TABLE XV

Saturation moments, Curie temperatures and cell edges in the system $NiFe_{2-a}Al_aO_4$ ($NiFe_2O_4$-$NiFeAlO_4$)

Al content a	formula	cell edge annealed (Å)	Θ (°C)	n_B annealed	n_B quenched from 1350 °C
0	$NiFe_2O_4$	8·3370 ± 4	580	2·29	2·29
0·25	$NiFe_{1·75}Al_{0·25}O_4$	8·3062 ± 7	506	1·30	1·59
0·45	$NiFe_{1·55}Al_{0·45}O_4$	8·2769 ± 4	465	0·61	1·19
0·50	$NiFe_{1·50}Al_{0·50}O_4$	8·2705 ± 6	430	0·44	0·99
$0·62_5$	$NiFe_{1·37_5}Al_{0·62_5}O_4$	8·2521 ± 7	360	0-0·045	—
0·66	$NiFe_{1·34}Al_{0·66}O_4$	8·2420 ± 20	368	*)	—
0·68	$NiFe_{1·32}Al_{0·68}O_4$	8·2485 ± 1	356	*)	—
$0·68_6$	$NiFe_{1·31_4}Al_{0·68_6}O_4$	8·2388 ± 4	≈340	*)	—
$0·68_8$	$NiFe_{1·31_2}Al_{0·68_8}O_4$	8·2387 ± 2		*)	—
0·70	$NiFe_{1·30}Al_{0·70}O_4$	8·2385 ± 7		*)	—
0·75	$NiFe_{1·25}Al_{0·75}O_4$	8·2329 ± 7	294	0·38	0·58
1·0	NiFe Al O_4	8·1951 ± 7	198	0·64	0·42

*) extrapolation too uncertain, or not measured at liquid-hydrogen temperature.

The material with $a = 1$, $NiFeAlO_4$, has been quenched from various temperatures; the saturation moments are given in table XVI *).

TABLE XVI

Saturation moment of $NiFeAlO_4$ as a function of the quenching temperature

quenching temperature (°C)	saturation moment n_B
1350	0·42
1120	0·08
1020	0·05
1000	0·02
700	0·52
annealed	0·64

*) These experiments were carried out by Mr J. A. Schulkes.

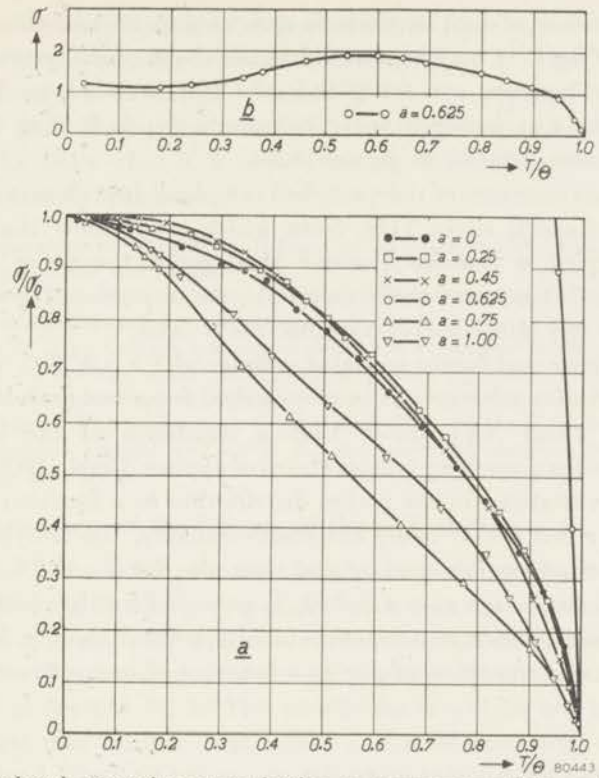

Fig. 28*a*. Reduced saturation-magnetization vs temperature (σ/σ_0 vs T/Θ) curves for the system $NiFe_{2-a}Al_aO_4$, for a = 0 - $0{\cdot}62_5$ and $a = 0{\cdot}75$ - 1·00
b. Saturation-magnetization (σ) vs reduced temperature (T/Θ) curve for $NiFe_{1{\cdot}375}Al_{0{\cdot}625}O_4$.

Maxwell, Pickart and Hall [101]) [102]) have investigated the same system up to $a = 2$. Their most recent results [102]) obtained for $a = 0$, 0·25, 0·50, 0·63, 0·75, 0·85 and 1·00 closely agree with ours. McGuire [103a]) has measured the effective *g*-factors of their annealed samples and reports the following values *):

a	= 0	0·25	0·50	0·63	0·75
g_{eff}	= 2·3	2·7	6·9	3·8	1·5 .

8.2.2. **Discussion of the Saturation Moments**

Our results for $a = 0{\cdot}25$, 0·45, 0·50, $0{\cdot}62_5$, 0·75 and 1·00 were first obtained. Table XV shows that values of the saturation moments of the annealed samples have a minimum near $a = 0{\cdot}62_5$. If it is assumed that for $a = 0{\cdot}75$ and 1·00 m is negative, a smooth curve for m vs a is obtained (fig. 27, curve I). Amongst the saturation magnetization vs

*) For details see [103b]).

temperature curves of fig. 28 there is one having an anomalous shape, of the type *d* of fig. 8. It may be noted that the shape of the curves changes discontinuously between $a = 0{\cdot}62_5$ and $a = 0{\cdot}75$, which is an indication that m changes sign between these compositions. A further discussion of the σ-T curves is given in section 8.2.4.

The saturation moments of the quenched samples do not show a minimum and lie on a smooth curve (II), from which we deduce that for the quenched samples m remains positive throughout the series of mixed crystals. The σ-T curves of these materials, not reproduced here, are all of Néel's type (Q) and concave towards the T axis.

In order to prove that for the annealed samples with $a \geqslant 0{\cdot}75$ m is negative, the preparation with $a = 1{\cdot}0$ was quenched from various intermediate temperatures. Table XVI shows that a minimum in the saturation moments occurs for quenching temperatures of approximately 1000 °C. Since discontinuous variations in the cation distribution as a function of *temperature* may be ruled out as being extremely unlikely, this proves that for the annealed sample m is negative, and thus also for $a = 0{\cdot}75$. A further proof that m changes sign near $a = 0{\cdot}62_5$ is provided by the measurements of g_{eff} by McGuire, which as a function of composition show a hyperbolic curve, like the measurements of g_{eff} as a function of temperature reported previously [87]).

8.2.3. **Discussion of the Cation Distribution**

The general formula of these mixed crystals is

$$\mathrm{Ni}_y\mathrm{Al}_x\mathrm{Fe}_{1-x-y}[\mathrm{Ni}_{1-y}\mathrm{Fe}_{1-a+x+y}\mathrm{Al}_{a-x}]\mathrm{O}_4\,, \tag{8.5}$$

for which for antiparallel ionic moments in A and B positions, and assuming $(g_{\mathrm{Ni}^{2+}})_B = 2{\cdot}3$, $(g_{\mathrm{Ni}^{2+}})_A = p$ *)

$$n_B = |m_b - m_a| \quad \text{and} \quad m_b - m_a = 2{\cdot}3 - 5a + 10x + (7{\cdot}7 - p)y\,. \tag{8.6}$$

For $x = 0$, $y = 0$, therefore, the saturation moments would follow the dashed line III in fig. 27. For the annealed samples (curve I) and to a greater extent for the quenched samples (curve II) some Ni^{2+} or Al^{3+} ions, or both, must be present in the tetrahedral position.

Since the migration to the A sites of Ni^{2+} ions contributes much less to a rise of m than that of Al^{3+} ions, and in view of the ionic distribution recently found [105]) for $NiAl_2O_4$ by X-ray diffraction, viz. about $Al_{0{\cdot}76}Ni_{0{\cdot}24}Ni_{0{\cdot}76}Al_{1{\cdot}24}O_4$, it seems certain that it is mainly Al^{3+} rather than Ni^{2+} ions that are partly present in the tetrahedral sites.

*) See footnote in section 6.2.2.

The cation distributions may be calculated from n_B values and effective g-factors in the manner described in section 6.2.2. This has been done, independently from us, by Smart [104]) for the system $NiFe_2O_4$-$NiAl_2O_4$ from the data obtained at the U.S. Naval Ordnance Laboratory [102]) [103]); the results show that it is indeed mainly Al^{3+} rather than Ni^{2+} that is found in tetrahedral sites.

An investigation of the system $NiFe_{2-a}Ga_aO_4$ ($NiFe_2O_4$-$NiGa_2O_4$) has recently been reported by Maxwell and Pickart [102]).

The general formula is equal to formula (8.5), substituting Ga^{3+} for Al^{3+}, and, as long as no angles between the ionic moments in the B sites occur, the saturation moment n_B is given by (8.6). Gallium was expected to have a strong preference for the tetrahedral sites (i.e. $a \geqslant x \gg 0{\cdot}5a$), so that n_B is expected to increase with a, starting from $NiFe_2O_4$.

This behaviour has indeed been found: for $a = 0{\cdot}25$ it may be deduced from (8.6), assuming that all Ni^{2+} ions occupy B sites, that 32 % of the Ga^{3+} ions occupy B sites for the annealed samples and 38 % for the quenched samples, provided the above assumptions are correct.

8.2.4. Discussion of the Shapes of the σ-T Curves

In order to look for preparations showing anomalous σ-T curves of the types *b-f* of fig. 8, the preparations with $a = 0{\cdot}66$, $0{\cdot}68$, $0{\cdot}68_6$, 068_8, $0{\cdot}70$ were then prepared; the σ-T curves were measured both before annealing, i.e. after a slow cooling process (see section 3), and after annealing, as specified in section 8.2.1. The results for $a = 0{\cdot}75$ are also given. Figs 29*a-e* show that for $a = 0{\cdot}66$ before and after annealing a curve of type *b* is obtained. For 0·68 before annealing a curve of type *c* (Néel's type (P)) is shown; annealing changes this into a curve of an anomalous type not recognizable as one predicted by Néel. The latter type of curve is also shown by the preparations with $a = 0{\cdot}68_6$ and $a = 0{\cdot}68_8$ before annealing; after annealing curves closely resembling type *f* are obtained. The latter type of curve is again shown for $a = 0{\cdot}70$ before annealing, which is changed by annealing into a curve of Néel's type (Q), which is, however, still convex towards the T-axis. We recognize this latter type of curve for $a = 0{\cdot}75$ before annealing. Annealing changes this into a linear curve, also of type (Q). If we include the curves obtained for the other a values (fig. 28), it is seen that with increasing a there is a change from curves of the types *a*, *b* and *c* to curves of the types *f* and *g* *). Curves of type *d* (Néel's type (L)) and *e* (Néel's type (N)) are not found, but instead the curve of the type shown in figs 28*b* and *c*.

We shall show that this can be understood from the inhomogeneity of the preparations.

*) The fact that for the annealed sample with $a = 0{\cdot}62_5$ a curve of type *c* is obtained and for $a = 0{\cdot}66$ one of type *b* is probably due to the fact that the cooling rates during the annealing treatment for the preparations with $a = 0{\cdot}66$ - $0{\cdot}75$ were slightly different from those used for the other preparations.

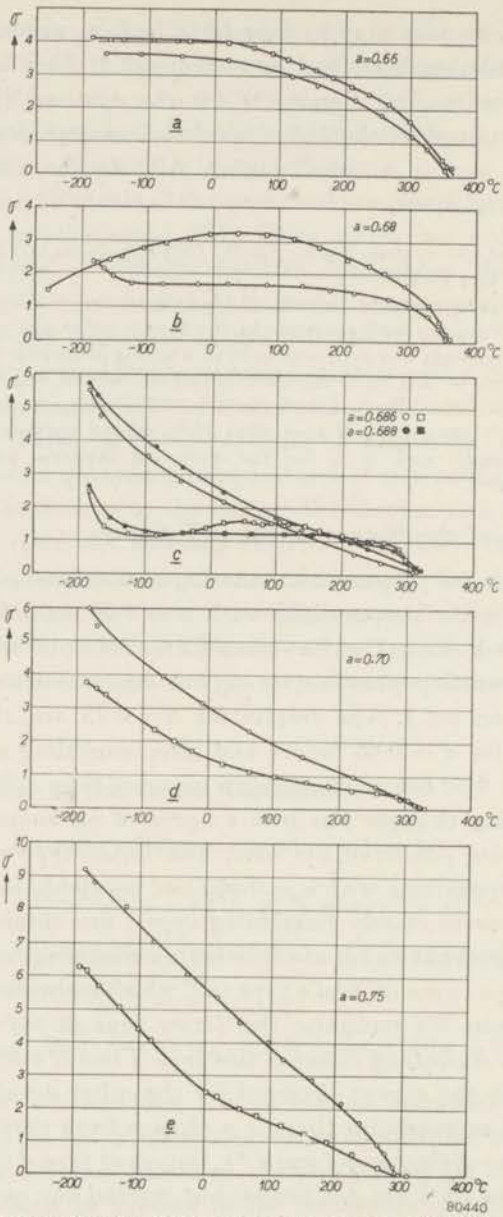

Fig. 29. Saturation-magnetization (σ) vs reduced temperature (T/Θ) curves for the system $NiFe_{2-a}Al_aO_4$, for $a = 0{\cdot}66 - 0{\cdot}75$.
□ — □ before annealing (section 8.2.1, sub (1));
○ — ○ after annealing (section 8.2.1, sub (2)).

From formula (8.2) it is deduced that a change in x of 0·01 results in a change in n_B of 0·1, i.e. a change in $\sigma_{T=0}$ of 2·6. From the fact that our annealing treatment results in a change of $\sigma_{T=0}$ of the order of 3 we may

deduce that this has produced a change — i.e. a decrease — of x of just over 0·01. Figs 29*a-e* show that this is sufficient to cause appreciable differences in type of σ-T curve. A change from type *d* (Néel's (type (*L*)) to type *f*, between which types curves of type *e* (Néel's type (*N*)) must occur with compensation temperatures ranging from 0 °K to the Curie temperature, will be brought about by a variation of x of a few hundredths at most.

An inhomogeneity of the material, caused by *local* variations of x of less than 0·01, therefore, will already result in a superposition of type *d* curves with widely varying compensation temperatures. Since saturation measurements only yield the absolute value of the spontaneous magnetization, such a superposition results in just the type of "hybrid" curves as found for $a = 0{\cdot}68$ (annealed) and for $a = 0{\cdot}68_6$ and $0{\cdot}68_8$ (slowly cooled).

In order to show that this explanation is correct we have measured the remanent magnetization of these preparations for several temperatures. The remanence indeed changes sign with temperature.

The samples of $FeNiAlO_4$, quenched from 1020 °C and 1000 °C also show the above-mentioned type of "hybrid" σ-T curve; here also the remanent magnetization changes sign with temperature.

The slight rise of σ towards $T = 0$ °K for the annealed sample with $a = 0{\cdot}62_5$ (fig. 28*b*) indicates that this σ-T curve is also such a "hybrid" curve with average $m_b - m_a$ very near to zero.

The above-mentioned small local variations of x will of course be present in the whole series of mixed crystals and, in fact, in all ferrimagnetic spinels having cation distributions that change with temperature. The σ-T curve, therefore, is in all these cases an average curve, but only for materials for which $m_b - m_a$ changes sign with temperature is the inhomogeneity detectable from the saturation-magnetization vs temperature curves.

REFERENCES

[93]) C. Guillaud and A. Michel, J. Phys. Radium **12**, 65, 1951.
[94]) C. Guillaud, J. Phys. Radium **12**, 239-248, 1951. (or J. Rech. C.N.R.S. nr. **12**, 1950).
[95]) E. J. W. Verwey, P. W. Haayman and F. C. Romeijn, J. chem. Phys. **15**, 181-187, 1947.
[96]) E. J. W. Verwey E. L. Heilmann, J. chem. Phys. **15**, 174-180, 1947.
[97]) G. O. Jones and F. F. Roberts, Proc. phys. Soc. Lond. **B 65**, 390-391, 1952.
[98]) G. H. Jonker, to be published.
[99]) G. E. Bacon, Acta cryst. **5**, 684-686, 1952.
[100a]) G. E. Bacon and F. F. Roberts, Acta cryst. **6**, 57-62, 1953.
[100b]) G. E. Bacon and A. J. E. Welch, Acta cryst. **7**, 361-363, 1954.
[101]) L. R. Maxwell, S. J. Pickart, and R. W. Hall, Phys. Rev. **91**, 206 (B7), 1953.
[102]) L. R. Maxwell and S. J. Pickart, Phys. Rev. **92**, 1120-1126, 1953.
[103a]) T. R. McGuire, Phys. Rev. **91**, 206 (B8), 1953.
[103b]) T. R. McGuire, Phys. Rev. **93**, 682-686, 1954.
[104]) J. S. Smart, private communication, to be published in Phys. Rev.
[105]) F. C. Romeijn, Philips Res. Rep. **8**, 304-342, 1953.

9. OTHER FERRIMAGNETIC OXIDES CONTAINING CHROMIUM: THE SYSTEM $Mn^{II}Fe^{III}_{2-a}Cr_aO_4$ ($MnFe_2O_4$-$MnCr_2O_4$)

9.1. Introduction

The general formula for the mixed-crystal series $MnFe_2O_4$-$MnCr_2O_4$ is

$$Cr_x(Fe^{III} + Mn^{II})_{1-x}\left[(Fe^{III} + Mn^{II})_{2-a+x}Cr_{a-x}\right]O_4, \qquad (9.1)$$

for which, for completely antiparallel ionic moments in A and B positions

$$n_B = |m| = |m_b - m_a| \quad \text{and} \quad m = m_b - m_a = 5 - 2a + 4x.$$

We have seen that Cr^{3+} has the strongest preference for sixfold coordination:

for $x = 0$, $m_b - m_a = 5 - 2a$ (fig. 30, line II).

For $MnCr_2O_4$ ($a = 2$) a value $n_B = 1{\cdot}5$, measured at liquid-helium temperature, has been reported [106]). We supposed that the discrepancy with the value $5 - 2a = 1{\cdot}0$ must be accounted for not by assuming $x = 0{\cdot}12_5$, but by the occurrence of angles between the ionic moments inside the B or A position. For angles in the A position equation 2.18 gives $a_2 = -1{\cdot}33$, and such a value is very unlikely from geometrical considerations. It was supposed that the strength of the Mn-O-Mn interaction is certainly not so much stronger than the Mn-O-Cr interaction as to counterbalance this geometrical argument.

When the angles between the moments occur in the B position, m will be <1, i.e. $-1{\cdot}5$. In this case in the system $MnFe_2O_4$-$MnCr_2O_4$ m will pass through zero as a result of these angles.

9.2. Experimental

A series of mixed crystals with the composition $MnFe_{2-a}Cr_aO_4$ was prepared with $a = 0$, $0{\cdot}12_5$, $0{\cdot}25$, $0{\cdot}50$, $1{\cdot}00$, $1{\cdot}08_5$, $1{\cdot}25$ and $1{\cdot}50$.

The following materials were used:
$MnCO_3$ (Na < appr. 0·1 %, Mg 0·01 %),
Fe (Ni $0{\cdot}01_6$ %),
CrO_3 (Ca < appr. 0·2 %, Cu $0{\cdot}01_2$ %, Si 0·01 %).

A chromic nitrate solution is prepared as described in section 7.1. The required weight of this solution is added to a solution of weighed quantities of Fe and $MnCO_3$ in dilute HNO_3, The materials were further prepared by method (C), pref. 2 h 700 °C, sint. 2 h 1250 °C.

The sintering was carried out in atmospheres containing N_2, H_2 and CO_2, of different compositions. X-ray diffraction patterns were obtained for all samples; the oxygen content was determined for those samples for which the diffraction patterns showed only spinel lines. The final adjustment of the oxygen content was carried out as described in section 6.4.

The magnetic investigations were carried out on samples which had the following excess oxygen contents:

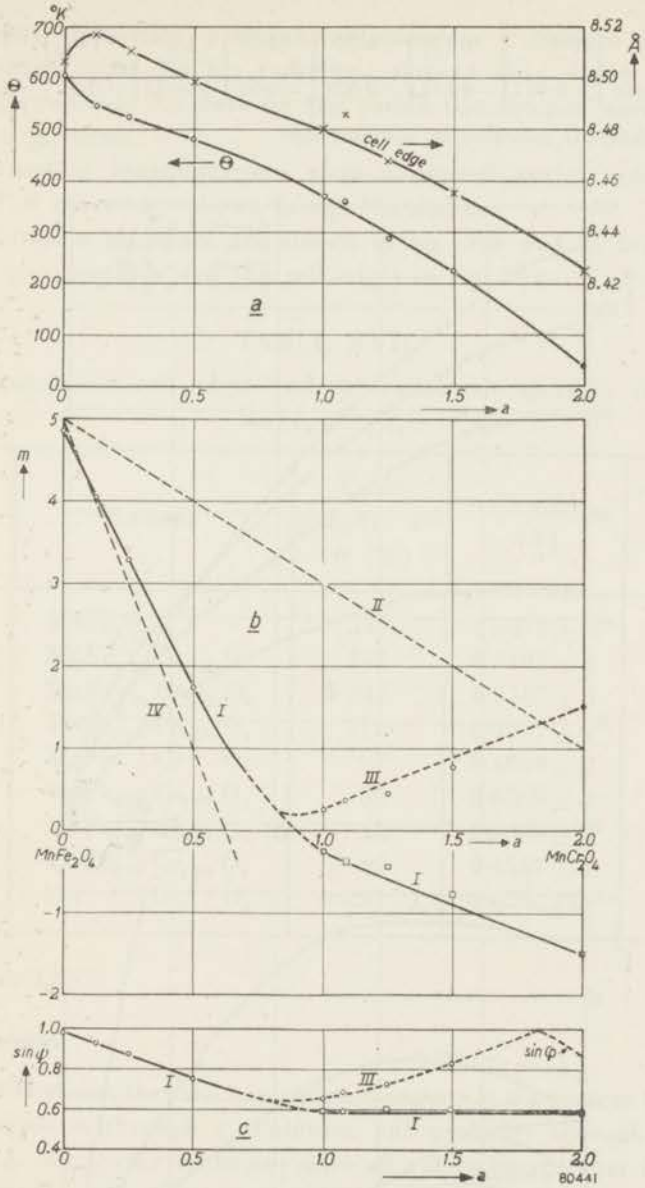

Fig. 30. Properties of the mixed-crystal series $MnFe_{2-a}Cr_aO_4$.
a. Curie temperatures (Θ in°K, left-hand scale) and cell edges (in Å, right-hand scale).
b. Saturation moments.
Curve I: saturation moments (most probable curve); curve I-III: saturation moments (other possible curve); line II: values calculated for all Cr^{3+} in the octahedral position and without angles between the ionic moments inside one sublattice; line IV: saturation moments calculated for the same assumptions as for line II, but with the moment of the Cr^{3+} ions (in the *B* position) *parallel* to those of the ions in the *A* sublattice.
c. sin ψ for angles $180° - 2\psi$ occurring between the directions of the ionic moments in the *B* position for the cases I and III of fig. 30*b*. On curve III above $a = 1{\cdot}8$, $\sin\psi = 1$, but $\sin\varphi < 1$.

a	0	$0{\cdot}12_5$	0·25	0·50	1·0	$1{\cdot}08_5$	1·25	1·50
wt % oxygen	+0·007	−0·075	−0·025	+0·05	−0·015	+0·05	+0·03	+0·01

An oxygen deficit is indicated by a minus sign.

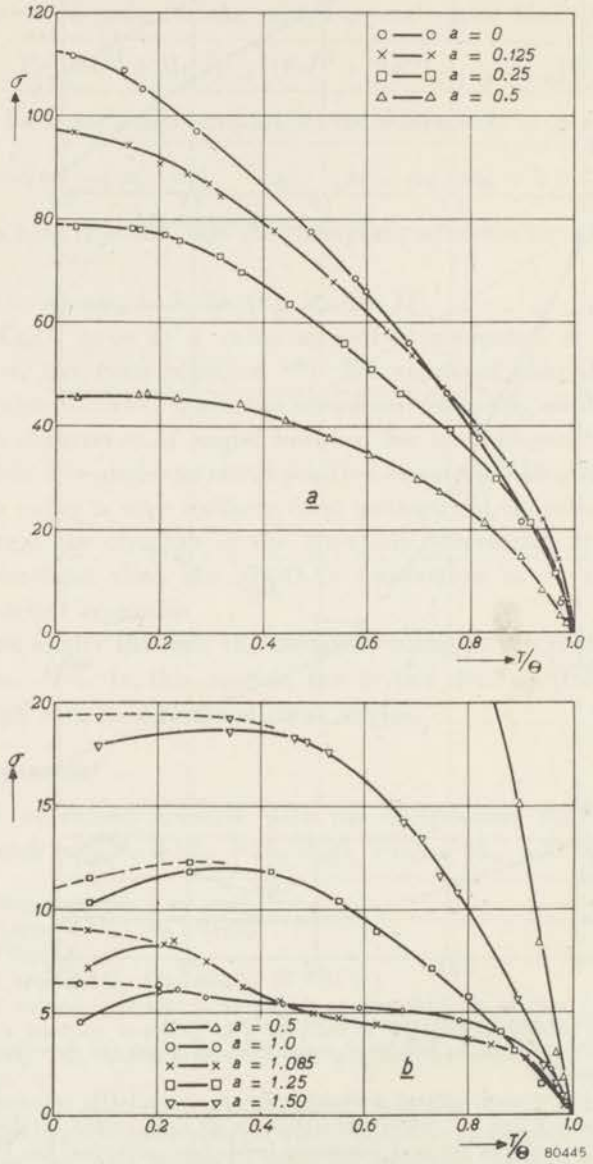

Fig. 31 *a* and *b*. Saturation-magnetization vs reduced temperature curves for the system $MnFe_{2-a}Cr_aO_4$. The values down to 77 °K were measured in fields up to 6000 oersteds, those at 77 and 20 °K up to 23000 oersteds. For $a = 1 - 1{\cdot}5$ the drawn curves represent measurements at 6000 oersteds, the dashed curves those at 23000 oersteds.

The X-ray diffraction patterns, obtained on a Norelco High-angle Diffractometer using Mo $K\alpha$ radiation, showed only spinel reflexions for all compositions. No data on the cation distribution were obtained from these patterns.

The saturation magnetizations were measured against temperature: the σ vs T/Θ curves are shown in figs 31*a* and *b*.

The saturation moments are shown in fig. 30*b* and in table XVII, the Curie temperatures and the cell edges in fig. 30*a*.

TABLE XVII

Curie temperatures, cell edges and saturation moments in the system $MnFe_{2-a}Cr_aO_4$

Cr content a	formula	Curie temperature Θ (°C)	cell edge (Å)	saturation moment n_B
0	$MnFe_2O_4$	330	$8{\cdot}5074 \pm 2$	4·85
$0{\cdot}12_5$	$MnFe_{1{\cdot}87_5}Cr_{0{\cdot}12_5}O_4$	272	$8{\cdot}5185 \pm 1$	4.04
0·25	$MnFe_{1.75}Cr_{0.25}O_4$	247	$8{\cdot}5107 \pm 3$	3·28
0·50	$MnFe_{1{\cdot}50}Cr_{0{\cdot}50}O_4$	210	$8{\cdot}4977 \pm 2$	1·73
1·00	$MnFeCrO_4$	97	$8{\cdot}4809 \pm 2$	0·25
$1{\cdot}08_5$	$MnFe_{0{\cdot}91_5}Cr_{1{\cdot}08_5}O_4$	88	$8{\cdot}4869 \pm 2$	0·37
1·25	$MnFe_{0{\cdot}75}Cr_{1{\cdot}25}O_4$	15	$8{\cdot}4680 \pm 2$	$(>)0{\cdot}45$
1·50	$MnFe_{0{\cdot}50}Cr_{1{\cdot}50}O_4$	—49	$8{\cdot}4567 \pm 1$	$0{\cdot}77_5$
2·00	$MnCr_2O_4$	—233 *)	8·426 **)	1·5 *)

*) [106])
**) see section I.2.5.1.

9.3. **Discussion**

Table XVII shows that the saturation moments in the system $MnFe_2O_4$-$MnCr_2O_4$ m passes through a minimum, and probably through zero like drawn in fig. 30*b* (curve I): in any case all values except that for $a = 2$ lie below line II, so that an assumption $x \neq 0$ is not sufficient to account for them.

The maximum in the cell edges for $a = 0{\cdot}12_5$ is probably due to the migration of a fairly large amount of Mn^{2+} ions to the tetrahedral position as a result of the introduction of a small amount of Cr^{3+} in the B position. The linear decrease of the cell edge for $a > 0{\cdot}12_5$ shows that the migration of Mn^{2+} to the A sites there proceeds more gradually. It is possible that the steep decrease of m for $a < 0{\cdot}5$ must be ascribed to angles between the

moments in the B sites. It seems rather surprising, however, that even the introduction of only $0{\cdot}12_5$ Cr lowers the saturation moment by $0{\cdot}8\ n_B$. This may be explained, like the maximum in the cell edges, by the migration of a fair amount of Mn^{2+} to the A sites, thus further decreasing the number of Fe_A-Fe_B interactions, which make the strongest contribution to the total AB interaction.

If the saturation moment m changes sign (line I), it follows from (2.19) that $\gamma_2 = -1$ for $m = 0$ and $\gamma_2 = -1{\cdot}43$ for $m = -1{\cdot}5$ ($a = 2{\cdot}0$). This is quite possible if the Cr^{3+}-Cr^{3+} interaction is much stronger than the Mn^{2+}-Cr^{3+} interaction, so that the geometrical reasons for γ_2 being small are counterbalanced.

If m would not change sign (line I-III) this would mean that γ_2 at first decreases to almost -1, i.e. $\sin\psi$ to $0{\cdot}6$, that $\sin\psi$ then increases to 1 for $a \approx 1{\cdot}8$, after which angles $180° - 2\varphi$ in the A position would start to occur and $\sin\varphi$ would decrease to $0{\cdot}9$, i.e. a_2 to $-1{\cdot}33$: this behaviour is extremely unlikely.

Finally, it may be suggested that the possibility of the interaction Fe_A-Cr_B being positive in the present system cannot be ruled out.

In section 2.3.3 we saw that the superexchange interaction between an ion with less than five 3d electrons and one with five 3d electrons may be either positive or negative: in the system $Li_{0{\cdot}5}Fe_{2{\cdot}5}O_4$-$Li_{0{\cdot}5}Fe_{0{\cdot}5}Cr_2O_4$ (cell edges about 8·3 Å) the Fe_A-Cr_B interactions are negative, but it is possible that in the present system, where for $a < 0{\cdot}5$ the cell edges are of the order of 8·5 Å, this interaction is positive.

Line IV shows the saturation moments for the case that the Cr_B^{3+} ions would have moments parallel to those of the ions in the A position. We have seen that it is very probable that Mn^{2+} ions migrate to the A position as a increases, so that in this case the number of positive Fe_A-Cr_B interactions may decrease rapidly with increasing a, i.e. the saturation moments will be expected to deviate from line IV for increasing a.

The saturation vs temperature curves do not show one of the anomalous curves predicted by Néel: for $a = 1{\cdot}25$ σ does decrease with decreasing temperature, but probably only as a result of the saturating field of 23 000 oersteds not being large enough.

A change of sign of m without the occurrence of anomalous curves of the types shown in fig. 8 was expected for a mixed-crystal series in which angles between the ionic moments in one of the sublattices (i.e. the B sites) occur at all temperatures (section 2.2.2).

It may be that the present series is an example of such a case.

REFERENCE

106) W. G. Schindler, T. R. McGuire, L. N. Howard and J. S. Smart, Phys. Rev. **86**, 599 (J14), 1952.

The author is indebted to Dr E. J. W. Verwey, director of Philips Research Laboratories, for his stimulating interest in the work, and for his consent to publish these results.

The assistance of Messrs T. T. A. M. Geraerts, G. Menkveld and M. Vrolijks in the experiments described in section 4 is gratefully acknowledged.

The experimental assistance of Mr E. Hondema in section 6.2-3, of Mr F. Herbschleb in section 8 and particularly of Mr J. A. Schulkes in sections 5.1, 6.4, 7, 8 and 9 has been invaluable.

The author should like to express his sincere thanks to Mr P. B. Braun, who obtained all X-ray data for him, to Mr J. Smit for instructive discussions on theoretical problems, and to Dr J. H. van Santen for his constructive criticism of the manuscript.

SAMENVATTING

De verzadigingsmagnetisatie (σ) van een aantal mengkristallen van oxyden met spinelstructuur werd gemeten als een functie van de temperatuur. De resultaten zijn in overeenstemming met Néel's theorie van het *ferrimagnetisme*: het resulterende magnetische moment m is het verschil der momenten van de tetraeder- (A) en octaeder- (B) deelroosters, hetzij: (a) met volledig evenwijdige ionenmomenten binnen ieder deelrooster, of (b) met hoeken tussen de ionenmomenten in een van de deelroosters.

De spinelstructuur is beschreven in (1.1); experimentele en theoretische gegevens uit de literatuur over de kationenverdeling zijn samengevat in (1.2). Een bespreking van de theorie van Néel is gegeven in (2.2.1), met de wijziging door Yafet en Kittel (2.2.2). Wanneer de momenten der beide deelroosters ongeveer gelijk zijn, voorspelt Néel een aantal anomale σ-T krommen. Deze moeten alle optreden in een reeks mengkristallen van type (a) waarin het resulterende moment m van teken wisselt. De experimentele methoden door ons gebruikt zijn gegeven in (3).

Uit de metingen aan enkelvoudige ferrieten $Me^{II}Fe_2^{III}O_4$ met $Me^{II} = Mn^{2+}$, Fe^{2+}, Co^{2+}, Ni^{2+}, Cu^{2+}, Mg^{2+} of ($0{,}5\ Li^{+} + 0{,}5\ Fe^{3+}$) blijkt dat deze tot groep (a) behoren; de mengkristallen $Me^{II}_{1-a}Zn_aFe_2O_4$ vanaf $a >$ ong. 0,4 behoren tot groep (b) (4).

Het moment van $Ca_{0,35}Zn_{0,65}Fe_2O_4$ is hoger dan van alle MgZn ferrieten, wellicht omdat de hoek A-O-B groter wordt doordat het grote Ca^{2+} ion voornamelijk op de B-plaats aanwezig is; daardoor wordt de AB wisselwerking vergroot, in overeenstemming met de theorie van Anderson (5.1) (voor een bespreking van de theorie van Anderson zie (2.3.2)). Het moment van ferrimagnetische oxyden met andere kristalstructuren kan uit de hoeken metaalion — zuurstofion — metaalion voorspeld worden, zoals b.v. voor $BaFe_{12}^{III}O_{19}$ en $KFe_{11}^{III}O_{17}$ (5.2).

In een aantal reeksen mengkristallen is gezocht naar anomale σ-T krommen: deze worden niet gevonden in de systemen $Ni_{1+a}Fe^{III}_{2-2a}Ti_aO_4$ en $Ni_{1,5-a}Zn_aFe^{III}Ti_{0,5}O_4$, doordat, tegen de verwachting in, Ti^{4+} ionen op tetraederplaatsen optreden, hetgeen voor $Ni_{1,5}Fe^{III}Ti_{0,5}O_4$ door meting van de effectieve g-factor bewezen is (6.1-2).

In het systeem $Li_{0,5}Fe^{III}_{2,5-a}Cr_aO_4$ ($0<a<2{,}0$) treedt een onverwachte verdeling der Li^{+} en Fe^{3+} ionen over de beide roosterplaatsen op, tengevolge van korte afstandsordening. Het resulterende moment m blijft positief, en slechts één anomale σ-T kromme, n.l. die waarvoor de spontane magnetisatie met de temperatuur van teken wisselt, treedt op, en wel in een breed gebied van samenstellingen. Voor $a \leqslant 1{,}25$ behoren deze stoffen tot groep (a) (7).

Een verandering van teken van het resulterend moment treedt wel op in het systeem $NiFe^{III}_{2-2a}Al_aO_4$. Anomale σ-T krommen zijn hier gevonden in een smal gebied van samenstellingen, maar niet alle typen door Néel voorspeld; de oorzaken hiervan worden besproken (8).

De aanwezigheid van Mn^{2+} ionen bevordert blijkbaar het optreden van hoeken tussen de ionenmomenten op de B-plaatsen: het gehele systeem $MnFe^{III}_{2-a}Cr_aO_4$, behoort tot groep (b), evenals $MnFe_2O_4$ bereid door anderen (4) en een gedeelte van het systeem $Ni_{1,5-a}Mn_aFe^{III}Ti_{0,5}O_4$ (6.3). In het eerstgenoemde systeem wisselt m van teken slechts tengevolge van deze hoeken.

Résumé

Les mesures de l'aimantation de saturation (σ) en fonction de la température ont été faites pour un certain nombre de cristaux mixtes d'oxydes à structure spinelle. Les résultats concordent avec la théorie de Néel sur le ferrimagnétisme: le moment magnétique résultant m est la différence des moments des sous-réseaux tétraèdrique (A) et octaèdrique (B), soit:
(a) avec parallélisme complet des moments ioniques à l'intérieur de chaque sous-réseau, ou
(b) avec des angles entre les moments ioniques à l'intérieur d'un des sous-réseaux.
La structure spinelle est décrite dans la section 1.1, données expérimentales et théoriques, tirées de la litérature, sur la distribution des cations sont résumées dans la section 1.2. La théorie de Néel est revue dans la section 2.2.1, avec la modification par Yafet et Kittel (section 2.2.2). Quand les moments des deux sous-réseaux sont à peu près égaux, Néel prévoit un certain nombre de courbes σ-T anormales. Il faut trouver toutes ces courbes dans une série de cristaux mixtes du type (a) dans laquelle le moment résultant m change de signe.
Nos méthodes expérimentales sont données dans la section 3.
Les mesures sur les ferrites simples $Me^{II}Fe^{III}_2O_4$, avec $Me^{II} = Mn^{2+}$, Fe^{2+}, Co^{2+}, Ni^{2+}, Cu^{2+}, Mg^{2+} ou $(0{\cdot}5\,Li^{+} + 0{\cdot}5\,Fe^{3+})$ montrent que celles-ci appartiennent au groupe (a); les cristaux mixtes $Me_{1-a}Zn_aFe_2O_4$ à partir de $a >$ appr. 0,4 appartiennent au groupe b (section 4).
Le moment de $Ca_{0{\cdot}35}Zn_{0{\cdot}65}Fe_2O_4$ est plus élevé que celui d'une ferrite quelconque Mg-Zn, probablement parce que l'angle A-O-B est agrandi par la présence de la plupart des grands ions-Ca dans les sites B, accroissant ainsi l'interaction A-B. Ce comportement est conforme à la théorie d'Anderson (section 5.1). La théorie d'Anderson est revue à la section 2.3.2. L'on peut prévoir le moment d'oxydes ferrimagnétiques à structures crystallographiques différentes d'après les angles (ion-métal)-(ion-oxygène)-(ion-métal), cf: $BaFe^{III}_{12}O_{19}$ et $KFe^{III}_{11}O_{17}$ (section 5.2.)
Dans un certain nombre de séries de cristaux mixtes on a cherché des courbes σ-T anormales; on ne les trouve pas dans les systèmes $Ni_{1+a}Fe^{III}_{2-2a}Ti_aO_4$ et $Ni_{1{\cdot}5-a}Zn_aFe^{III}Ti_{0{\cdot}5}O_4$ à cause de la présence inattendue d'ions Ti^{4+} dans les sites tetraèdriques, démontrée pour $Ni_{1{\cdot}5}Fe^{III}Ti_{0{\cdot}5}O_4$ par des mesures du facteur g efficace (section 6.1-2).
Dans le système $Li_{0{\cdot}5}Fe^{III}_{2{\cdot}5-a}Cr_aO_4$ $(0 < a < 2{\cdot}0)$ la distribution des ions Li^{+} et Fe^{3+} est anormale à cause d'une ordre à courte distance. Le moment résultant reste positif, et il apparaît dans une large gamme de compositions un seul type de courbe anormale σ-T, notamment

celui où l'aimantation spontanée change de signe avec la température. Pour $a < 1.25$, les produits appartiennent au groupe (a) (section 7). Il se produit bien un changement de signe dans le système $NiFe^{III}_{2-a}Al_aO_4$. L'on trouve ici des courbes anormales σ-T dans une étroite gamme de compositions, mais non tous les types prévus par Néel: les raisons sont discutées (section 8).
La présence d'ions Mn^{2+} apparemment favorise la formation d'angles entre les moments ioniques dans les sites B: le système complet $MnFe^{III}_{2-a}Cr_aO_4$ appartient au groupe (b), comme $MnFe_2O_4$ préparé par d'autres auteurs (section 4) et une partie du système $Ni_{1.5-a}Mn_aFe^{III}Ti_{0.5}O_4$ (section 6.3). Dans le premier système cité, le changement de signe de m n'est que le résultat de ces angles.

Zusammenfassung

Es wurde die Sättigungsmagnetisierung (σ) einer Anzahl Mischkristalle von Oxyden mit Spinellstruktur in Abhängigkeit von der Temperatur gemessen. Die Ergebnisse entsprachen der Néelschen Theorie des Ferrimagnetismus: das resultierende magnetische Moment ist der Unterschied der Momente der Tetraeder- (A) und Oktaeder- (B) Teilgitter, und zwar entweder
(a) mit vollständig parallelen Ionenmomenten innerhalb jedes Teilgitters, oder
(b) mit Winkeln zwischen den Ionenmomenten in einem der Teilgitter.
Die Spinellstruktur ist in (1.1) beschrieben, experimentelle und theoretische Daten aus der Literatur über die Ionenverteilung sind in (1.2) zusammengefaßt. Eine Besprechung der Néelschen Theorie ist in (2.2.1) gegeben, dazu die durch Yafet und Kittel gelieferte Abänderung (2.2.2). Wenn die Momente der zwei Teilgitter einander nahezu gleich sind, sagt Néel eine Anzahl anomaler σ-T Kurven vorher. Alle diese Kurven müssen in einer Reihe von Mischkristallen vom Typus (a), in welcher das resultierende Moment m das Vorzeichen ändert, vorkommen.
Die von uns benutzten experimentellen Methoden werden in (3) beschrieben.
Aus den Messungen an einfachen Ferriten $Me^{II}Fe^{III}_2O_4$ mit $Me^{II} = Mn^{2+}$, Fe^{2+}, Co^{2+}, Ni^{2+}, Cu^{2+}, Mg^{2+} oder ($0{,}5\ Li^+ + 0{,}5\ Fe^{3+}$) geht hervor, daß diese zur Gruppe (a) gehören; die Mischkristalle $Me^{II}_{1-a}Zn_aFe_2O_4$ von a > ungefähr 0,4 an gehören zu Gruppe (b) (4). Das Moment von $Ca_{0,35}Zn_{0,65}Fe_2O_4$ ist höher als das aller MgZn-Ferrite, vielleicht weil der Winkel A-O-B infolge der Anwesenheit der Mehrzahl der großen Ca^{2+}-Ionen am B-Platz größer wird: dadurch wird die AB-Wechselwirkung im Einklang mit der Theorie von Anderson vergrößert. ((5.1), eine Besprechung der Theorie von Anderson gibt (2.3.2)).
Das Moment von ferrimagnetischen Oxyden mit anderen Kristallstrukturen kann aus den Winkeln Metallion-Sauerstoffion-Metallion vorhergesagt werden, wie z.B. für $Ba\ Fe^{III}_{12}O_{19}$ und $K\ Fe^{III}_{11}O_{17}$ (5.2).
In einer Anzahl von Mischkristallreihen ist nach eventuellem Auftreten von anomalen σ-T Kurven gesucht worden: man findet diese nicht in den Systemen $Ni_{1+a}Fe^{III}_{2-2a}Ti_aO_4$, weil entgegen den Erwartungen Ti^{4+}-Ionen an Tetradeerplätzen auftreten, was für $Ni_{1,5}Fe^{III}Ti_{0.5}O_4$ durch Messung des effektiven g-Faktors bewiesen worden ist (6.1-2).
Im System $Li_{0,5}Fe^{III}_{2,5-a}Cr_aO_4$ ($0 < a < 2{,}0$) tritt eine unerwartete Verteilung der Li^+- und Fe^{3+}-Ionen über die beiden Gitterplätze auf als Folge einer Ordnung kurzer Reichweite. Das resultierende Moment bleibt positiv, und es tritt nur eine anomale σ/T-Kurve auf, nämlich diejenige, bei der die spontane Magnetisierung mit der

Temperatur das Vorzeichen ändert, und zwar in einem breiten Gebiet von Zusammensetzungen. Für $a \leqslant 1{,}25$ gehören diese Stoffe zu Gruppe (a). (7).

Eine Änderung des Vorzeichens von m tritt dagegen in dem System $NiFe^{III}_{2-2a}Al_aO_4$ auf. Anomale σ/T-Kurven treten hier in einem schmalen Gebiet von Zusammensetzungen auf, aber nicht alle Typen die von Néel vorhergesagt worden sind; hiervon werden die Ursachen besprochen (8).

Die Anwesenheit von Mn^{2+}-Ionen begünstigt anscheinend das Auftreten von Winkeln zwischen den Ionenmomenten an den B-Platzen: das ganze System $MnFe^{III}_{2-a}Cr_aO_4$, gehört zu Gruppe (b), ebenso wie das von anderen hergestellte $MnFe_2O_4$ (4) und ein Teil des Systemes $Ni_{1,5-a}Mn_aFe^{III}Ti_{0,5}O_4$ (6.3). Im erstgenannten System ändert das Vorzeichen nur infolge dieser Winkel.

STELLINGEN

I

De in de biochemie ingeburgerde term "high-energy phosphate bond" is misleidend, en is wellicht aansprakelijk voor de voorkomende verwarring van de begrippen enthalpie en vrije enthalpie.

R. J. Gillespie, G. A. Maw en C. A. Vernon, Nature **171**, 1147, 1953.

II

Bij ferrimagnetische spinellen zullen verzadigingsmagnetisatie-temperatuurkrommen van de typen *d* (Neel's type (*L*)) en *f* (dit proefschrift, fig. 8) slechts kunnen optreden als in de verdeling der kationen over de beide roosterplaatsen geen plaatselijke schommelingen optreden. In een reeks mengkristallen, waarin $m_b - m_a$ van teken wisselt, zullen deze typen krommen wel optreden bij de remanentie-temperatuurkrommen.

Dit proefschrift, § 8.2.4.

III

Het gebruik van een "fullness factor", $(BH)_{max}/B_rH_c$, als maat voor de practisch bereikte kwaliteit van permanentmagnetische materialen met betrekking tot de theoretisch bereikbare, is zinloos, niet alleen ter vergelijking van verschillende typen materialen, maar ook ter vergelijking van verschillende monsters van eenzelfde soort materiaal.

R. M. Bozorth, *Ferromagnetism*, D. van Nostrand, 1951, blz. 351-352.

IV

De gronden waarop Bertaut en Delorme aannemen dat $Cu_{0.5}Fe_{2.5}O_4$ cupriferroferriet is, zijn evenzeer onvoldoende als die, waarop Kordes en Röttig aannamen, dat deze stof als kationen slechts cupro- en ferri-ionen bevat.

E. Kordes en E. Röttig, Z. anorg. Chem. **264**, 34, 1951.
F. Bertaut en C. Delorme. C. R. Acad. Sci. Paris, **236**, 74, 1953.

V

De opvatting van Rutten over de continentale oorsprong van de Zechstein-evaporieten is aanvechtbaar.

M. G. Rutten, Geol. en Mijnb. **16** (3) 61, 1954.

VI

De door Robin en Bénard bij 300 °C bereide metastabiele mengkristallen met spinelstructuur tussen γ-Fe_2O_3 en Co_3O_4 zijn inderdaad [1]) mengkristallen tussen deze verbindingen, en hebben dus niet, zoals later[2]) door de auteurs werd aangenomen, dezelfde samenstelling als de bij hogere temperatuur stabiele mengkristallen tussen Fe_2O_3 en $CoFe_2O_4$ en tussen $CoFe_2O_4$ en Co_3O_4.

[1]) J. Robin en J. Bénard, C. R. Acad. Sci. Paris **232**, 1830, 1951.
[2]) J. Robin en J. Bénard, C. R. Acad. Sci. Paris **234**, 956, 1952, J. Robin, Thèse, Paris, 1953.

VII

Afgezien van andere overwegingen, is het op chemische gronden niet waarschijnlijk dat het voorkomen van gangen, lava's en sedimenten met een aan het aardveld tegengesteld gerichte remanente magnetisatie te danken is aan de aanwezigheid van ferrimagnetische spinellen met een compensatie-temperatuur.

L. Néel, Ann. Géophys. **7**, 90, 1951, dit proefschrift, § 6.1.

VIII

Ter bestrijding van de verontreiniging van de zee door stookolie is het dringend gewenst dat de regeringen der voornaamste zeevarende landen zich verstaan, teneinde tot een wettelijke regeling dienaangaande te komen. Reeds voordien moet door propaganda bij reders en scheepsofficieren op de belangen van zeevogels, robben, badgasten en hotelexploitanten gewezen worden.

Report of the Committee on the Oil Pollution of the Sea, Ministry of Transport. London, H.M.'s Stationery Office, 1953.
Report of the proceedings of the International Conference on Oil Pollution of the Sea, 27 Oct. 1953.

IX

Uit de metingen van de effectieve g-factor van $Li_{0.5}Fe_{1.25}Cr_{1.25}O_4$ door van Wieringen volgt dat de g-factor van het Cr^{3+} ion kleiner is dan die van Fe^{3+} ion.

J. S. van Wieringen, Phys. Rev. **90**, 488, 1953, of dit proefschrift, § 7.2.3.

X

De instelling van een baccalaureaatsstudie als bedoeld in het ontwerp Hoger Onderwijswet, art. 87, zou in de faculteit der wis- en natuurkunde in een behoefte voorzien; door de toelating tot het baccalaureaatsexamen uitsluitend open te stellen voor candidaten zou echter òf de baccalaureaatsstudie òf de studie voor het doctoraalexamen geschaad worden.

Prof. Dr. J. J. L. Duyvendak, *Rede bij de overdracht van het Rectoraat* op 21 Sept. 1953.

XI

De conclusie van Von Euler en Kispecky, dat de reactie tussen 1, 3, 4-xylenol en formaldehyde in zuur milieu een bimoleculaire reactie is, volgt niet uit hun meetresultaten.

H. von Euler en S. Kispecky, Z. phys. Chem. **A 189**, 104, 1944.

XII

Een bestudering door bezoekers aan het buitenland van de daar heersende omgangsvormen en nationale gevoeligheden kan een bijdrage leveren tot de internationale verstandhouding; de in „Le savoir-vivre international" aanbevolen gedragingen zijn voor niet-Fransen echter niet altijd aanbevelenswaardig.

P. Daninos en D. Ogrizek, *Le Savoir-vivre international, code de la Susceptibilité et des Bons Usages à travers le monde*, Odé, 1950.

XIII

Hoewel in verschillende der gegeven bepalingen de gegevens ontoereikend zijn, is in principe een ruwe schatting van de leeftijd van meteorieten uit een bepaling van de He, U en Th gehalten, na correctie voor het door kosmische straling geproduceerde helium door bepaling van de $^3He/^4He$ verhouding, geoorloofd.

J. C. Dalton, F. A. Paneth, P. Reasbeck, S. J. Thomson en K. I. Mayne. Nature, **172**, 1168, 1953.